Biogeochemical Characterisation of an Alum Dosed Stream: Implications for Phosphate Cycling in Lake Rotoehu

A thesis

submitted in partial fulfilment

of the requirements for the degree

of

Masters of Science

in Earth Sciences

at

The University of Waikato

by

Christopher Andrews Eager

THE UNIVERSITY OF
WAIKATO
Te Whare Wānanga o Waikato

2017

Lake Rotoehu at sunset from the eastern shoreline (Photo by Chris Eager)

“Eventually, all things merge into one, and a river runs through it. The river was cut by the world's great flood and runs over rocks from the basement of time. On some of the rocks are timeless raindrops. Under the rocks are the words, and some of the words are theirs. I am haunted by waters.”

— Norman Maclean, A River Runs Through It and Other Stories

Abstract

Lakes are highly valued freshwater ecosystems which provide many goods and services upon which humans are reliant. Eutrophication of waterways, driven by the over-enrichment of nutrients such as phosphorus and nitrogen, is a threat to the future quality of water resources globally. Lake restoration methods are increasingly being employed to improve eutrophic waterways, via numerous catchment derived and in-lake approaches. However, spatio-temporal heterogeneity in physicochemical and biogeochemical conditions within lakes may restrict the efficacy of restoration methods. This thesis explores in-stream alum dosing as a lake remediation strategy for the purpose of dissolved phosphorus inactivation, and its physicochemical and biogeochemical interaction and fate within Lake Rotoehu, New Zealand.

Laboratory and field measurements were undertaken at Lake Rotoehu, on New Zealand's North Island. The shallow, polymictic lake resides in an active volcanic area with geothermal inputs, and is subject to several management issues including elevated nutrient concentrations, invasive macrophytes, and frequent cyanobacteria blooms. The geothermal Waitangi Springs, which discharge into Lake Rotoehu, contribute ~69 % of the lake's total ionic content, and are responsible for enhanced concentrations of biologically limiting nutrients including phosphorus, silicon, nitrate, ammonium, and iron. In an effort to curb in-lake phosphorus levels, in-stream alum-dosing has been employed in order to floc out dissolved reactive phosphorus (DRP), through chemical adsorption and sedimentation.

The results presented here, culminate from an investigation of the physicochemical and geochemical dynamics across the mixing zone from the Waitangi Springs geothermal stream outlet across Te Wairoa Bay to the main lake body. A combination of approaches was used: two field experiments with fixed location and transect measurements, laboratory analysis and geochemical speciation modelling with PHREEQC.

Results show sharp changes in physicochemical water properties across the mixing zone within the bay: pH, O_2 and dissolved reactive

phosphorus values increased with distance from the stream outlet, whereas major ion concentrations, temperature and conductivity values decreased. Initial in-stream phosphorus stripping through alum dosing is effective in reducing the DRP load by ~50 % of background concentration. As alum is introduced to the stream water (~pH 6) it precipitates to form amorphous aluminium hydroxide ($Al(OH)_{3(am)}$) and adsorbs phosphorus via hydroxyl ligand exchange. However, elevated levels of iron in amorphous hydrous ferric hydroxides $Fe(OH)_{3(am)}$ are also likely to be contributing to natural phosphorus binding capacity. Sediment core data also indicated that settled $Al(OH)_{3(am)}$ floc and $Fe(OH)3_{(am)}$ particulates were primarily concentrated within the inner portion of Te Wairoa Bay near the Waitangi Springs outlet. Surface water physicochemical and geochemical concentrations were spatially resolved and indicated distinct mixing boundaries (pH, DO, temp) and patchiness (Al, Fe, DRP) within Te Wairoa Bay associated with the locations and configuration of dense submerged macrophytes (*Ceratophyllum demersum*). Geochemical speciation modelling also indicated that the primary dissolved Al species was $Al(OH)_4^-$ under the observed daytime conditions, and that Fe was primarily in colloidal form $Fe(OH)_{3(am)}$, which was confirmed through diffusive gradients in thin films (DGT) measurements.

A diel sampling experiment also confirmed that as alum-dosed water enters the lake, daytime biogeochemical conditions driven by *C. demersum* alter physicochemical water properties from ~pH 6 to ~pH 9, and DO (supersaturation) via increased photosynthesis. Diel-fluxes in geochemical solubility (Al, Fe, and DRP) responded to physicochemical shifts (pH, O_2,) and demonstrate that *C. demersum* have the capacity to influence Al solubility and DRP availability within Te Wairoa Bay.

This work highlights the complexity of biogeochemical processes within aquatic freshwater ecosystems. Moreover, the results emphasise the need to account for the significant spatial and temporal heterogeneity of physicochemical parameters in the development of effective lake remediation strategies.

Acknowledgements

First and foremost, I would like to thank my chief supervisor Dr. Adam Hartland and co-supervisor Professor David Hamilton for their guidance, support, and allowing me the opportunity to undertake this research. Furthermore, I would especially like to thank Dr. Grant Tempero, whose helpful advice, assistance with data, time, and patience were invaluable.

I would also like to thank many other faculty and staff members who have supported me throughout my time at Waikato including Karin Bryan, Conrad Pilditch, Ian McDonald, Brendan Hicks, Moritz Lehmann, Mat Allan, Erik Horstman, and Adrian Pittari.

To the technicians who have put up with me as an undergrad researcher and as a MSc student over the past five years and who are truly unsung heroes in so many circumstances. Dean Sandwell, Ronald Ram, Warrick Powrie, Dudley Bell, Peter Jarman, Annie Barker, Steve Cameron, Steve Hardy, Lee Laboryie, Janine Ryburn, Ivan Bell, Lynn Parker, and, Annette Rodgers. Many thanks go to Chris McBride and the BOPRC lakes group for designing, constructing, and maintaining the lake monitoring stations, they are world class.

I thank fellow students, in particular Huma Saeed and Andy Pearson who I am immensely indebted to for your help and guidance in both the lab and the field. Also, Geoff Tait, Grace, Ingrid, and Helena, Nicola Lovett, Noel Bates, and John Montgomery, as well as others in the WEG, LERNZ and CMG groups.

Many thanks go to Iain MacDonald at NIWA for assisting with equipment needs, and Niroy Sumeran at Bay of Plenty Regional Council, for supporting this project, keeping me up to date throughout the project, and answering requests for data and reports.

Furthermore, this project would not have been possible without the funding support of The Hillary Jolly Memorial Scholarship, The University of Waikato MSc Scholarship, the Bay of Plenty Regional Council, the Waikato

Environmental Geochemistry Group, and the Bay of Plenty Chair in Lake Restoration at the University of Waikato .

Thanks to my family and friends who have given me support, in particular my parents Marel and Jim, grandmother Susan H. Emerson for her inspiring curiosity , sister Emily, Jan and Terry Mullarney, Daniel and Kara Laughlin, Doug McCauley and Sylvia Lindeman and others overseas.

Finally, infinite thanks to my partner Julia Mullarney, for your unwavering patience, love and support.

This thesis is dedicated to the memories of James C.Eager, William G. Emerson, Dorothy W. Eager, and Corey M. Morris.

Table of Contents

List of Figures

List of Tables

List of Abbreviations

ANC	Acid Neutralizing Capacity
Al	Aluminium
Al_{dis}	Dissolved Aluminium
Al_{tot}	Total Aluminium
$Al_2Si_2O_5(OH)_4$	Kaolinite
$AlPO_4$	Variscite
As	Arsenic
B	Boron
Ba	Barium
BD	Bicarbonate Dithionite
BOPRC	Bay of Plenty Regional Council
C	Carbon
CO_2	Carbon Dioxide
CO_3^{2-}	Carbonate
Ca	Calcium
$CaCO_3$	Calcium Carbonate
Cl	Chlorine
Cl^-	Chloride
Cu	Copper
DIC	Dissolved Inorganic Carbon
DIP	Dissolved Inorganic Phosphorus
DIN	Dissolved Inorganic Nitrogen
DON	Dissolved Organic Nitrogen
DOP	Dissolved Organic Phosphorus
DOM	Dissolved Organic Matter
DO	Dissolved Oxygen
DRP	Dissolved Reactive Phosphorus
Eh	Reduction-Oxidation Potential
Fe	Iron
Fe_{dis}	Dissolved Iron
Fe_{tot}	Total Iron
FeS_2	Pyrite
FeO(OH)	Goethite
Fe_2O_3	Hematite

$Fe^{2+}Fe^{3+}O_4$	Magnetite
$(Fe^{3+})_2OH_{3(am)}$	Ferrihydrite
$(Fe^{2+})_3(PO_4)_2$	Vivianite
H	Hydrogen
HFO	Hydrous Ferric Oxide
HCO_3^-	Bicarbonate
HPO_4^{2-}	Monophosphate
H_2S	Hydrogen Sulfide
$H_2PO_4^-$	Dihydrogen Phosphate
IAP	Ion Activation Product
K	Potassium
K_{sp}	thermodynamic solubility product
$KAl(SO_4)_2$	Alum
logK	Equilibrium constant
LMA	Law of Mass Action
Mg	Magnesium
Mo	Molybdenum
Mn	Manganese
N	Nitrogen
Na	Sodium
NaOH	Sodium Hydroxide
NH_4^+	Ammonium
NO_3^-	Nitrate
NO_2^-	Nitrite
NOM	Natural Organic Matter
O	Oxygen
O_2	Dioxygen
OH^-	Hydroxide
P	Phosphorus
pH	Hydrogen Potential
PIP	Particulate Inorganic Phosphorus
POP	Particulate Organic Phosphorus
PIN	Particulate Inorganic Nitrogen
PON	Particulate Organic Nitrogen
PO_4^{3-}	Orthophosphate

REDOX	Reduction-Oxidation
S	Sulfur
SAV	Submerged Aquatic Vegetation
SI	Saturation Index
SO_4^{2-}	Sulfate
Se	Selenium
Si	Silicon
Sr	Strontium
TDP	Total Dissolved Phosphorus
TDN	Total Dissolved Nitrogen
TN	Total Nitrogen
TPN	Total Particulate Nitrogen
TPP	Total Particulate Phosphorus
TP	Total Phosphorus
Zn	Zinc

CHAPTER ONE

GENERAL INTRODUCTION

1.1 Motivation

1.1.1 Eutrophication and Lake Ecosystem Restoration

Water is an essential resource required by all life. The ongoing deterioration of freshwater quality in both surface and groundwater, driven by a variety of point source and non-point source inputs from numerous anthropogenic influences, has been known for many decades (Vollenweider 1968; Liu *et al.* 2007). Increasing pressure from global population growth, nutrient inputs, land use change, water resource manipulation, invasive species, and climate change are simultaneously driving freshwater ecosystems to ecological tipping points (Vorosmarty *et al.* 2000; Scheffer *et al.* 2001; Foley *et al.* 2005). For example, Scheffer *et al.* (1993) relate how shallow lakes can transition from oligotrophic macrophyte dominated ecosystems to eutrophic algal dominated ecosystems, and how numerous feedback loops within the system contribute to the resulting altered stable states. Such eutrophication scenarios which were once out of the ordinary, have now in many areas, become the norm, a consequence of the impacts of multiple stressors on ecosystem health (Vitousek *et al.* 1997).

Freshwater ecosystems deliver numerous good and services with high economic value, including the supply of water for drinking and industrial use (energy, agriculture, wastewater), as well as for recreation and tourism (Pretty *et al.* 2003; Mueller *et al.* 2016). Thus, the need to ameliorate or maintain the quality and quantity of freshwaters is a critical but costly undertaking, upon which government and citizens are reliant (Hutton & Haller 2004). Furthermore, government legislation in many regions now mandates bottom-line water quality targets, and these targets will require improved water management strategies moving into the future (European Parliament and the Council of the European Union 2000; Government of New Zealand 2014; Ministry for the Environment 2017).

Lakes represent a large proportion of global surface freshwaters, and are exposed to the influence of terrestrial and atmospheric inputs. Lakes have been shown to act as effective sentinels of both climate and land-use changes (Carpenter *et al.* 2007; Adrian *et al.* 2009; Williamson *et al.* 2009). Decline in lake water quality is often attributed to increased external and internal nutrient loading (Carpenter *et al.* 1998). Given the impetus to undertake lake ecosystem rehabilitation, a diverse range of methods have been utilised to improve both external and internal factors contributing to lake ecosystem deterioration (Cooke *et al.* 2005). Often an integrated remediation strategy is required. These strategies incorporate both catchment (external) and in-lake (internal) approaches, and often result in differing rates of remediation response. Such restorative operations often focus on nitrogen (N) and phosphorus (P) inputs, but may extend to biomanipulation, physical alteration (mixing, diversion), and invasive species removal (Jarvie *et al.* 2013; Hamilton *et al.* 2016).

Studies have indicated that the remediation of lakes from eutrophication is a slow process, primarily due to the accumulation of internal "legacy" nutrient loading and the accompanying physical and biogeochemical drivers which are responsible for nutrient cycling (Welch & Cooke 1995; Søndergaard *et al.* 2003; Burger *et al.* 2007; Jarvie *et al.* 2013). Therefore, over the last half century, lake restoration management plans have employed restorative methods such as chemical nutrient locking and sediment capping techniques primarily with alum ($KAl(SO_4)_2$) in an attempt to control both external nutrient loading and internal nutrient cycling (Browman *et al.* 1977; Eisenreich & Armstrong 1978; Cooke & Carlson 1986; Huser *et al.* 2016b and references therein). The focus of such chemical geo-engineering methods has revolved primarily around P which has been identified as a major biologically-limiting nutrient in freshwater ecosystems (Schindler 1977). The limitation of P is a function of the its chemical behaviour and the physicochemical conditions within water bodies (Froelich 1988; Reynolds & Davies 2001). However, P load increases in freshwater ecosystems have occurred primarily by the increased use of P fertilizers coupled with high rates of erosion, and the increased discharge of wastewaters (Smith *et al.* 2006; Withers & Jarvie 2008).

Although P limitation has been a focal point in eutrophication and lake restoration methods, it is now widely accepted that nutrient limitation in lakes may be driven by P, N+P, and N (Scheffer *et al.* 1993; Lewis & Wurtsbaugh 2008) and on occasion by micronutrients (Sterner *et al.* 2004). Such nutrient limitation studies have been highlighted in several inter-lake comparison studies (Abell *et al.* 2010; Lewis *et al.* 2011; Søndergaard *et al.* 2017).

Additionally, research coupling algal physiology, biogeochemistry and ecology highlights the potential shifts in ion specific N:P ratios (Anderson *et al.* 2002). When limitation and control of either N or P is undertaken through remediation, the respective dissolved N (ammonium (NH_4^+), nitrite (NO_2^-), nitrate (NO_3^-), dissolved organic nitrogen (DON)) to P (phosphate (PO_4^{3-}), dissolved organic phosphorus (DOP)) concentrations and relative ratios between ions, may have a pronounced effect on ecosystem function, community composition, and food web dynamics based on phytoplankton nutrient requirements (Glibert *et al.* 2016). Therefore, any undertaking of lake remediation using such nutrient-limiting techniques should be based on a thorough understanding of the major processes controlling elemental behaviour and fate (Spears *et al.* 2014). Moreover, informed freshwater management and discussion is a vital iterative process, and management approaches should consider longer-term consequences due to factors such as climate change as more research becomes available on advancing remediation techniques and practices (Trolle *et al.* 2011; Mackay *et al.* 2014; O'Reilly *et al.* 2015).

1.1.2 Chemistry of Natural Waters: Phosphorus, Iron, and Aluminium

Natural waters contain a host of chemical ions which are derived from a wide range of environmental processes. These processes vary both spatially and temporally, and can be accounted for by; 1) physical conditions and processes, inclusive of water body morphometry, weather, and climate, 2) local and regional geology, and 3) the biological constituents within the water body and the surrounding catchment (Likens 2009). The dominant ions within natural freshwaters consist of the major dissolved gases (oxygen (O_2)

and carbon dioxide (CO_2)), the major cations (calcium(Ca^{2+}), magnesium (Mg^{2+}), sodium (Na^{+}), potassium (K^{+})) and the major anions (bicarbonate (HCO_3^{-}), carbonate (CO_3^{2-}), sulfate (SO_4^{2-}), and chloride (Cl^{-})). Additionally, inorganic nutrients (P, N, silicon (Si)), metals (iron (Fe), manganese(Mn), aluminium (Al)), as well as other trace elements (e.g. Cu, Mo, Zn) contribute both directly and indirectly to many biological processes. The primary mechanisms by which chemical ions are mobilised and cycled include both wet and dry atmospheric deposition, soil and rock mineral weathering, and a diverse array of biogeochemical processes (Stumm & Morgan 1996; Nimick *et al.* 2011). Hydrologic connectivity acts to transport ions through a continuum from uplands, into wetlands and streams, progressing into larger lentic and lotic water bodies. Such hydrologic ion transport is inclusive of both ground and surface waters (Boano *et al.* 2014). Additionally, the many transition zones along these hydrologic continuums are coupled to the biogeochemical potential and physical conditions present, resulting in variable concentrations, behaviour, and fate of chemical ions within freshwater systems (Schlesinger & Bernhardt 2013).

Within any aquatic biogeochemical system, the reactions of ions are classified into two categories; 1) reactions involving the state of oxidation or REDOX reactions and 2) reactions which control chemical coordination (acid-base, complexation, and precipitation) (Luther 2016). Whereas some ions in water show very conservative properties (low reactivity) such as Na^{+} or Cl^{-}, many other ions such as metals (e.g. Fe and Al) and limiting nutrients (e.g. N and P) are cycled via chemical and biochemical reactions (high reactivity) (Stumm & Morgan 1996). This reactivity often results in the phase partitioning of many ions into soluble, particulate, and solid form, which act to control the (bio)availability of many elements in the aquatic environment (Figure 1.1)(Elder 1989).

The rates of such reactions fluctuate due to temporal and spatial variations in equilibrium physicochemical conditions including temperature, acid neutralizing capacity (ANC), pH, Reduction-Oxidation (REDOX) potential, light, ionic strength, solution speciation/concentration, and reaction surfaces.

Moreover, equilibrium conditions allow that reactions between ions may be both specific and reversible (Warren & Haack 2001). Additionally, the availability of O_2 within the aquatic environment is fundamentally tied to the speciation of N, Mn, Fe, sulfur (S), and carbon (C). Through REDOX reactions, via chemically and biologically mediated transfers, oxidised forms of these elements are sequentially reduced within the water column and within aquatic sediments when O_2 has been depleted (Mortimer 1941; Emerson 1976; Emerson & Widmer 1978).

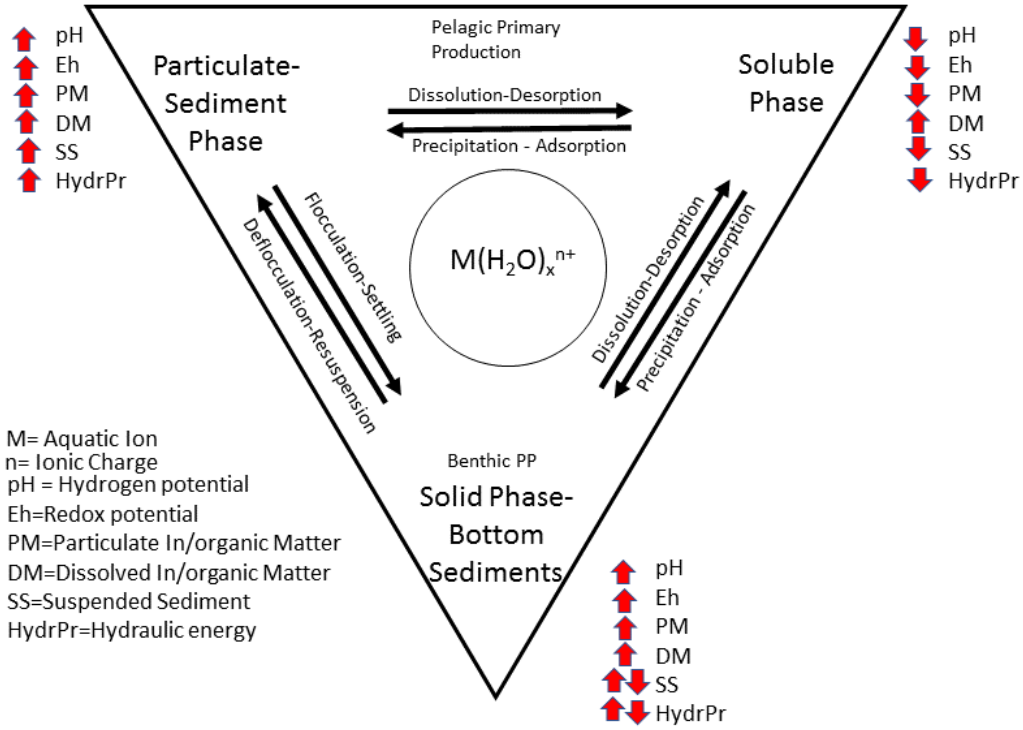

Figure 1.1 Reactive phase partitioning (Soluble, Particulate-Sediment, Solid-Sediment) in aquatic biogeochemical systems, and some physicochemical conditions which favour each phase (outside triangle). Biological primary producers are located near phases which they most closely associate (pelagic, benthic). (Figure adapted from Elder, 1989).

Lakes display a wide range of ionic compositions, and therefore are constrained or relieved by physicochemical processes, which act to control the reaction rates, availability, speciation, and fate of many biologically-limiting elements. One such control is that of P, through the aqueous metal interactions of Fe and Al (Lijklema 1980). I introduce the role each of these major components below.

Phosphorus

A key element in the contribution to inland water eutrophication is P and its environmental availability. Considered a limiting nutrient in freshwater ecosystems and required by all biota, relative P fractions in aquatic systems can be divided into inorganic and organic components as well as size classes: dissolved (<0.45 μm) and particulate (>0.45 μm), (Carpenter *et al.* 1998). Together, dissolved inorganic (DIP) and dissolved organic (DOP) phosphorus constitute total dissolved phosphorus (TDP). Similarly, the particulate inorganic (PIP) and particulate organic (POP) phosphorus components account for the (TPP) with the total phosphorus (TP) being the sum of TDP+TPP. Inorganic P and organic P may also be divided into labile and recalcitrant pools, which reflect their capacity to be easily bio-degraded or retained within their current form. Differentiation between inorganic P and organic P is based on the class of ion, compound, or molecule in which P is integrated. While inorganic P compounds are primarily associated with minerals and colloids within the aquatic environment, organic P is primarily composed of chemical compounds and molecules which have been incorporated into living organisms. Such organic P molecules include larger particulate fractions and dissolved components such as nucleic acids and phospholipids, as well as colloidal organic P (Worsfold *et al.* 2008).

According to Bostrom *et al*. (1988), there are six P transfer mechanisms which account for P mobilization between the pelagic and sedimentary compartments in lakes. These transfer mechanism are; 1) Detrital sedimentation of P bearing minerals from external inflows to the littoral zones, 2) Adsorption and precipitation reactions involving P and inorganic compounds (e.g. complexation-precipitation with Ca, Al, Fe, Mn, adsorption to amorphous metal hydroxides, P associated with carbonates, 3) Sedimentation of externally sourced P associated with metal-organic matter complexes, 4) Internal production and sedimentation of P associated organic matter, 5) Biological P assimilation and mineralization within the water column and sediments by primary producers (phytoplankton, macrophytes, periphyton) and prokaryotes, 6) Transfers of P at the sediment water interface (Boström *et al.* 1988).

Within oxic aquatic systems the majority of inorganic P is found in particulate form bound to metal (oxy)hydroxides; yet the primary bioavailable fraction is the dissolved reactive fraction (DRP) which is a component of the TDP, and the fraction which reacts with molybdate (Murphy & Riley 1962; Reynolds & Davies 2001). DRP availability is limited by several environmental factors including reduced mobilisation during mechanical and chemical weathering of rocks and soil, plant/rootzone interception on land, an ephemeral gaseous phase (phosphine), and the high adsorption capacity of dissolved P to di/trivalent cationic elements and to natural organic matter (NOM) (Reddy *et al.* 1999). These biogeochemical mechanisms are generally referred to as the phosphate buffering system (Figure 1.2). DRP is therefore primarily transported to the aquatic environment adsorbed to sediment, mineral precipitates, or complexed to NOM (Froelich 1988; Weng *et al.* 2012). High DRP loads are therefore often from anthropogenic point and non-point sources such as wastewater effluents, and decreased sediment binding capacities in eutrophic systems.

Although elemental P displays a range of oxidation states (-3 to 5+), in the aqueous environment it is primarily found in the highest oxidation state of orthophosphate ($H_nPO_4^n$). Therefore, aqueous DRP incorporation into both biological and mineral chemical compounds and molecules is generally as orthophosphoric acid species of orthophosphate (PO_4^{3-}), dihydrogen phosphate ($H_2PO_4^-$) or monophosphate (HPO_4^{2-}) that are dependent on pH (Correll 1998; Reynolds & Davies 2001). Individually P also displays very little activity with respect to REDOX cycling. However, due to PO_4^{3-} compatibility with other ions, inorganic P is often found in association with major cations and therefore susceptible to REDOX cycling through adsorption-desorption reactions (Lijklema 1980). P can bind with cations (Ca^{2+}, Fe^{3+}, Mn^{2+}, Al^{3+}) as inner sphere complexes of hydrated metal phosphates, or with respect to acid-base equilibria bound to hydroxide and oxyhydroxides which act to sorb P in solution and may precipitate out in a variety of colloidal, flocculated, or amorphous forms (Kumar *et al.* 2014). Longer-term reactions (days to months) allow inner sphere complexes to develop and this solid-solution transition leads to sedimentation and diagenetic burial, whereby further pH

and redox associated solubility reactions may crystallize or re-solubilize these minerals (Penn *et al.* 1995). Ultimately metal-P bearing authigenic minerals may be buried, dependent on the reductive dissolution of SO_4^{2-} to H_2S and S species interactions, such as pyrite formation with primarily Fe-P minerals. Furthermore, inorganic P in sediments and the water column may be cycled via microbial reductive metabolisms under anoxic conditions which play a major role in the internal P loading in lakes (Gächter & Meyer 1993).

Given the reduced availability of essential inorganic P in lakes, much of the P which is transported into these systems is taken up and recycled through organic forms or within microbial loops (Vanni 2002; Turner *et al.* 2005). Many primary producers have developed mechanisms in which to cleave PO_4^{3-} from organic P molecules, when inorganic forms are in short supply using alkaline and acid phosphatases (Jansson *et al.* 1988). Therefore, increased loading of inorganic DRP from external or internal sources, favours increased algal productivity within lakes, and the accumulation of P in lake sediments (Boström *et al.* 1988). Increased autotrophic uptake, organic cycling, and death return the organic matter and P back to lake sediments where it may be recycled via mineralization or undergo diagenesis through sediment burial (Wetzel 1995; Correll 1998). Additionally, the heterotrophic breakdown of the C rich organic matter may reduce oxygen driving the sediment water interface to anoxia, and reducing minerals such as Mn_3O_4/Mn^{2+} and Fe^{3+}/Fe^{2+}. Through dissolution, such minerals may control a large fraction of P sorption within sediments (Moore & Reddy 1994). Therefore, if external P loads cannot be managed effectively, sediments will eventually exceed their adsorptive capacity for P, leading to heightened eutrophication.

Many chemical sediment extraction methods have been developed to quantify inorganic P within sediments. Some extraction methods relate TP from the sediment such as that of Martin *et al.* (1994), whereas others further fractionate the sediment-P by; labile or exchangeable-P, iron-hydroxide-P (mobile-P), aluminium hydroxide bound-P, Mineral bound-P, and refractory-P (Psenner *et al*. 1988). More advanced methods such as nuclear magnetic resonance spectroscopy have allowed the examination of organic fractions of

P (Özkundakci *et al.* 2014a). While such methods have advanced knowledge of P cycling a great deal, variation in numerous spatially and temporally driven lake processes, including hydrodynamics, sediment dynamics (settling, resuspension, focusing), as well as climatic factors may account for the variation of TP in freshwater aquatic ecosystems.

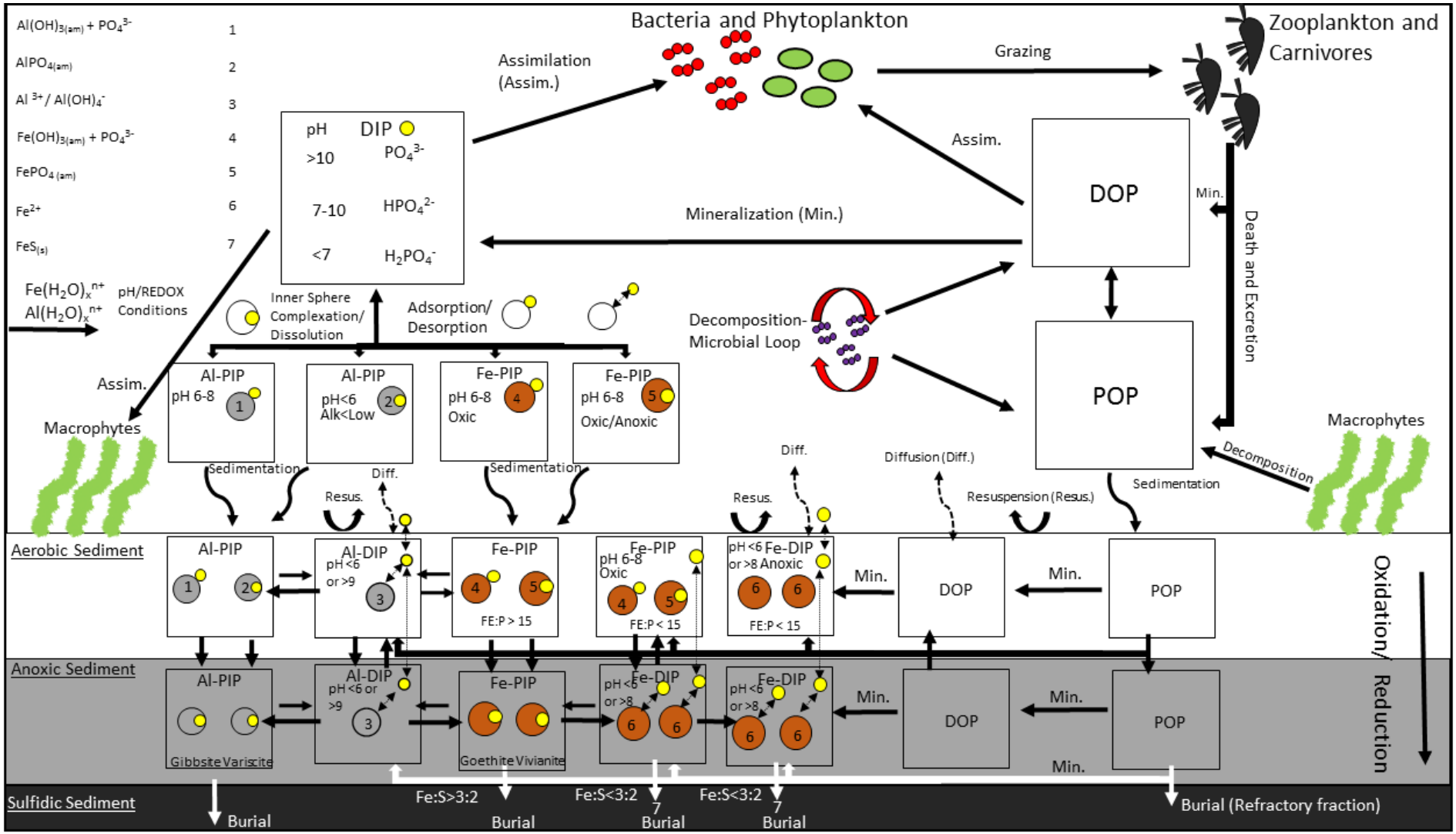

Figure 1.2. Conceptual model of biogeochemical cycling of phosphorus within lakes. In particular, the model highlights the controls on the inorganic components of phosphorus with respect to Al, Fe and S dynamics. Numbers correspond to relevant Al and Fe phase species: 1. Amorphous Aluminium Hydroxide + Phosphate, 2. Amorphous Aluminium Phosphate, 3. Dissolved species of Aluminium, 4. Amorphous Hydrous Ferric Oxide + Phosphate, 5. Amorphous Iron Phosphate, 6. Dissolved Ferrous Iron, 7. Pyrite. PIP and DIP correspond to particulate and dissolved inorganic phosphorus, respectively. DOP and POP refer to dissolved and particulate organic phosphorus, respectively. Within the inorganic components, each box illustrates different conditions and associated forms of Al and Fe (with respect to Phosphorus within the water column and sedimentary compartments).

Iron and Aluminium

Aqueous cations (Ca^{2+}, Fe^{3+}, Mn^{2+}, Al^{3+}) all form solid-solution series in aquatic environments and play an integral role in P cycling within lakes. The amorphous and crystalline forms of these elements, may be buried, transformed, and re-cycled in diagenetic sedimentary processes (Emerson 1976). Minerals which incorporate P, and their associated dynamics are dependent on environmental pH, and redox conditions (Penn *et al.* 1995). A full treatment of the major mineral assemblages would include all of the above elements; however, the primary focus of this thesis is on Fe and Al dynamics and therefore Ca and Mn are only briefly covered.

Fe in the environment is a highly abundant element and is an essential micro-nutrient to most organisms. Iron incorporation in enzymes and proteins has been shown to modulate autotrophic metabolisms and bioavailability, and can be essential in the regulation of ecosystem dynamics (Orihel *et al.* 2016). Additionally, Fe may control crucial interactions with other trace elements (e.g., Cu, Mo) and nutrients (N), which is a function of its high reactivity (Schoffman *et al.* 2016). Within the aquatic environment Fe is found in both the oxidized (Fe^{3+}) or ferric and reduced (Fe^{2+}) or ferrous forms, and its solubility is highly dependent on local pH, and REDOX conditions (Lijklema 1980). The hydrolysis reactions for Fe in water are as follows (Eq. 1.1-1.4) (Flynn Jr. 1984):

$$Fe^{3+}_{(aq)} + H_2O \rightleftarrows FeOH^{2+}_{(aq)} + H^+_{(aq)} \qquad \log K_1 = -2.2 \qquad \text{(Eq. 1.1)}$$

$$Fe(OH)^{2+}_{(aq)} + H_2O \rightleftarrows Fe\,(OH)_2{}^+_{(aq)} + H^+_{(aq)} \qquad \log K_2 = -3.5 \qquad \text{(Eq. 1.2)}$$

$$Fe\,(OH)_2{}^+_{(aq)} + H_2O \rightleftarrows Fe\,(OH)_{3\,(s)} + H^+_{(aq)} \qquad \log K_3 = -6 \qquad \text{(Eq. 1.3)}$$

$$Fe\,(OH)_{3\,(s)} + H_2O \rightleftarrows Fe\,(OH)_4{}^-_{(aq)} + H^+_{(aq)} \qquad \log K_4 = -10 \qquad \text{(Eq. 1.4)}$$

Soluble and reactive Fe^{2+} is the dominant species found within anoxic and acidic aquatic environments such as anoxic stratified lake waters and sediments. In the well-mixed water column under oxic and circumneutral to alkaline pH (pH 6-8), Fe is found as a number of precipitated hydrous ferric

(oxy)hydroxides (HFO), and constitutes 99% of iron in the aquatic surface waters (Davison 1993).

These hydrous (oxy)hydroxides can also be found as precursors to the minerals goethite (FeO(OH), hematite (Fe_2O_3), magnetite ($Fe^{2+}Fe^{3+}O_4$), or in amorphous hydrated forms such as ferrihydrite ($(Fe^{3+})_2OH_{3(am)}$). Ferrihydrite is often present under oxic conditions where Si concentrations are high, and is comprised of nano-particle sized colloids which can form a large component of the dissolved Fe fraction (Lofts *et al.* 2008; Hartland *et al.* 2015b). The precipitation of Fe as an hydroxide $Fe(OH)_3$, provides surfaces in which anions such as PO_4^{3-} can form outer sphere non-covalent bonds via surface adsorption, or as an inner sphere complexes through the formation of hydrated phosphate minerals such as vivianite $(Fe^{2+})_3(PO_4)_2$ (Dzombak & Morel 1990). Moreover, larger particulate inorganic Fe-P precipitates may floc with surrounding NOM, adhering to surfaces and settling to the lake sediment surface (Tipping *et al.* 2002; Hartland 2013).

Under oxidised conditions regardless of the chemical bonding mechanism, Fe retains P within the sediments and is not released to the water column. However, during thermal stratification of lakes, dissolved O_2 (DO) is reduced through organic matter breakdown, and lake sediments proceed through the redox gradient where $Fe(OH)_3$ in surface sediments may be chemically and microbially reduced to soluble Fe^{2+}, in the process releasing sorbed PO_4^{3-}. Although P release from sediment is often attributed to de-oxygenation of the lake hypolimnion and the reduction of organic matter, sediment diagenetic processes are far more involved. Jensen *et al.* (1992) showed that the total Fe:P ratio in the upper portion (1-5 cm depth) within shallow-lake sediments is critical to the gross internal loading of P. This ratio represents the potential for Fe to sorb P and control the rate of P flux to the water column, irrespective of DO concentrations. Other studies have highlighted the intricacies of how pyrite (FeS_2) formation through the coupled Fe-S process affects P mobility through a combination of REDOX-controlled reactions, sedimentation rate, S concentration, and microbial metabolism (Caraco *et al.* 1989; Gächter & Meyer 1993; Gächter & Müller 2003). Further

work from Bostrom *et al.* (1988), Moore & Reddy (1994) and Kopáček *et al.* (2005) has gone on to improve the understanding of Fe-P cycling with respect to Ca and Al fractions within sediments.

Within aquatic systems Al, like Fe, may form insoluble (oxy)hydroxides, and displays very similar speciation dynamics. Al abundance in the Earth's crust is the highest of any metal, and takes its primary form as an elemental component in many oxide and silicate minerals. Aluminium is highly reactive and therefore does not occur in pure elemental form (Ščančar & Milačič 2006). In freshwater systems, the availability of Al is controlled primarily by pH, mineral weathering, and transport and it is of great influence due to its high adsorption capacity. Al is known to complex with a variety of inorganic and organic molecules (Tipping *et al.* 2002). Therefore, Al is often found in low soluble concentration as it enters the aquatic ecosystem, primarily as particulate matter and as a component of sediments. However, Al displays amphoteric behaviour as an acid neutralizing base or as a base neutralizing acid (Driscoll & Schecher 1990). Al is also a component of the Acid Neutralizing Capacity (ANC) of natural waters contributing to the ability of natural waters to buffer acidification (Sullivan *et al.* 1989).

Much of the work associated with Al in the natural environment has stemmed from its interaction with acid rain, and mobilization as a potentially eco-toxic and highly reactive soluble Al^{3+} ion, although more recent work has highlighted the potential impacts of $Al(OH)_4^-$ to biota on the alkaline end of the spectrum (Schafran & Driscoll 1987; Sullivan *et al.* 1989; Gensemer & Playle 1999). Given the appropriate conditions of highly acidic or alkaline pH, Al solubility increases. Therefore, due to the variability in catchment soils, rainwater chemistry and, ion concentrations in natural waters, environmental equilibrium conditions with respect to Al mobilization may change rapidly (Sullivan & Cosby 1998). The hydrolysis reactions are described in the following equations (Eq. 1.5-1.8). Under acidic pH (<4) Al is soluble as the tri-valent Al^{3+} reacts with a water molecule incorporating a hydroxyl(OH-) (Eq. 1.1). These reactions lead to the formation of an amorphous solid Al hydroxide ($Al(OH)_{3(am)}$) the precursor of mineral Gibbsite ($Al(OH)_{3(s)}$) at circumneutral

pH (6.5-8) (Eq. 1.6-1.7). At higher pH (>8.5) values, $Al(OH)_{3(am)}$ passes its point of zero charge (PZC) and resolubilizes as $Al(OH)_{4^-(aq)}$ (Eq. 1.8).

$Al^{3+}_{(aq)} + H_2O \rightleftarrows AlOH^{2+}_{(aq)} + H^+_{(aq)}$ $\log K_1 = -4.97$ (Eq. 1.5)

$Al(OH)^{2+}_{(aq)} + H_2O \rightleftarrows Al(OH)_2^+{}_{(aq)} + H^+_{(aq)}$ $\log K_2 = -4.3$ (Eq. 1.6)

$Al(OH)_2^+{}_{(aq)} + H_2O \rightleftarrows Al(OH)_{3\,(s)} + H^+_{(aq)}$ $\log K_3 = -5.7$ (Eq. 1.7)

$Al(OH)_{3\,(s)} + H_2O \rightleftarrows Al(OH)_4^-{}_{(aq)} + H^+_{(aq)}$ $\log K_4 = -8.0$ (Eq. 1.8)

Further polymerization may occur during the formation of $Al(OH)_{3(am)}$ and this process contributes to Al's flocculation behaviour, and ability to coagulate and bind anions, and organic particles such as NOM (Martell *et al.* 1996). Additionally increased silicic acid concentrations may result in the precipitation of aluminium silicates such as kaolinite $Al_2Si_2O_5(OH)_4$ (Zänker *et al.* 2006). Upon precipitation $Al(OH)_{3(am)}$ may be transported and eventually settle as a metastable species in sediments. Within, sediments under ideal physicochemical conditions crystallization may proceed to form gibbsite ($Al(OH)_{3(s)}$) and this process is thought to occur over periods of days to weeks (Goldberg *et al.* 1996). Moreover any adsorbed ligands such as PO_4^{3-} may be become incorporated into the crystalline structure under reducing conditions potentially stabilising as variscite ($AlPO_4$) (Wisawapipat *et al.* 2017). Furthermore, Douglas *et al.* (2016a) state that the approximate order and preference in adsorption of P is Al-amorphous > Fe-amorphous >> goethite, haematite, magnetite > gibbsite, and is dependent on a number of external factors including size of particles, pH, ionic strength, age, drying, crystallinity of particular minerals, the time of P-adsorption, and initial P concentration.

With respect to lake sediments, Kopáček *et al.* (2005) indicated using the sequential extraction method of Psenner *et al.* (1988), that with a molar $Al_{sodium\text{-}hydroxide(NaOH)}$:$Fe_{bicarbonate\text{-}dithionite(BD)}$ ratio >3 or Al_{NaOH}:$P_{(H2O+BD)}$ > 25 one could delineate between high and low P adsorptive capacity within lake sediments. This Al_{NaOH}:Fe_{BD} ratio has thus been identified as an important mechanisms in the delivery of DRP to aquatic systems, and can be dependent

on regional hydro-geological conditions. For example in more acidic hydrological systems such as northern North America and Sweden, some lakes display high Al-P control within lake sediments (Huser & Rydin 2005; Norton *et al.* 2008). In certain cases, this has been attributed to photo-oxidation of Al-DOM, species, which subsequently dissociate and the free Al ion precipitates and acts to bind P (Norton *et al.* 2008). Under more temperate and tropical conditions soils are consistently more weathered and eroded as a consequence of increased rainfall rates favouring Fe mobilisation and Fe-P binding (Raiswell & Canfield 2012). Furthermore, in volcanic geological settings such as New Zealand, hydrothermal dissolution of dissolved ions such as Fe and P may result in large concentrations of these elements in sediments (Timperley 1983; Timperley & Vigor-Brown 1986).

Calcium and Manganese

Ca also plays a crucial role in the formation of P-binding minerals such as calcite ($CaCO_{3(s)}$) and hydroxyapatite ($Ca_{10}(PO_4)_6(OH)_2$) in the aquatic environment. Additionally, Ca is vital for numerous biological components in animals such as cell walls, bones and shells, and biological functions including cell signalling and osmotic regulation (Likens 2009). Furthermore, the direct interaction of Ca with the C cycle through the precipitation and dissolution of calcite can be a major influence and an important regulator of ANC. Ca may be found in colloidal and particulate forms, and the form is often dependent on the precipitation of calcite in high pH (>7.0) waters. Such high pH conditions may occur in areas of intense photosynthesis by aquatic primary producers. During calcite precipitation, co-precipitation of P may occur, and can act as a transport mechanism to transfer P from the water column to the bed (Reddy & DeLaune, 2008).

Under acidic conditions, Mn is generally found in dissolved form, and forms oxyhydroxides with increasing pH. Mn displays similar behaviour to Fe in terms of redox cycling in the aquatic environment. However, the chemical oxidation of Fe occurs at a much faster rate than that of Mn. Mn has the capacity to bind P in much the same manner as Fe, but cycling of Mn-P

complexes is thought to be more reliant on microbial reduction (Canfield *et al.* 2005).

1.1.3 Alum dosing in the context of Natural Water Remediation

The continued effects of P loading to lakes often results in lake nutrient enrichment coupled by an over-abundance in lake primary productivity (Istvánovics 2008). Numerous supporting cases have demonstrated that such conditions can persist for extended periods of time even after external loading of P had been reduced (Cullen & Forsberg 1988; Jeppesen *et al.* 1991, 2005; Welch & Cooke 1995). Differences in lake mixing regime play a large role in P cycling within lakes (Søndergaard *et al.* 2003). Most lakes store the greatest fraction of P within their sediments due to particle settling. Thus, lake mixing frequency, mixing mechanism (wind, thermal), depth, and water residence time are integral factors in P cycling as both PP and DP can be redistributed when lakes are mixed. Shallow polymictic lakes often have increased rates of sediment re-suspension into the water column, promoting internal P cycling, where deeper dimictic and monomictic lakes thermally stratify for longer periods of time, effectively de-coupling hypolimnetic and epilimnetic waters and their respective nutrient budgets (Fee 1979). Such morphological characteristics are important considerations when considering nutrient inactivation lake restoration methods. Furthermore, it is evident from past studies that controlling the rates and magnitude of internal P loading within lakes is a requisite step if a shift in lake ecosystem health are to be realised (Cooke *et al.* 1993; Jeppesen *et al.* 2007; Jensen *et al.* 2015; Lurling *et al.* 2016).

The use of aquatic geo-engineering methods for the purpose of P-inactivation has been of increasing interest in lake remediation research for several decades (Cooke *et al.* 2005; Mackay *et al.* 2014). The methods employed for P-inactivation, have generally used charged solid -phase natural mineral floccing agents such as Al-salts (alum), ferric chloride ($FeCl_3$), and polymeric-Al-Chloride (PAC), as well as synthetic mineral analogues such as zeolites, or lanthanum modified clays (Phoslock) (Hickey & Gibbs 2009; Douglas *et al.* 2016b). Many of these P-inactivation agents have originated

from their application in the wastewater and drinking water remediation sectors, as both coagulants for the settling of suspended solids (NOM) and their role in the binding of P (Jiang & Graham 1998; Kumar *et al.* 2014). Here, for the purpose of delineating between methods of P-inactivation we will refer to in-lake application as P-occlusion and in-stream as P-stripping. While these two methods are effectively interchangeable, this delineation seeks to separate the respective differences in P-inactivation application purpose. In-lake application often seeks to reduce internal mobile-P cycling between the sediment and the water column (Garrison & Knauer 1984), whereas in-stream applications focus on the removal of TDP from the water column primarily as an external P-stripping method (Cooke & Carlson 1986).

While, many P-inactivation agents have been trialled for lake remediation methods, the majority of cases have been undertaken using alum for the purpose of P-occlusion. The application of alum is most frequently undertaken by boat, in fluidized form through a manifold applicator and dispersed in the water column. However, the use of alum for in-stream applications has also been undertaken (Kennedy & Cooke 1982). Alum ($KAl(SO_4)_2$) reactions are chemically consistent to those in the previous section (Eq. 1.5-1.8), whereby at pH (6-8) the $KAl(SO_4)_2$ dissociates in water, K^+ and two SO_4^- ions are replaced by OH^- (ligand) forming an Aluminium hydroxide $Al(OH)_{3\ (am)}$ precipitate. This hydrolysis reaction contributes to a reduction in pH as it consumes OH^- and therefore pH changes arising from alum dosing are an important consideration with respect to lake ANC. At lower pH (<4) and higher P concentrations, Al^{3+} ions are more abundant and may form a hydrated metal phosphate solid such as vivianite, via inner sphere complexation (Eq. 1.9). At pH ranges between 6 and 8 the $Al(OH)_{3(s)}$ precipitate is favoured and under most concentrations HPO_4^{2-} will adsorb (Eq. 1.10):

$$Al^{3+}_{(aq)} + PO_4^{3-}{}_{(aq)} \rightarrow AlPO_{4(s)} \qquad \text{(Eq. 1.9)}$$

$$Al(OH)_3 + HPO_4^{2-}{}_{(aq)} + H_2O \rightarrow AlOH(HPO_4)\bullet H_2O_{(s)} + 2OH^-_{(aq)} \qquad \text{(Eq. 1.10)}$$

At high pH (>8.5), the amphoteric behaviour of aluminium drives the $Al(OH)_{3\ (am)}$ through its PZC and induces the dissolution of $Al(OH)_{3\ (am)}$ to the soluble $Al(OH)_{4^{-}\ (aq)}$ species. This dissolution reaction may also result in the desorption and release of PO_4^{3-} adsorbed to the Al hydroxide (Eq. 1.6) (Karamalidis & Dzombak 2010; Reitzel *et al.* 2013). For P-occlusion, alum application leads to $Al(OH)_3$ floc formation and subsequent settling to the sediment surface. Under the appropriate conditions non-complexed Al ions continually complex with P, effectively sequestering internal P fluxes and, inhibiting availability of P to the water column. This P-occlusion thus limits the P available to primary producers and may lead to a reduction in the lake trophic state (Cooke *et al.* 2005). In general, the consensus in the literature has been to base alum dose on the fraction of mobile-P (sum of porewater-P, iron bound-P, and in some cases nonreactive-P (polyphosphates and organic-P) within lake sediments, although the dose ratio has varied widely between studies (Rydin & Welch 1999; Reitzel *et al.* 2005; de Vicente *et al.* 2008a; Huser & Pilgrim 2014). Sediment-mobile-P within lakes may be dependent on numerous physical, morphological and biogeochemical factors (Paludan & Jensen 1995; James 2011). Therefore, more recently a predictive model (AlMobP) developed by (Huser & Pilgrim 2014) allows for the dose Al:P application ratio to be optimized, based on the mobile-P fraction within the sediment. This approach allows for a reduction in associated alum dose costs and a minimization of internal P cycling.

Alum treatments for the purpose of P-occlusion have been undertaken throughout a wide range of lakes globally. However, up until recently, there has been very little synthesis between studies in regards to the longer-term effectiveness of dosing. Alum treatments have been conducted primarily in the U.S. (States of FL, ME, MI, MN, NH, VT, WA, WI) (Garrison & Knauer 1984; Welch & Cooke 1999; Rydin *et al.* 2000; Huser *et al.* 2011), Europe (Sweden , Denmark, Germany (Reitzel *et al.* 2005; Egemose *et al.* 2011; Jensen *et al.* 2015)), and New Zealand (Paul & Hamilton 2008; Özkundakci *et al.* 2010; Tempero 2015). A synthesis of 114 lakes treated with alum by Huser *et al.* (2016b), showed that treatment longevity of applied dosing was effective for a mean of 21 years in stratified lakes and a mean of 5.7 years in polymictic

lakes. Eighty two percent of the variation in treatment success was shown to be related to Al dose, watershed (catchment) to lake area ratio, and lake morphology. Furthermore, in-lake biogeochemical conditions such as benthic feeding fish impacted the effectiveness of alum dosing, while the same effect was weak in lakes with Al-dose based on mobile-P (Fe hydroxide bound-P), (Huser *et al.* 2016a). Other studies have focused on the impacts of alum-treated sediments that are resuspended, in-lake sediment focusing, and dissolution of Al under high pH conditions (Egemose *et al.* 2009, 2013; Reitzel *et al.* 2013). These studies have indicated how alum-treated lake sediments in productive shallow polymictic lakes, were at risk of elevated dissolved $Al(OH)_4^-$concentrations if they were to encounter high pH conditions (>9.5). Furthermore, the post-depositional alum floc could easily be transported and focused based on lake morphology and conditions. Given the ability of highly productive lakes to increase lake pH through CO_2 drawdown, such conditions (>pH, sediment mobilization) may present within shallow lake sediments as well as in the water column (Maberly 1996; Han *et al.* 2016; Reid & Mosley 2016). Thus, the solubilisation of Al and the potential desorption of P from Al-P stores due to sediment and or water column pH shifts should be a major consideration when employing the use of alum for P-inactivation.

While the use of alum has been used frequently for in-lake P-occlusion, its application for the reduction of external P loading or P-stripping has been utilised far less for lake remediation purposes. According to Fastner *et al.* (2016) external P load reductions for in-lake water quality improvement may take the form of three main methods; 1) wastewater and sewage treatment, 2) diversion of inflows, 3) P-stripping at the inflow. Therefore, point source treatment of external P inflows may cover a broad range of treatment options. It is well established that external P loading to waterways increases eutrophication, and this resultant knowledge has led to the development of many wastewater treatment facilities which undertake P load reduction. The methods for P reductions in wastewater treatment are numerous and constitute a field in themselves; however, they often involve coagulation, filtration, and microbial bioreactors which span multi-tiered systems. If wastewater treatment is not a viable option, diversion of inflows may provide

significant reductions in nutrient inputs (Fastner *et al.* 2016). Much work has been conducted using artificial wetlands, and bioreactor beds, which allow natural biogeochemical processes to cycle high loads of nutrients helping to reduce inflow concentrations (Tanner *et al.* 1995; Ballantine & Tanner 2010; Egemose *et al.* 2012). Finally, P-stripping may be undertaken in situations where not only point source, but also non-point source P loads contribute to the inflows. This effective removal of P is similar to that of wastewater treatment systems which often use alum within a coagulation and settling phase of in-stream treatment. Thus, along with DRP adsorption to Al, the active coagulation also removes suspended solids and promotes particle settling. This however may result in the accumulation of $Al(OH)_{3(am)}$ floc dependent on stream velocity and discharge. Often, longer term P-stripping systems have moved towards the use of detainment bunds, or in-stream bypasses in order to remove the accumulated floc (Bernhardt 1980; Harper 1990; Heinzmann & Chorus 1994; Pilgrim & Brezonik 2005a). The continuous nature of such systems is costly and should be considered only in situations where other remediation measures are unsuitable or unfeasible.

Continuous P-stripping within lake inflows has been conducted in several cases, primarily in the US (States FL, MN, OH) (Cooke & Carlson 1986; Harper 1990; Pilgrim & Brezonik 2005a), Europe (Germany and the Netherlands) (Bernhardt 1980; Heinzmann & Chorus 1994), and New Zealand (McIntosh 2012; Hamilton *et al.* 2015; Tempero 2015; Smith *et al.* 2016). P-stripping in the Cuyahoga River in Ohio was one of the first attempts at in-stream continuous dosing (Cooke & Carlson 1986). The dosing was undertaken at 1-2 mg Al L^{-1}. Although successful in reducing DRP by 50-60 %, in-lake TP reduction was low. Additionally, the low volume stream resulted in floc accumulation which was detrimental to the downstream ecosystem (Barbiero *et al.* 1988). Other, in-stream P-stripping systems have been primarily in heavily urbanized areas which experience increased storm-water flows. These systems generally used detainment structures, or in-stream processing in order to remove the accumulating alum floc. The Wahnbach reservoir and Lake Tegel in Germany have been using continuous alum dosing since the 1980s and undertake multi-tiered stripping and settling using both

alum and Fe salts, via constructed P treatment systems (Bernhardt 1980; Heinzmann 1998). In Florida, Harper (2007) has been involved in storm-water alum treatment facilities in upwards of 50 lakes. Initially, early versions of treated inflows discharged alum directly to the lakes, and sediment extractions indicated that there was increased P-retention as well as retention of heavy metals within lake sediments. However, local government eventually legislated the requirement for floc removal, which in recent years led to the development of novel in-stream P-stripping and floc settling systems. Other storm-water systems in Minnesota on Fish Lake and Tanners lake have employed in-stream P-stripping and discharge into detention ponds (Pilgrim & Brezonik 2005a; b). Finally, in New Zealand, P-stripping treatment systems have been installed on both Lakes Rotorua commencing in 2006 (two inflows, one of which is geothermal) and Rotoehu commencing 2011 (with a single geothermal inflow). Both operations discharge alum directly to the lakes and have been shown in Lake Rotorua to be correlated with reductions in TP and chlorophyll-a (Smith *et al.* 2016). However, it is uncertain as to how the in-lake P-occlusion is occurring as high concentrations of Al have been found only in littoral sediments near the stream mouths, and climatic effects may potentially be a factor (Özkundakci *et al.* 2014b; Hamilton *et al.* 2015). The elevated TP and DRP in two of the alum-dosed geothermal streams have been attributed to hydrothermal dissolution of P within groundwater (Timperley & Vigor-Brown 1986). Therefore, aside from the potential impacts of agriculturally derived nutrient inputs, a strong background concentration of naturally elevated levels of DRP, as well as DIN, may be present (Timperley 1983; Hoellein *et al.* 2012).

1.2 Thesis Objectives

1.2.1 Major Research Questions

The use of alum as a P locking agent for both discrete application in lakes and for in-stream application in the wastewater sector is well-documented. However, the continuous in-stream application of alum for the purpose of external load P reduction has been undertaken far less frequently. As with any lake restoration method, site-specific knowledge is essential if the

optimisation of restorative methods is to be achieved. This thesis aims to further the understanding of in-stream alum applications and their effects on the biogeochemistry of lake ecosystems, through a field investigation of a geothermal stream-lake transition zone currently receiving in-stream alum application. The aim of the field investigation was to establish high resolution physicochemical and geochemical coverage of the transition zone to gain improved knowledge of the biogeochemical dynamics of the system. This investigation was undertaken primarily to: 1) Quantify the changes in Al, Fe, and P phases based on the variability of conditions within the transition zone, and 2) Explore the impact that high submerged macrophyte biomass has on Al, Fe, and P dynamics over a diel cycle within the transition zone. Furthermore, the unique geothermal setting in this study provides a test case which to the author's knowledge is the first of its kind. Chapter 2 introduces the study site in detail including a brief review of previous research related to the lake. The chapter also summarises the analytical methods common to the subsequent two chapters. Chapter 3 focuses on the spatial geochemical and physical characterisation of the Waitangi Springs and its dispersal plume entering Te Wairoa Bay within Lake Rotoehu. This field study compares the summertime low stream discharge and a large rainfall event which resulted in an increase in stream discharge, plume dispersal, and coincided with a lake destratification event. The primary motive for this approach was to characterise the dynamics of the physicochemical factors which control the behaviour and fate of Al, Fe, and P within the system. Geochemical water column analyses are synthesized through PHREEQC geochemical equilibrium/speciation modelling. Long-term lake data is also analysed to elucidate the in-lake response to the alum application. Key findings from Chapter 3 spurred further inquiry into the effects of the invasive submerged macrophyte *Ceratophyllum demersum*, and its role in the biogeochemical dynamics of Te Wairoa Bay. Chapter 4 focuses on the diel biogeochemical cycling within Te Wairoa Bay, and more specifically how the *C. demersum* beds alter the physicochemical environment with respect to Al, Fe and P dynamics. Chapters 3 and 4 are structured to be read as stand-alone pieces of work, or as part of the overall thesis. Each of these chapters includes the methods and

discussion of results specific to the chapter. Chapter 5 provides a summary of the body of research in terms of the wider context of the use of in stream P stripping as an effective form of lake remediation and offers recommendations for future research and management with regards to in-stream alum application. An appendix (Appendix 1) with raw data is also attached.

CHAPTER TWO

SITE OVERVIEW AND ANALYTICAL METHODS

2.1 Site Overview

The Te Arawa Rotorua Lakes consist of twelve major volcanic lakes occupying the area surrounding Rotorua on the North Island of New Zealand (Figure 2.1a,b). Due to the active geology of the region, the lakes have a rich and complex, geophysical and geochemical past (Lowe & Green 1987). Located within the Taupo Volcanic Zone (TVZ) an active and currently rifting Quaternary silicic volcanic region, most of the lakes within the area have been formed by large caldera forming rhyolitic eruptions, smaller volcanic craters, and through damming by lava deposition (Jolly & Brown 1975; Wilson & Rowland 2016). The lakes reside primarily within the Rotorua and Okataina volcanic complexes, are relatively young geologically and have had varying morphological development over the last 500,000 years.

Lake Rotoehu and the Waitangi Springs the focus of this study are a direct product of the active volcanic, geothermal and geomorphological processes occurring within the TVZ. Both Lake Rotoehu and the Waitangi Springs are located in the northern portion of the Haroharo-Okataina caldera. This large caldera has evolved over approximately the last 50,000-400,000 ka and is the product of multiple explosive plinian style eruptions (Hodgson & Nairn 2004).

2.1.1 Lake Rotoehu

Lake Rotoehu (Figure 2.1) is a medium sized (area 7.95 km^2, total volume 6.2 x 10^7 m^3), shallow (mean depth 8.2m, max. depth 13.5 m), eutrophic (Trophic Level Index, TLI=4.5 in 2014), polymictic lake, and sits at ~297 m above sea level. The lake forms part of the Te Arawa Rotorua lakes found within the TVZ on the North Island of New Zealand. Lake Rotoehu has a polymictic regime and its water column is generally well-mixed due to its marginal depth; however, it often displays thermally stratified periods during

episodic high pressure events in summer and can develop anoxic bottom waters, which enhance internal nutrient loading (Fish 1970; Burns *et al.* 2009).

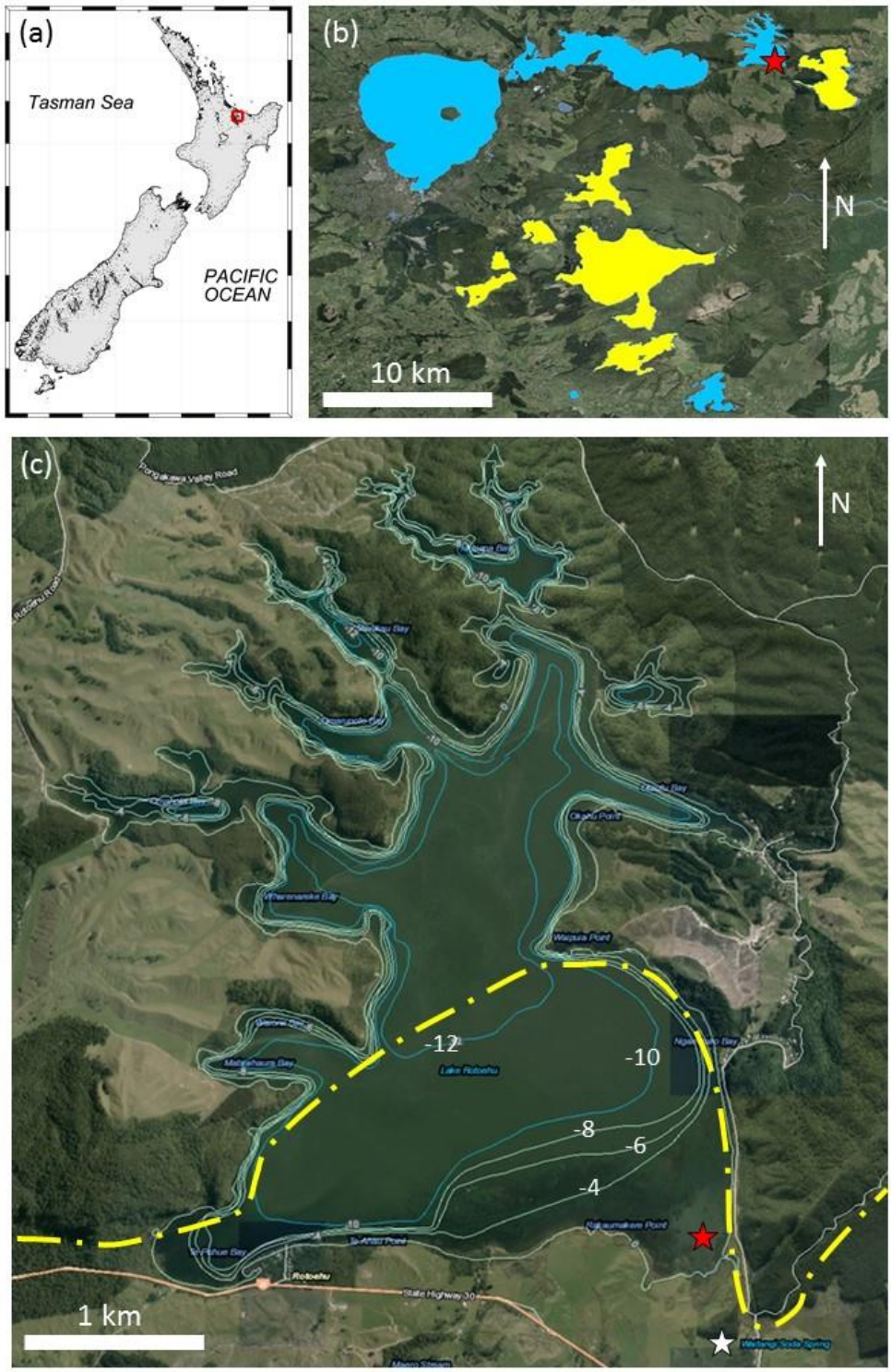

Figure 2.1. A map of (a) New Zealand and the location (red square) of the Te Arawa Rotorua lakes, (b) the Te Arawa lakes denoting those which are actively being managed (blue) and those in a natural condition (yellow) with respect to the location of lake Rotoehu (red star), and (c) Lake Rotoehu, bathymetric profile (blue lines (m)), location of Te Wairoa Bay (red star) and the Waitangi Springs (white star) in relation to the lake. Yellow dashed line shows the northern boundary of the Haroharo caldera rim in relation to the lake.

Lake morphology includes the northern section of the lake which is characterised by seven digitate arms, while the southern portion of the lake consists of a larger open basin. The unique morphology of the lake was developed by the active volcanic and geomorphic processes of the area, and its current form is the result of several eruptive phases (Lowe & Green 1987). The lake basin was once a larger valley which drained Lakes Rotorua and Rotoiti and the digitate northern arms represented stream valley's which once drained in a southerly direction into the modern day Tarawera river valley system (Hodgson & Nairn 2004). Large episodic phreato-plinian volcanic eruptions (Okataina eruptions 50,000-400,000 ka) and caldera collapse acted to form the Haroharo caldera rim. The rim itself runs through the central portion of the lake and forms a portion of its northern boundary, effectively splitting the northern and southern portions of the lake and demarcating the southern basin (Figure 2.1c). Later eruptions from the from the Haroharo complex south-southwest of the Lake Rotoehu area raised the topography within the area, infilling the riverine valley and effectively impounding the lake from the south. The lake is estimated to be 8500-9000 ka in age (Jolly & Brown 1975).

There are four major streams (Te Pohue stream, Te Maero stream, Raukaumakere stream, and the Waitangi Springs) and numerous springs and smaller surface water inputs to Lake Rotoehu. Additionally, groundwater input/output is thought to be a significant component of the water balance. A consequence of the formation of the lake by impoundment is that Lake Rotoehu has no surface outlet. However, it is stated that that a sinkhole outlet likely exists in one of the northern arms, draining to northward flowing springs (Jolly & Brown 1975). The lake level shows significant variability over decadal time scales, and due to its shallow depth, has demonstrated large fluctuations in water level in the past (Burns *et al.* 2009). The lake is also estimated to have a water residence time of 1.4-1.7 yr based on the period of 2003-2006 (Trolle *et al.* 2011). The lake catchment area (47.1 km^2) is of mixed land use consisting of 34 % pasture, 31 % native forest, 30 % exotic forest, 5 % wetland, exotic shrub, and 1 % urban (BOPRC 2007). A nutrient budget based on 2003 data estimated that the total external nutrient loads to the lake

were 53.1 t y^{-1} TN and 2.45 t y^{-1} TP, with internal loads from lakebed sediments contributing 5.6 and 1.4 t y^{-1} of TN and TP (1990-2002), respectively (BOPRC 2007).

Records of in lake limnology extend back to work conducted in the 1950s (Jolly 1968; Jolly & Chapman 1977), and 1960s (Fish 1970), which covered Lake Rotoehu's physical, optical, chemical, and biological conditions. Lake Rotoehu was recognised as being thermally mixed, shallow and prone to algal blooms (Cassie 1978), as well as having a unique chemistry as a consequence of the large geothermal inputs (Timperley & Vigor-Brown 1986). Further work began to explore the increased abundance of invasive submerged aquatic vegetation, such as *Lagarosiphon major* and *Elodea canadensis* (Carter 1973), and the current major infestation of the invasive hornwort *Ceratophyllum demersum,* which contributes a large amount of N and P to the lake. Of all the Te Arawa lakes, the submerged plant indicator (Lake SPI) index (18 %) in Lake Rotoehu is the poorest with low native condition (25 %) and high invasive impact (92 %) (Burton & Clayton 2015). In 1993 a significant and prolonged drop in lake water resulted in high internal nutrient loading, resulting in an elevated TLI of 5.2 (Burns *et al.* 2009).

In 2007, the Bay of Plenty Regional Council enacted the Lake Rotoehu Action Plan which aims to address lake and catchment remediation through a number of catchment and in-lake remediation methods in an effort to improve the TLI (BOPRC 2007). The Action Plan remediation strategies have included catchment-related work such as, land use conversions from pastoral to forestry, stream denitrification, and reduction of external P loads through continuous in-stream alum application of the geothermal Waitangi Springs since 2011 (Anderson & Taylor 2008; Tempero 2015). In-lake remediation measures have included the removal of aquatic weeds (*C. demersum*) targeting N and P since 2008, instalment of a floating wetland at the Te Maero stream outlet focusing on N removal, and in lake aeration/destratification from 2011-2015 (McBride *et al.* 2015; Scholes & Hamill 2016). Lake surface and bottom water flows were measured by Gibbs *et al.* (2011b) and showed a dependency on wind direction and stratification. When the lake was fully mixed, flows in

the upper and bottom layers were coupled and velocity decreased with increasing depth. When the lake was thermally stratified, upper layer flows were in the direction of the wind with a bottom water return flow in the opposite direction. During south-westerly winds this resulted in a north-easterly surface current with a south and south-westerly bottom return flow from both the mid and southerly basins, thus downwelling of surface waters and upwelling bottom waters were hypothesized. Sustained wind velocities >4 m s^{-1} were required to de-couple the flow during periods of stratification. Maximum flow speeds (u) of 17 and 13 cm s^{-1} were observed at the surface and bottom (13 cm s^{-1}), respectively, with mean velocities ranging between 3.6-5 cm s^{-1} (surface) and 2.3-3.4 cm s^{-1} (bottom). Under quiescent conditions, a mean southerly flow direction was observed in bottom waters. Furthermore, monthly monitoring by the BOPRC for key water quality parameters (TN, TP, PO_4-, NO_3-, NO_2-, NH_4^+, Chl-a, Secchi depth) has been ongoing since 1993, and have been instrumental in tracking longer term trends in lake trophic status.

In recent years, real time monitoring of in-lake conditions from a telemetered buoy, measures numerous vertically integrated water-column properties and physical surface conditions. Combined, longer term records have been used on several occasions to calibrate aquatic ecosystem models, such as DYRESM-CAEDYM, ELCOM-CAEDYM, and GLM which has improved understanding of in-lake processes and lake behaviour under a range of conditions, and assisted in management decisions (Trolle *et al.* 2011; Allan *et al.* 2016). Trolle *et al.,* (2011) investigated the future impacts of climate-related temperature change of lake water moving into the future. Model simulations demonstrated that the effects of increased temperatures could be the equivalent of increasing external TP and TN loading by up to 50 % and could result in a potential increase of >15 % in the cyanobacterial contribution of in-lake Chl-a. The work of Allan *et al.* (2016) used remote sensing techniques to measure lake skin temperatures, and validated these measurements using high-frequency temperature data. Results from remote sensing of lake skin temperature displayed heterogenous temperature patches across the lake on many occasions. Additionally, the surface temperature signature of the Waitangi Springs geothermal plume was well resolved. They subsequently

developed a three-dimensional hydrodynamic model (ELCOM) for Lake Rotoehu. ELCOM model results estimated the magnitude of plume dispersion well in most cases, although, responses to wind direction were not always correlated with the lake skin temperature distribution (Allan *et al.* 2016).

2.1.2 Waitangi Springs

The persistent quaternary silicic volcanism, characteristic of the TVZ has been an integral geomorphic driver within the central North Island of New Zealand (Nairn 1992). The actively rifting arc is spreading between 7-15 mm per year from South to North respectively, and this spreading has resulted in a very shallow continental crust (~7 km). This coupled magmatic-volcanic-hydrothermal system is globally unique and only comparable in magnitude to the Yellowstone region in the United States (Hurwitz & Lowenstern 2014; Wilson & Rowland 2016). The presence of numerous geothermal fields across the TVZ is a function of the significant magmatic heating of groundwaters within the permeable crust of the region. High temperatures and convective flows within country rock leads to mineral alteration and dissolution of minerals into geothermal waters, resulting in high total dissolved solids concentrations (Ratouis & Zarrouk 2016). Chemical compositions of geothermal waters are regulated by the water temperature, the chemical composition of the host rock, and the oxidation state, all of which affect mineral dissolution reactions (Henley & Ellis 1983). Such chemical alterations may produce a gradient of hydrothermal water chemistry. These water types are generally classified as; 1) neutral-chloride, 2) acid-sulphate-chloride, and 3) acid-sulphate and are dependent on the underlying hydrogen sulphide (H_2S) concentrations and phase (aqueous or gas) within the host rocks. Thus, many geothermal waters in the TVZ contain high concentrations of dissolved boron (B), Na^+, K^+ Cl^-, Si, Ca^{2+}, Mg^{2+}, SO_4^{2-}, and HCO_3^- in comparison with stream water and rainwater (Timperley & Vigor-Brown 1986). Additionally, pumice soils naturally high in PO_4^{3-} minerals are common within the TVZ. Groundwater contact with these soils, results in acid-dissolution of P on account of high CO_2 and low Ca^{2+} concentrations which can bind PO_4^{3-}. This

dissolution therefore results in high dissolved P concentrations not only in geothermal waters but in cold water springs within the region (Timperley 1983). More recent work has highlighted nutrient cycling in geothermal stream reaches, and the saturation of NH_4^+ (Hoellein *et al.* 2012).

The Waitangi Spring emanates from the Tikorangi-Rotoma geothermal field located between Lakes Rotoehu and Rotoma (Figure 2.2) (Simpson & Bignall 2015). The geothermal field extends along what is considered the eastern boundary of the Okataina caldera, and measured subsurface temperatures exceed >220 °C at 700-1000 m depth at Tikorangi. A resistivity low located north of Tikorangi is thought to be the source of the spring waters. This resistivity low results in a shallow condensate aquifer which has been hydrothermally altered and produces the sodium-bicarbonate-chloride waters at the Waitangi and Otei (Rotoma) springs (Bromley *et al.* 1988).

The Waitangi springs drains an area of 1.7 km^2 and flows through a wetland area before converging with a larger cool water spring. The spring temperature ranges between 35-40 ^oC and the streambed is visually red due to HFO precipitation. The Waitangi Spring base flow has been estimated at 210 L s^{-1}, and a combined flow after converging with the Manawahe Road cold spring of 345 L s^{-1} based on 2016 flow records. Discharge at the lake mouth was estimated using and ADCP and an order of magnitude estimate was calculated to be ~315 L s^{-1} on 07/04/17. In total, geothermal waters have been estimated to deliver 0.8 tonnes of TP (32. 9 % of gross input) and 4.7 t of TN (8.9 % of gross input) to Lake Rotoehu (Bioresearches 2003).

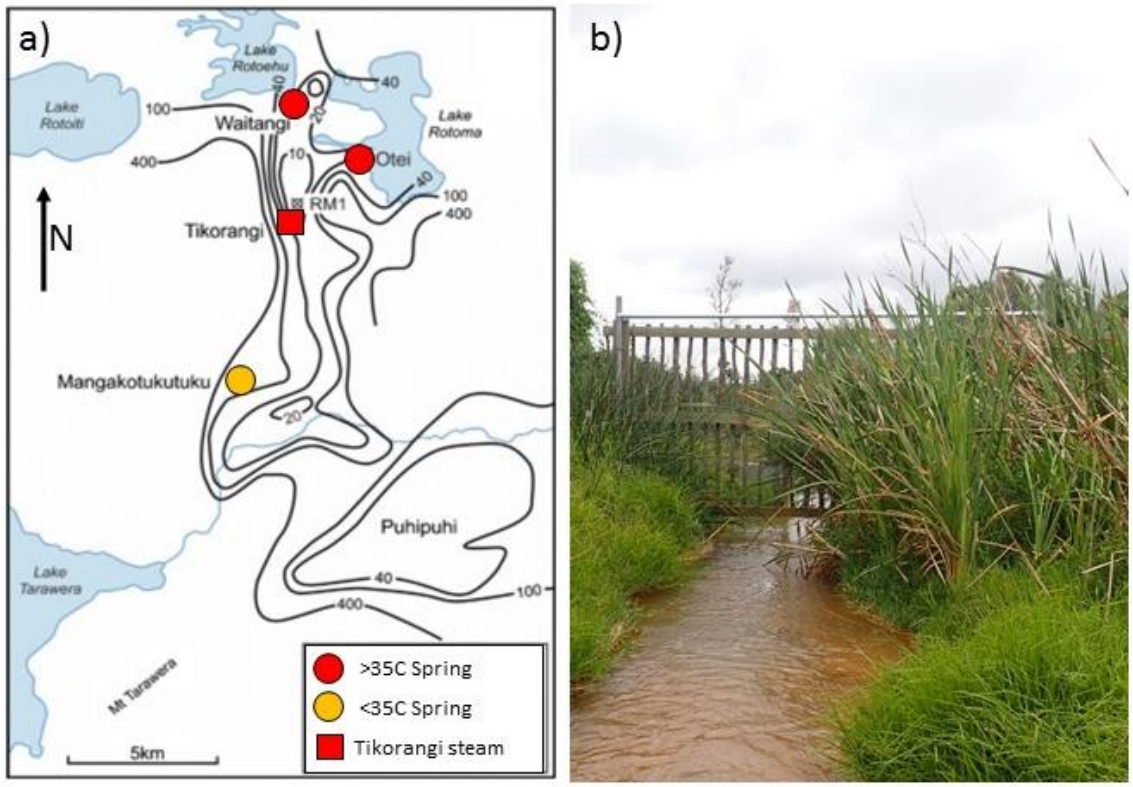

Figure 2.2. The Tikorangi-Rotoma geothermal field (a) depicting geothermal features and resistivity contours (black lines in ohms) (adapted from Bromley, 1988 and Simpson, 2016). (b) Photo of the Waitangi Springs looking downstream above the alum dose point.

2.1.3 Alum Dosing

Alum dosing at the Waitangi Springs for the purpose of P-stripping has been consented since mid-2011, with the aim of reducing TP levels within the lake. Variation in dosing rates since 2011 were due to the ranges of acceptable TP levels which were 0.014-0.017 g m^{-3} up until October 2014 and 0.02-0.025 g m^{-3} thereafter. An auto-dispensing system injects an alum slurry from a 20,000 L capacity tank at a specified fixed rate of 45 L h^{-1} since October 2014. Dosing protocol is to reduce (or increase) the dose by 5 L h^{-1} if the lower (or upper) control levels of TP are breached over a three-month rolling average. Alum dosing levels were calculated based on the change in the alum storage tank level (using tank level data taken from BOPRC website). Data were averaged to provide daily values and were de-spiked to remove erroneous measurements and times of tank refilling. Rates were then estimated assuming a tank capacity of 20,000 L and a specific gravity of 1.32 for the alum slurry (Figure 2.3). Tonnes of alum and aluminium added and phosphorus-

locked per year assuming 4.2 % of the slurry is aluminium, and a reaction ratio for aluminium: phosphorus of 7:1 (McIntosh 2012; Tempero pers. com.) are shown in Table 2.1.

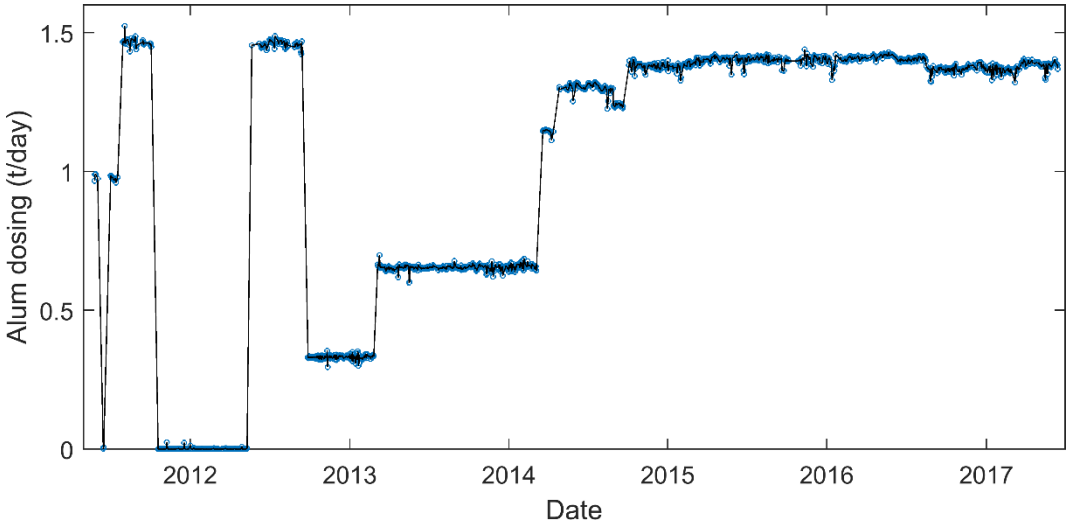

Figure 2.3. Alum dosing rate (t^{-1} per day Alum) from the Waitangi Springs P locking facility. Data spans the commencement of dosing (mid) 2011- (mid) 2017. Data provided by BOPRC real time monitoring, and de-spiked for inaccuracies in tank level.

Table 2.1. Alum dosing totals for the Waitangi Springs.

Dates	Alum (t)	Aluminium (t)	P locked (kg)
1/7/2011 to 31/12/2011	121	5	0.73
1/1/2012 to 31/12/2012	186	8	1.11
1/1/2013 to 31/12/2013	219	9	1.31
1/1/2014 to 31/12/2014	420	18	2.52
1/1/2015 to 31/12/2015	511	22	3.06
1/1/2016 to 31/12/2016	510	22	3.06
1/1/2017 to 14/6/2017	227	10	1.36
Total	2193	93	13.16
Total (kg m^{-2} lake area)	0.2758	0.0117	0.0017

2.2 Sampling Protocols, Analytical Methods and Geochemical Modelling

2.2.1 Sampling Protocol

Sampling of Waters: Dissolved and Total Fractions

All water sampling equipment (polypropylene 'falcon' tubes, syringes) were washed in 10 % HCl, 10 % HNO_3 (with the exception of those used for N

nutrient sampling) and subsequently triple-rinsed in ultrapure deionised water. Sampling equipment was then air dried in a clean room for 24 h before being capped, labelled, and allocated into sampling site containers.

Dissolved fraction water sampling was undertaken via personal watercraft or by wading (stream sites) and sought to minimise any disturbance to the water column. Surface samples were collected approximately 15 cm below the water surface using BD Luer-Lok 60 ml syringes and immediately filtered into falcon tubes (3 x 50 ml for alkalinity, IC, and FIA analysis, 1 x 15 ml for ICP-MS analysis) using Minisart cellulose acetate/surfactant free 0.45 μm filters. Bottom water samples were collected (only for 07/04/17) in the same aliquot numbers; however, was collected through 4-mm diameter neta tubing attached to a luer fitting and lowered to the lake bottom. The tubing was flushed several times with ambient water and discarded before retaining the sample to ensure residual water was not incorporated into the samples. Upon filtration, all falcon tubes were sealed and wrapped with parafilm to reduce any potential for gaseous exchange, and immediately put on ice. Upon return from the field site, samples were either kept at < 6 °C in a refrigerated dark cooler (Alkalinity IC, ICP-MS), or frozen immediately (FIA-DIN_DRP, FIA-TN_TP) dependent on the analyses to be performed.

Sampling of Waters: Diffusive Gradients in Thin Films (DGT)

The use of in-situ sampling diffusive hydrogels for the quantification of analytes in the environment has been undertaken for several decades. Diffusive Gradients in Thin Films (DGT) are based on the progressive accumulation of analytes across a diffusive membrane/diffusive hydrogel/resin binding gel interface, where the resin acts to bind the solutes which diffuse across the solution-sampler interface (Figure 2.4). The accumulation of solutes in the sampling device effectively perturbs the system in which it is deployed and can segregate chemical species based on the environmental (redox, pH) conditions. Such devices are particularly useful for capturing the dynamic chemical fluxes in aquatic solutions and solid-solution

chemical environments. The use of DGTs in numerous environments from water column to sediments and soils, has allowed increased temporal and spatial analysis of many inorganic and organic analytes. When the DGT device is deployed in natural waters, it passively accumulates analytes over time. Upon retrieval, the binding resin is eluted and analysed via ICP-MS. Calculations are required in order to obtain the DGT measured concentration which is interpreted based on environmental conditions. In order to obtain the mass of metal M on the binding resin Eq 2.1 is required. Where c_e is the concentration of metal obtained in the acid eluent, V^{bl} is the volume of the binding layer, V_e is the volume of the acid eluent, and f_e is the elution factor or the fraction of bound metal released based on controlled conditions. Based on Fickian diffusive law, the flux of solute J is equal to the diffusion coefficient D^{mdl},where *mdl* refers to diffusion within the materials of the device, and is multiplied by the concentration gradient $\frac{dc}{dx}$ where c is the solute and x is distance (Eq 2.2). Furthermore, J may also be obtained by M over the diffusive area A_p of the DGT window by deployment time t (Eq 2.3), which is explained by Davison (Davison 2016). Thus $cDGT$ (Eq. 2.4) or the interpreted DGT concentration may be calculated based on the previous equations and Δg which is the total thickness of the material diffusive layer (Fig 2.4). $cDGT$ has been shown to predict that the measured mass of solutes increase linearly with time, and has been has been verified with respect to Fe and Al under environmentally stable conditions (Panther *et al.* 2012). $cDGT$ is considered an interpreted measurement, because environmental conditions may change, and chemical speciation may influence the accumulation of solutes in the binding resin. Here, we have utilised a well-tested method (Zhang & Davison 1995), for the capture of trace metals using the Chelex-100 resin binding gel in order to capture labile Al and Fe fractions within the water column.

$$M = \frac{c_e(V^{bl}+V_e)}{f_e} \quad \text{(Eq. 2.1)}$$

$$J = D^{mdl}\frac{dc}{dx} \quad \text{(Eq. 2.2)}$$

$$J = \frac{M}{A_p t} \quad \text{(Eq. 2.3)}$$

$$cDGT = \frac{M\Delta g}{D^{mdl} A_p t} \quad \text{(Eq. 2.4)}$$

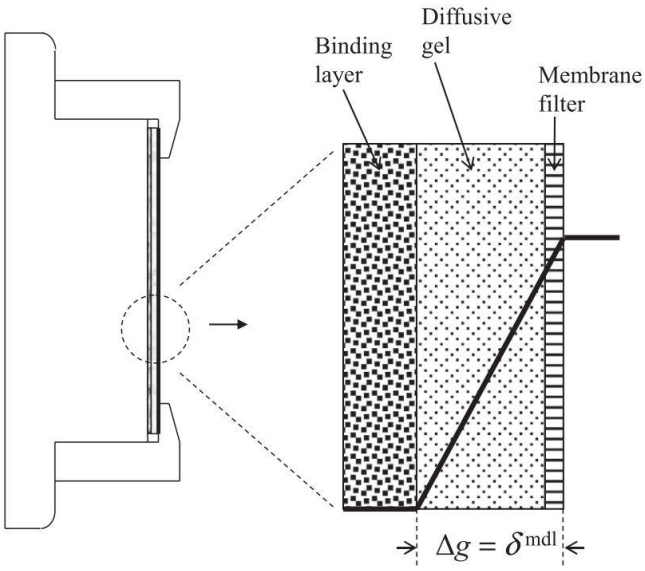

Figure 2.4. Schematic of diffusive gradient in thin films (DGT) probe. The right-hand shows a close up view of the thin film construction. The solid line is an example of a concentration profile across the thin film. Figure taken from Davison (2016).

Sediment Cores

Sediment cores were collected by the Lake Ecosystem Research New Zealand (LERNZ) research group from the University of Waikato on March 2, 2016 using a Swedish gravity corer (Pylonex HTH 70 mm). Plexiglas core barrels had dimensions of 60 x 600 mm and captured between 10-20 cm of sediments along with ~20 cm of the overlying water. A gas-tight fitting was installed over the core barrels for transport and, cores were kept upright and stored in a refrigerator at <6 ^{o}C.

2.2.2 Analytical Methods

Potential of Hydrogen (pH)

pH was measured in dissolved water samples on a Eutech 700 pH meter at 25 ^{o}C (APHA-4500-H+, 2005).

Total Alkalinity (TA)

Bicarbonate alkalinity was analysed using a Mettler-Toledo (Columbus, OH, USA) auto-titrator system, using 0.1M HCl and titrated against pH to the CO_2 equivalence point pH 4. The auto-titrator was calibrated using a 3-point pH calibration (buffers 4,7,9). Alkalinity was then quantified using the Gran method (Gran 1952, 1988).

Ion Chromatography (IC)

Major inorganic anions (Cl^-, SO_4^{2-}) were resolved using a Dionex ICS-2000 Ion Chromatograph fitted with a Dionex IonPac AS18-4mm hydroxide-selective anion-exchange column (Thermo Scientific, Waltham, MA, USA), (APHA-4110, 2005). A seven-anion multi-standard solution (Thermo Fisher) was run using a 25 mM KOH isocratic method with electrolytic ion suppression at 2700 psi pressure. Samples (5 ml) were run in duplicate within 24 h of collection using the same method as described for the standards.

Inductively Coupled Plasma Mass Spectrometry (ICP-MS): Water samples

ICP-MS was undertaken for the analysis of major cations and trace elements due to its high analytical resolution (generally 1 ppb) (APHA-3125, 2005). ICP-MS samples were filtered (10 ml) into 15 ml Falcon tubes using 0.45 µm filters (see Sampling Protocol). Samples were immediately acidified with 2 % concentrated high-purity HNO_3 by volume upon return to the laboratory and analysed on a Perkin Elmer (Waltham, MA, USA) quadrupole ICPMS calibrated with Merck multi-element QC (Merck KGaE, Darmstadt, Germany) and NRC-SLRS-6 Ottawa River water standards (National Research Council, Ottawa, ON, Canada). Procedural blanks consisting of ultra-pure deionised water resulted in values below detection limits (1 ppb). Total dissolved phosphorus (TDP) was compared with FIA-DRP values and often showed good correlation between samples as per Hartland *et al.* (2015a), thus TDP and DRP were considered interchangeable. The mean concentrations of elements in procedural blanks were reported as negligible and are included in the appendix.

Inductively Coupled Plasma Mass Spectrometry (ICP-MS): Sediment Digestions

Sediment digestions were performed by the LERNZ group at Waikato University. Core sediments were extruded at 1 cm increments to a depth of 4 cm and then at 2 cm increments to a maximum of 20 cm total depth. Sediments were dried at 50 ^{o}C for 1 week, ground with mortar and pestle, and ~0.2 g was weighed and allocated to a clean 50 ml falcon tube for each extrusion increment. A reverse aqua regia (1HNO_3:0.33HCl) solution was added and left overnight in a digestion block. A 1-h digestion at 50 ^{o}C was undertaken (Martin *et al.* 1994). Upon digestion completion 50 ml of deionised water was pipetted into each sample and centrifuged for 10 minutes at 4000 rpm. A 10-ml aliquot of supernatant was extracted from each sample into a 15 ml Falcon tube and analysed on a Perkin Elmer (Waltham, MA, USA) quadrupole ICPMS calibrated with Merck multi-element QC (Merck KGaE, Darmstadt, Germany) and NRC-SLRS-5 Ottawa River water standards (National Research Council, Ottawa, ON, Canada). Procedural blanks consisting of ultrapure deionised water resulted in values below detection limits (1 ppb).

Nutrient Analysis: Spectrophotometric Flow Injection (FIA)

Spectrophotometric flow injection methods were undertaken for dissolved nutrients DIN: nitrate (NO_3^-), (cadmium reduction), nitrite (NO_2^-), ammonium (NH_4^+), and dissolved reactive phosphorus (DRP), using method APHA-4500 (APHA-4500, 2005). Samples were analysed on a Lachat QuickChem Flow Injection Analyser (FIA 8000 Series, Zellweger Analytics, Inc.). Total N (TN) and Total P (TP) were detected simulateously using the APHA-4500-P J method (APHA-4500-P, 2005), after undertaking an manual alkaline persulphate digestion. A WaterCheck Round WCP19 (IANZ, Auckland, New Zealand) was used as an internal standard. The limits of detection were 0.001 mg N L^{-1} for NO_2^- and NO_3, 0.002 mg N L^{-1} for NH_4^+, and 0.001 mg P L^{-1} for DRP.

2.3 Geochemical Modelling

Thermodynamic equilibrium geochemical modelling was undertaken to ascertain the spatial distribution and changes in hydro-geochemical speciation across the Waitangi Spring/Te Wairoa Bay interface. Furthermore, mineral saturation indices were calculated based on the over/under-saturation of primary Al and Fe minerals with respect to P binding.

The freely available PHREEQC software (version for Notepad ++ 3.3) from the United States Geological Survey (USGS) was used for all modelling (Parkhurst & Appelo 2013). PHREEQC is a law of mass action based modelling package, in which inputs of temperature, pressure, and total elemental concentrations (master species) are used to calculate aqueous chemical species and mineral phase concentrations in molar units. The model is based on thermodynamic equilibrium (logK) databases for hydro-geochemical speciation and mineral saturation constants. Several thermodynamic databases are available for use with PHREEQC; however, for this research the WATEQ4f.dat database was used as it included the largest library of Al species available. A brief description of the relevant model concepts is given below:

Chemical Equilibrium:

If we consider a chemical reaction where A + B are the reactants and C + D are the products and a, b, c, d represent the stoichiometric coefficients then

$$aA + bB = cC + dD. \quad \text{(Eq. 2.5)}$$

PHREEQC calculations assume local equilibrium conditions and are based on the Law of Mass Action (LMA) (Eq. 2.6) where K the temperature dependent equilibrium constant is equal to the quotient of the products over reactants where curly brackets denote activities. The equilibrium constant may also be expressed as logK or pK = -logK, where

$$K = \frac{\{C\}c\{D\}d}{\{A\}a\{B\}b}. \quad \text{(Eq. 2.6)}$$

In order for the PHREEQC model to calculate equilibrium conditions, it is necessary to have both the model framework (LMA) algorithm (e.g. PHREEQC) and a thermodynamic database of log K's (e.g WATEQ4f) for all species reactions. For each species in a thermodynamic database both a stoichiometric reaction formula and a temperature dependent logK value are required for example:

$Al^{+3} + H2O = AlOH^{+2} + H+$ logK=-4.97 (25 ^{o}C) (Eq. 2.7)

$AlOH^{+2} + H+ = Al^{+3} + H2O$ -logK=4.97 (25 ^{o}C). (Eq. 2.8)

Therefore Eq. 2.7 corresponds to the first dissociation step of Al. As many of the reactions in natural waters are reversible the thermodynamic database can also represent the opposite reaction (Eq. 2.8) and is represented by the -logK. Variation in temperatures are compensated for within the PHREEQC model based on Van't Hoff's equation.

Mineral Saturation:

Mineral saturation indices are based on LMA dependent precipitation/dissolution reactions. For example, where AaBb may precipitate or dissolve based on the equation below (Eq. 2.9) and a thermodynamic solubility product K_{sp}, then

AaBb = aA+bB, (Eq. 2.9)

where the LMA defines the K_{sp} as

$$Ksp = \frac{\{A\}a\{B\}b}{\{AaBb\}} = \{A\}a\{B\}b \quad \text{(Eq. 2.10)}$$

and

solid phase $\{A\}a\{B\}b = 1.$ (Eq. 2.11)

The K_{sp} represents whether a mineral is soluble or insoluble at a given chemical equilibrium (e.g. $K_{sp} \leq 1$ is insoluble, and $K_{sp} \geq 1$ is soluble). Furthermore, an ion activation product (IAP) based on the actual activities in

solution is calculated dependent on the whether the solution is actually in equilibrium:

$$IAP = \{A\}a\ actual\{B\}b\ actual. \quad \text{(Eq. 2.12)}$$

This IAP is used to calculated the Saturation Index (SI) based on the ratio of the Ksp:IAP as

$$SI = \log_{10} (IAP / K_{sp}). \quad \text{(Eq. 2.13)}$$

The SI is used to determine if the solution is therefore saturated, under-saturated, or supersaturated with respect to a mineral from

SI = 0	IAP = K_{sp}	saturated (in equilibrium)	(Eq. 2.14)
SI < 0	IAP < K_{sp}	undersaturated	
SI > 0	IAP > K_{sp}	Supersaturated.	

Thermodynamic equilibrium in many hydro chemical reactions are reversible based on solution composition and thermodynamics. PHREEQC has been used for numerous hydrogeochemical purposes including use in lakes (Oelßner *et al.* 2003; Andersen *et al.* 2011) and with respect to P and mineral saturation indices (Berg *et al.* 2004; Das *et al.* 2009).

The limitations of PHREEQC are primarily that the model assumes that reactions culminate in equilibrium conditions. Therefore, chemical speciation and mineral stability are predictions based on the thermodynamics within the system and a function of the thermodynamic databases used. The PHREEQC databases also do not account for reaction kinetics and thus depending on the system energetics, differences in mineral stability/dissolution may be misrepresented.

CHAPTER THREE

GEOCHEMICAL CHARACTERISATION OF THE ALUM-DOSED WAITANGI SPRINGS GEOTHERMAL PLUME, LAKE ROTOEHU: IMPLICATIONS FOR ALUMINIUM, IRON, AND PHOSPHORUS BEHAVIOUR AND FATE

3.1 Introduction

Eutrophication science has been a focal point in aquatic research for over a century. The increased loading of nutrients such as N and P to natural water bodies has reduced water quality worldwide as the over-enrichment of these nutrients leads to eutrophication, increased algal blooms, and loss of ecosystem function (Scheffer *et al.* 2001). Furthermore, anthropogenic alterations to vital biogeochemical cycles (N and P) are fundamentally altering the rates at which changes in ecosystems occur (Vitousek *et al.* 1997; Smith *et al.* 2006). Natural water resource management and remediation, due to anthropogenic reliance on water quality for energy and food sustainability, is a costly undertaking, yet cost-benefit analyses indicate that such actions are economically favourable (Pretty *et al.* 2003; Hutton & Haller 2004; Dodds *et al.* 2009). Several decades of limnological research has identified that with reduced loading of TP to freshwater ecosystems, both algal productivity and accompanying water quality can be controlled (Vollenweider 1968; Schindler 1977). This understanding has led to decreases in point source inputs of P to aquatic systems and resulted in improved water quality in many cases (Jeppesen *et al.* 2005; Smith & Schindler 2009). However, aquatic ecosystems span a broad range of complexities and not all degraded waters respond to remediation strategies at the same rates or in the same manner (Hamilton *et al.* 2016; Huser *et al.* 2016b). Additionally, with increasing climatic uncertainty moving into the future, implementing water management schemes, and remediating degraded aquatic systems, will likely be a common scenario moving into the future (Trolle *et al.* 2011; Jarvie *et al.* 2013).

Lakes represent a primary source of surface fresh water, and provide a diverse range of ecosystems across climatic gradients. While attempts to

restore degraded lake ecosystems through nutrient reductions have resulted in improvement in many cases (Jeppesen *et al.* 2007), spatiotemporal heterogeneity within lake ecosystems represents a fundamental challenge when concerning nutrient cycling and lake restoration (James 2011; Mackay *et al.* 2011b; Abell & Hamilton 2015). More specifically within lakes, ecosystem processes are influenced by both physical and biogeochemical variability (Kratz *et al.* 2005). Nutrient transport pathways (P and N) to lakes consist of external atmospheric and terrestrial catchment processes as well as internal cycling mechanisms. Transport and accumulation of nutrients to and within lakes is affected by a plethora of ecosystem processes that fluctuate both spatially and temporally and at multiple length scales (Wetzel 2001).

Physical processes in lakes are a function of lake morphometry, water residence time, inflows/outflows (surface, groundwater), as well as a host of atmospheric processes and climatic conditions such as wind speed and direction, gas exchange across interfaces, temperature, and precipitation (Imberger & Patterson 1989). Furthermore, physical lake conditions including light availability, water temperature, water body stratification, and water transport processes including, particle settling and resuspension, heavily influence the rates and magnitudes of numerous macro and trace element biogeochemical cycles (e.g. O, Si, P, N, Mn, Fe, S, H, C, Cu, Mo, Al and others) (Davison 1993; Maberly 1996; Tipping *et al.* 2002; Nimick *et al.* 2011). Conversely, these cycles may affect lake physical conditions, through nutrient availability and primary productivity, light attenuation due to phytoplankton self-shading or mineral precipitation (Stumm & Morgan 1996; Warren & Haack 2001). Also, many elemental cycles often involve multiple pathways and feedback mechanisms, and many chemical elements display coupled cycling (e.g. C-O, Fe-S) behaviour over a variety of temporal scales (hours, days, seasons, years) (Lohse *et al.* 2009; Aufdenkampe *et al.* 2011; Couture *et al.* 2016a). Elemental speciation and mineral saturation, which are governed primarily by acid-base equilibria and redox transformations, also play pivotal roles in the phase transformation and subsequent bioavailability of many elements within the environment. Therefore, the distributions and

magnitudes of these processes can exert a significant impact on lake water quality (Schlesinger *et al.* 2011).

Transition zones between stream outlets and lakes are often the sites of steep gradients in physicochemical conditions and elemental concentrations within lakes (Izydorczyk *et al.* 2008; Mackay *et al.* 2011a; Abell & Hamilton 2015). Streams act as conduits which disperse high loads of dissolved and particulate matter to lake ecosystems. As such, streams are a major physical linkage between terrestrial and aquatic systems (Lohse *et al.* 2009; Marion *et al.* 2014). The external nutrient loads delivered to lake ecosystems by streams often contribute to a large fraction of the nutrients required to bolster primary production within pelagic lake waters (Pacini & Gachter 1999; Peryer-Fursdon *et al.* 2014). Furthermore, both physical and biogeochemical conditions across stream-lake transition zones may change rapidly due to environmental forcing mechanisms (Rueda & MacIntyre 2009; Kalinowska & Rowiński 2015). Stream inflows in lakes may be either buoyant or plunging dependent on the water temperature and density differential between the stream outflow and the receiving lake body (Na & Park 2006; Marti *et al.* 2011). Additionally, these physical characteristics may affect the mixing behaviour of these features, dependent on the outlet flow speed, orientation, and nearshore bathymetry (Fischer *et al.* 1979). Flow can also interact with aquatic vegetation: emergent and submerged aquatic vegetation (SAV) can reduce flow (Madsen *et al.* 2001; Nepf 2012a), enhance sediment deposition (Hamilton & Mitchell 1996; Jeppesen *et al.* 1997), and alter biogeochemical processes within littoral environments (Maberly 1996; Xing & Liu 2011; Hartland *et al.* 2015b).

In New Zealand, geothermal streams can deliver high nutrient loads to lakes. Works of Timperley & Huser (1996) and Hoellein *et al.* (2012) have shown that both P and NH_4^+ are often saturated in the dissolved phase within geothermal streams, which may influence the balance between N and P limitation within specific lakes (Scheffer *et al.* 1993, 2001; Lewis & Wurtsbaugh 2008; Conley *et al.* 2009). More recent work has demonstrated that many freshwater bodies may show P, N+P, or N limitation, often requiring

the management of both macronutrients in order to improve water quality (Abell *et al.* 2010; Lewis *et al.* 2011; Søndergaard *et al.* 2017).

The response of lakes to remediation is variable due to the complex nature of ecosystem processes. Lake recovery can be inhibited by external nutrient loading as well as the internal cycling of nutrients (primarily P) between the sediment and the water column (Søndergaard *et al.* 2003; Spears *et al.* 2014). Therefore, effective management of such complex systems often requires an integrated case-by-case approach (Spears *et al.* 2015; Hamilton *et al.* 2016). In Lake Rotoehu, one approach which has been taken is the in-stream stripping of P.

Over the last fifty years, the use of lake geo-engineering methods such as P-inactivation has been adopted in some circumstances to speed up lake recovery. These methods were developed primarily for wastewater treatment and use P adsorbent metal-salts either applied to sediments in order to occlude P, or applied to the water, generally at high concentration point source inflows (Cooke *et al.* 2005). Adsorption agents are added to the water body under the appropriate conditions, these agents hydrolyse, and through ligand exchange adsorb DRP (Kumar *et al.* 2014). Trivalent metal salts such as alum ($KAl(SO_4)_2$), have been the most widely used agents for P locking, as well as the use of ferric hydroxides and chlorides. More recently, other P adsorbent materials have become available including aluminosilicate-modified zeolites (Gibbs *et al.* 2011a), lanthanum-modified bentonite clays (Phoslock) (Douglas 2002), and lanthanum-aluminium hydroxide composites (LAHC) (Xu *et al.* 2017). Dissolved reactive phosphorus (DRP) in the water column is generally found in the soluble hydrated anionic phosphate ($H_2PO_4^-$, HPO_4^{-2}) form. In general, the approach of P locking agents is to sequester DRP into non-mobile redox insensitive mineral fractions, such as, $Al(OH)_3$ (gibbsite) or Al-polyphosphates which crystalize and lock out P through inner sphere complexation reactions. However, the physical and biogeochemical dynamics found in lake systems are not always conducive for ideal sequestration of DRP (de Vicente *et al.* 2008b; Egemose *et al.* 2010; Reitzel *et al.* 2013). Alum floc formation and binding capacity are heavily reliant on the overriding hydro-

geochemical conditions including transport and resuspension, floc age, pH, ionic strength, alkalinity, and organic matter within the water body (de Vicente *et al.* 2008a; Egemose *et al.* 2011).

Elemental speciation is dependent on numerous biogeochemical variables. DRP availability in the aqueous environment is often limited by inorganic and organic particle reactions, incorporation into minerals via solid-solution phase transformation, and through biological uptake. As a biologically limiting nutrient in freshwater aquatic ecosystems, DRP can exert control on both primary production through assimilation, and may select for specific primary producers (e.g. phytoplankton species, macrophytes). Moreover, secondary production may also be limited by P limitation, through control of primary production (quality and quantity) as well as the availability of organic P provided through cycling from phytoplankton and prokaryotes (Vanni 2002). Inorganic control of DRP by major cations in solution Ca^{2+}, Fe^{3+}, Mg^{2+}, $Al^{3+}$and Mn^{2+} under circumneutral pH (6-8.5) is a primary natural means of limiting DRP in freshwater ecosystems. However, the pH and/or REDOX dependent nature of Fe and Al may lead to their increased solubility dependent on environmental conditions.

Here, we seek to characterise the geochemical dynamics in the transition zone between the alum-dosed geothermal Waitangi Springs and Lake Rotoehu. In particular, we examine if pH changes within the bay are responsible for reduced efficacy of in-stream P-stripping remediation approach. We use an ensemble of in-situ and spatial environmental monitoring techniques, coupled with geochemical modelling.

3.2 Methods

3.2.1 Study Site: Te Wairoa Bay

Te Wairoa Bay (-38.032161°, 176.544915°) is a small (0.42 km^2) shallow bay (mean depth of 1.96 m), located in the south-eastern corner of Lake Rotoehu in the Bay of Plenty region of New Zealand (Figure 3.1 a,b). The geographical position of the bay is a somewhat sheltered position dependent

on the direction of the wind. The catchment area is approximately 1.7 km^2 (estimated from topography using the Google Earth polygon tool), although the hydrological inputs may extend much further due to complex groundwater inputs. The catchment is composed of pastoral land, exotic forestry, native bush, and wetlands. Within the wetlands, both the geothermal Waitangi Springs and the Manawahe Road spring flow from a shallow aquifer and converge within a dense wetland, emerging via small channels into a sub-basin before entering Te Wairoa Bay. Te Wairoa Bay is heavily influenced by the geothermal stream input of the Waitangi Springs as the combined base flow (~345 L s^{-1}) is the largest contribution of surface water input to Lake Rotoehu and the unique physicochemical properties of the geothermal input are therefore continuously present (BoPRC, Sumeran unpublished data). Additionally, due to the volcanic soils of the area and through geothermal dissolution, biologically dissolved limiting nutrients (DRP and DIN) are continuously elevated within the Waitangi Spring (BOPRC data). Furthermore, the shallow bay is often inundated with the extremely dense and invasive floating macrophyte *C. demersum*, which likely plays a large role in the physical and biogeochemical dynamics of the stream-lake transition zone.

3.2.2 Sampling and Monitoring

The experiment took place over a period of nine days in the month of March 2017, near the end of the austral summer. High frequency temperature loggers and real-time lake monitoring data spanned the duration (9 days) of the experiment. The experiment coincided with two large rainfall events, and therefore the measurements reflect a low stream flow/low lake level to high stream flow/high lake level transition. Two days of intense sampling took place at the beginning (07/03/17) and final day of the (16/07/17) of the experiment. For these days, numerous physiochemical and biogeochemical variables were measured over the spatial extent of the bay at differing intervals. These measurements are described in detail below.

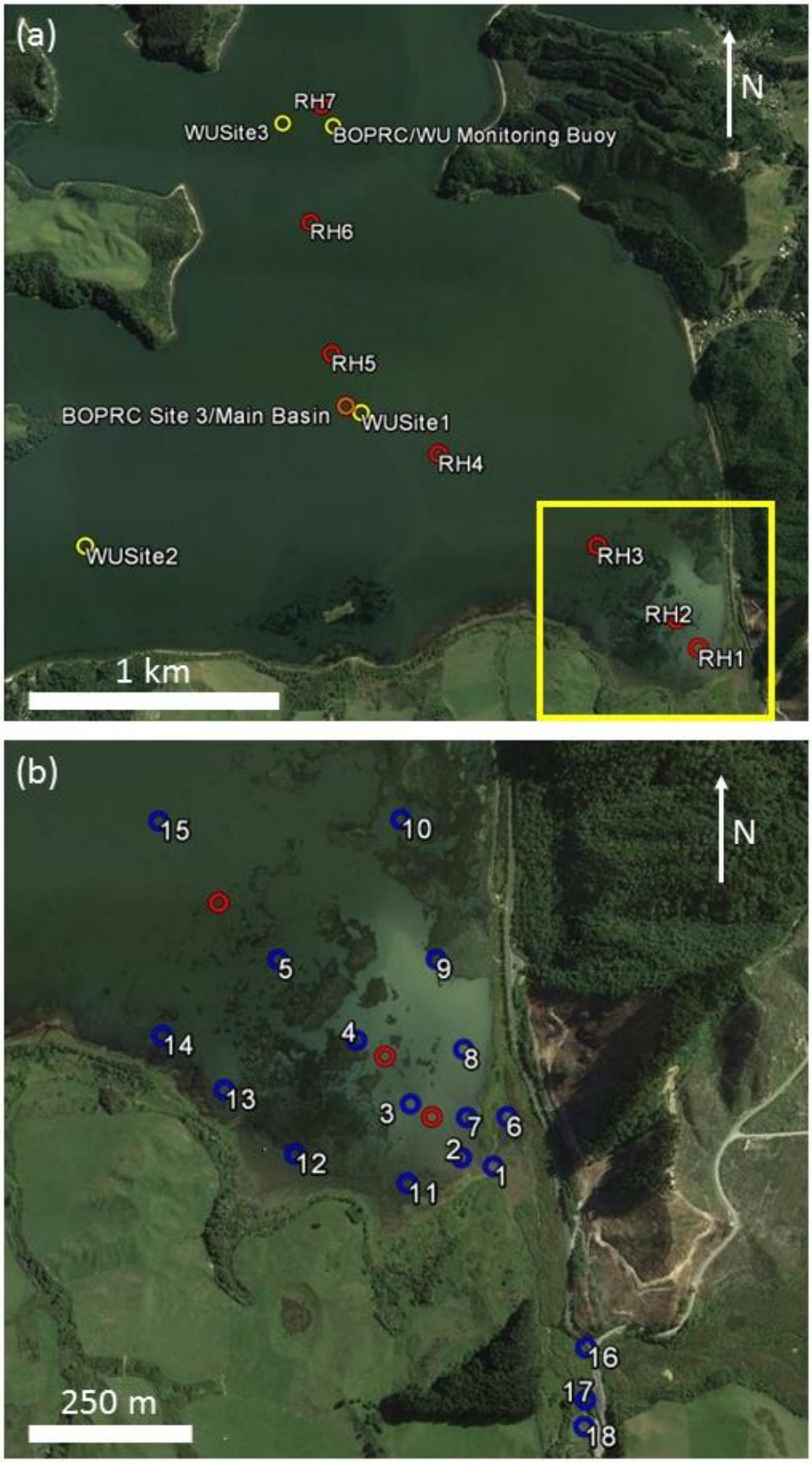

Figure 3.1. (a) BOPRC and Waikato University sampling sites in Lake Rotoehu's main basin (orange and yellow circles), and lake sediment core sites (red circles RH1-7) with yellow inset of Te Wairoa Bay location. (b) Te Wairoa Bay and the Waitangi Springs sampling locations. Water samples were taken at sites 1-18 (blue circles), DGTs were also deployed at sites 1-5. Sediment core locations (RH1-RH3) are represented by red circles.

Physicochemical Transects

Physicochemical transects of Te Wairoa Bay were carried out on 07/03/17 and 16/03/17 during daytime hours (09:00-16:00) using a Garmin E-Trex GPS (Garmin International, Olathe, KS, USA) which was time synched to a multiparameter YSI Sonde-600QS/650 MDS Display (Yellow Springs, OH, USA) mounted on a small kayak (Figure 3.2). Measured parameters were pH, DO sat (%), SpCond (µS cm^{-1}), depth (m), and temperature (^{o}C). All sensors were calibrated following the manufacturers specifications. The DO sensor was calibrated on each sampling day and adjusted for barometric pressure (MetService Rotorua) and site elevation. pH was calibrated using a three-buffer (4,7,9) calibration and checked before and after sampling at the field site. Logging frequency was set at 2-s until internal Sonde memory was depleted. Further monitoring was logged on the 650 MDS at 30-s second intervals until memory was full. Transects followed the circumference of the bay as well as several lateral crossings when possible (see results section). Large dense macrophyte beds (*C. demersum*) required that kayak transects occurred primarily in channels between or along the perimeter of macrophyte rafts. However, in order to capture the heterogeneity in conditions, transects did intersect the main central macrophyte bed located between sites 3 and 4 (Figure 3.1). Slow kayak velocities were maintained to allow sensors to equilibrate and to reduce the effects of flow on the sensors.

Figure 3.2. (a) Sonde profiler mounted on kayak in white pipe. (b) Instrument in-situ during sampling.

Temperature Moorings

Temperature moorings were installed across a central transect from the Waitangi Springs mouth into Te Wairoa Bay. Onset Hobo Tidbit temperature dataloggers were installed on the moorings at 20cm below the surface and 20 cm above the bottom at sites 1-5 (see Figure 3.1). Temperature loggers recorded every 30 s continuously from 07/03/17 to 16/03/17.

DGT Deployment

Chelex-100 DGTs were deployed on 15/03/17 for 24hrs, and attached to temperature mooring lines at mid-depth of the water column. DGTs were housed in pairs inside 1 litre BML specimen bottles which had been drilled out to allow high permeability. Each sample bottle, with paired DGTs also contained an Onset Hobo tidbit temperature logger to allow calculation of diffusion coefficients required for cDGT calculations.

Water Sampling

Sampling took place on two days at the beginning (07/03/17) and the end (16/03/17) of the experiment. Surface water samples were taken sites 1 to 15, in an effort to obtain a broad horizontal representation of the stream-lake transition zone within Te Wairoa Bay. Sampling protocols are given in Chapter 2. Samples were also collected at the Waitangi Springs, above and below the alum dose point, sites 18 and 17, respectively. The cold-water tributary springs at Manawahe Road (site 16), above the mixing point with the Waitangi Springs was sampled only on 16/03/17.

3.2.3 Data Analysis

Physicochemical Monitoring

Physicochemical data from the Sonde was processed by identifying times when the instrument was out of the water (from the pressure signal) and these points were removed. The remaining data obtained by kayak transect were used to generate georeferenced contour plots in MATLAB using the Open

Earth Toolbox (https://publicwiki.deltares.nl/display/OET/OpenEarth), which is a freely available MATLAB toolbox available from Deltares (Delft, Netherlands).

Water Sampling – Geochemical Modelling

Water sampling (ICPMS, IC, alkalinity, and pH) data was compiled in Excel and then imported into MATLAB for analysis and visualisation. Furthermore, element concentration values were compiled in the Notepad++ PHREEQC (version 3.3) and scripts were written to run equilibrium and speciation models for water samples at each site (site 1 to site 18) using the WATEQ4 database. The models provided output molar concentrations, molar speciation concentrations, mineral saturation indices, and equilibrium charge balances.

Sediment Coring Data

Sediment cores taken a year prior to this experiment (March 2, 2016) by the LERNZ group were extruded and digested for total elemental sediment concentrations. ICPMS analysis provided the elemental concentrations for sediment cores. Sediment dry weights were calculated based on sediment weight for extrusion depth increments (Martin *et al.* 1994).

Long Term and Real Time Monitoring Data

Long-term data provide by the BOPRC included water quality (TP, TN, Chl-*a*, Al, pH), high-frequency real time sensor monitoring obtained from the lake buoy (water temperature, DO, phycocyanin, Chl-*a*, wind speed and direction) and Waitangi Springs monitoring station (stage height, rainfall, alum dose rate, and lake level at Te Pohue Bay). The alum dosing times-series underwent a de-spiking routine, which successfully removed most anomalous points. Statistical methods applied to long-term water quality data included regression fits to the data. Dependencies between variables were examined using a linear fit. Time series of variables (TN, TP and Chl-*a*) were fitted using a robust loess local polynomial regression with a span of 50 %. 95 %

confidence intervals were obtained by a bootstrap method (with 2000 samples) using MATLAB scripts modified from Martinez & Martinez (2002).

3.3 Results

3.3.1 Spatial and Temporal Physicochemical conditions

Both the stream-lake transition zone within Te Wairoa Bay and the main body of the lake exhibited significant changes in physicochemical conditions over the course of the experimental period from 07/03/17 to 16/03/17. These changes are described within the following sections.

Environmental Conditions

The late summer hydrologic conditions during 2017 were characterized as a rapid event-driven transitional phase. Several large tropical systems resulted in regional rainfall accumulations during the month of April which were around 250-300 % of normal for the year (BOPRC website). During the experimental period, there were two sizeable precipitation events which delivered 88.5 and 160.5 mm of rainfall over 27 and 48 h, respectively (Figure 3.3a), which resulted in very rapid changes in the Waitangi Springs stage height which increased from 0.35 to 0.38 m (Figure 3.3b). Lake Rotoehu surface elevation level increased 0.2 m in height from 294.5 m to 294.7 m during the span of the nine-day experiment (Figure 3.3c). Conditions from 07/03/17 corresponded to the lowest stream stage height and lake surface elevations throughout 2017 (not shown), while the 16/03/17 sampling is a representation of post-rainfall-event conditions. Furthermore, observations during sampling indicated that the water depth at the Waitangi Springs outlet was <20 cm on 07/03/17, and approximately 40 cm on 16/03/17.

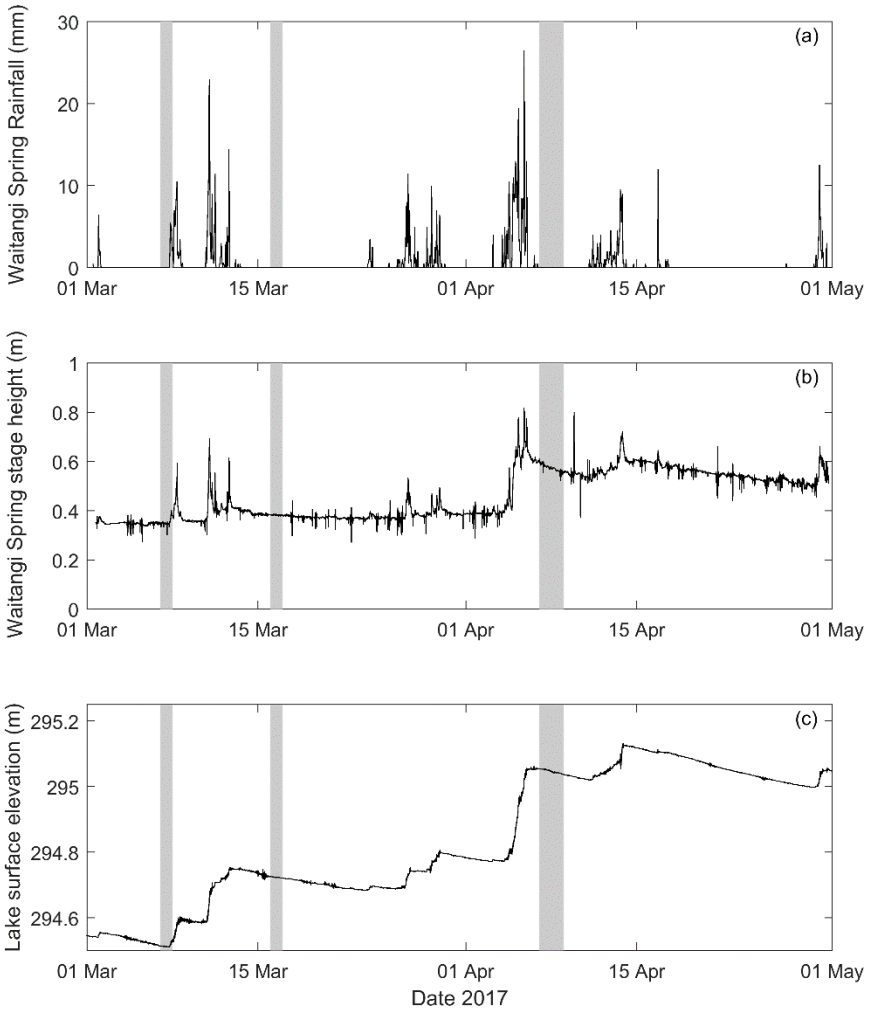

Figure 3.3. Conditions covering the experimental periods 7/03/17 – 16/03/17 (chapter 3) and 07/04/17-08/04/17 (chapter 4). Data is from BOPRC website and provided at 15 min intervals. (a) Rainfall measured at Waitangi Springs. (b) Waitangi Springs stage height. (c) Lake Rotoehu surface elevation. Grey shading indicates times of additional water sampling.

On the water sampling days, winds were relatively light (<6 ms^{-1}) and predominantly from the east. Winds were generally easterly throughout the 12-day deployment, although other directions were recorded over shorter periods (Figure 3.4). The two rain events were also associated with higher wind speeds (up to 14 ms^{-1} on 07/03/17 and around 12 ms^{-1} on 16/03/17, not shown).

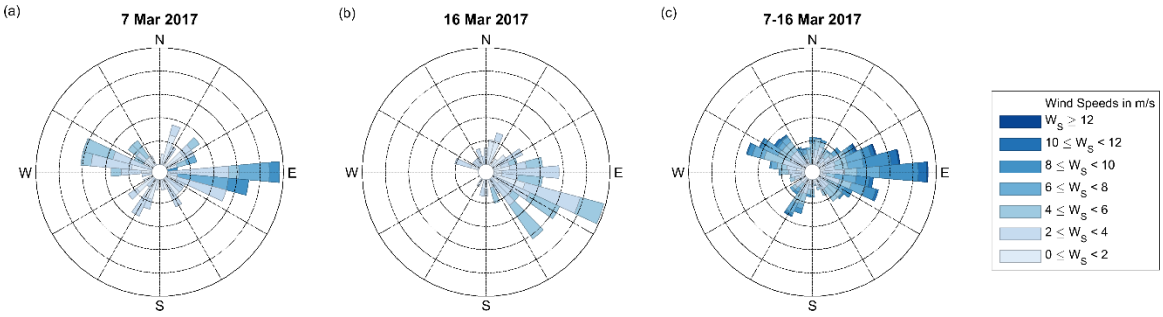

Figure 3.4. Wind conditions during (a,b) the times of water sampling, and (c) over the full experimental period 7/03/17 – 16/03/17. Bar lengths show the frequency of winds from each direction and colours indicate wind speeds.

Water Temperature

The Waitangi geothermal springs plume entering Te Wairoa Bay was characterised with data from temperature moorings at sites 1-5 (Figure 3.1b) within the shallow Te Wairoa Bay (depths<2.5 m), and data along transects covered by kayak-mounted multi-parameter Sonde. Site 1 and site 2 were situated directly within the discharge of the stream outlet and displayed high average temperatures at the surface (~24.3 ^{o}C, Figure 3.5b,c). Site 3 was situated within a large dense submerged macrophyte bed (*C. demersum*), which also displayed warm surface temperatures (mean 21.5^{o}C) and represented a mixing boundary between the area of geothermal influence and the lake (Figure 3.5d). Site 4 and site 5 recorded cooler mean surface temperatures of ~20^{o}C, closer to the general lake conditions (Figure 3.5e,f).

During the large rainfall event between 07/03/17 and 08/03/17, both surface and bottom temperatures at all sites decreased by approximately 5^{o}C (Figure 3.5). Temperatures at sites 1-3 appeared to re-establish to pre-rainfall event temperatures within 2-3 days, indicating the effect of geothermal buffering on the inner bay temperature. Sites more closely associated with lake conditions (sites 4-5) displayed far smaller daily fluctuations in temperature and did not return fully to pre-rainfall event temperatures, indicating the plume influence was diminished at these sites. A second larger rainfall event between 11/03/17 and 13/03/17 was also visible in the water temperature record and further reinforces the segregation of the transition zone.

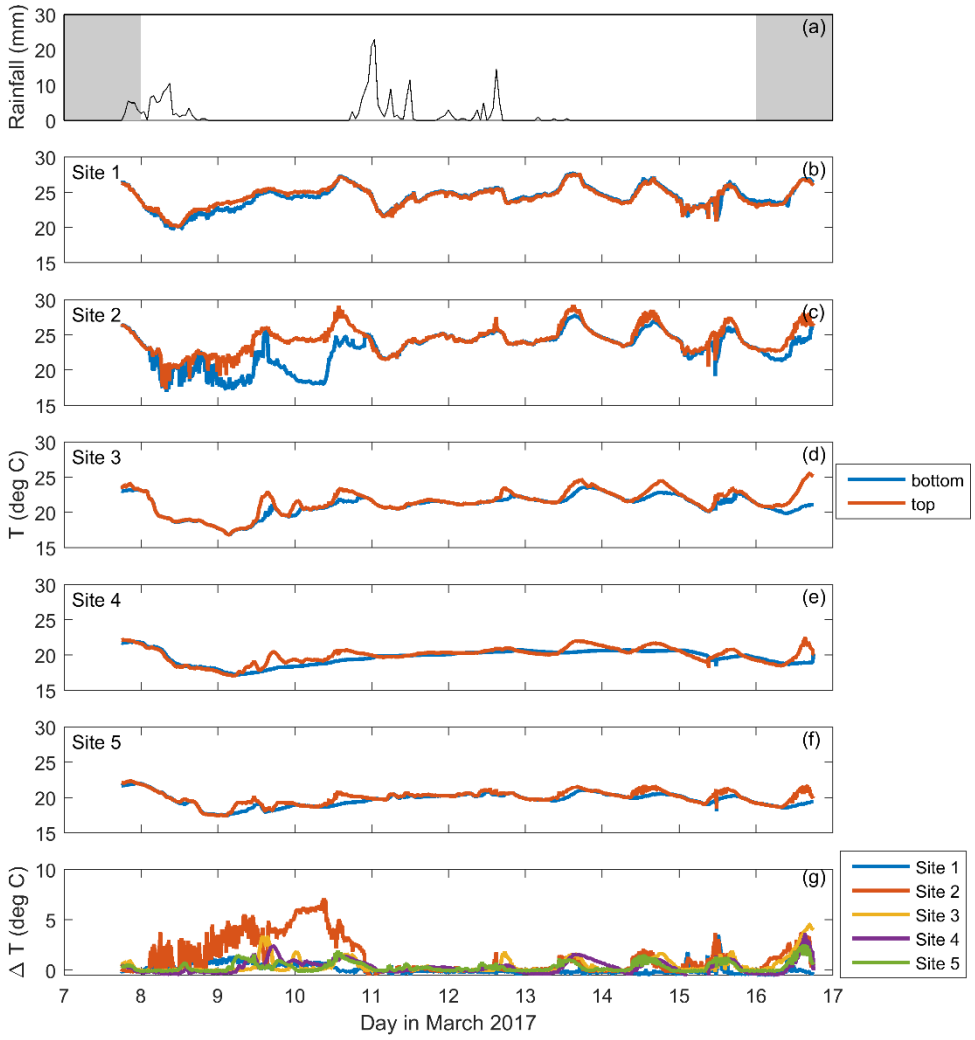

Figure 3.5. (a) Rainfall (mm) over the experimental period (measured hourly). (b-f) Te Wairoa Bay surface temperatures (red) and bottom temperatures (blue) from sites 1 to 5, from the Waitangi Springs outlet into the main southern lake basin. (f) Differences between surface and bottom temperatures from all sites. Measurements were taken every 30 s. Grey shading represents times of water sampling.

Lake water temperature and dissolved oxygen measured at the BOPRC high-frequency data buoy indicated that the water column was thermally stratified on 07/03/17 (Figure 3.6a). Correspondingly, dissolved oxygen concentrations in lake bottom waters were close to zero (Figure 3.6b). The combined effects of precipitation, winds, and inflow at the lake surface during the 07/03/17 rainfall event resulted in lake destratification and rapid mixing of bottom and surface waters by 08/03/17 (Figure 3.6a, first grey bar). This mixing event led to a rapid decrease in surface water temperature of ~3°C. Accompanying this thermal mixing event was a rapid re-oxygenation of

hypolimnetic waters which had been close to zero for approximately twenty days prior to lake overturning (Figure 3.6b).

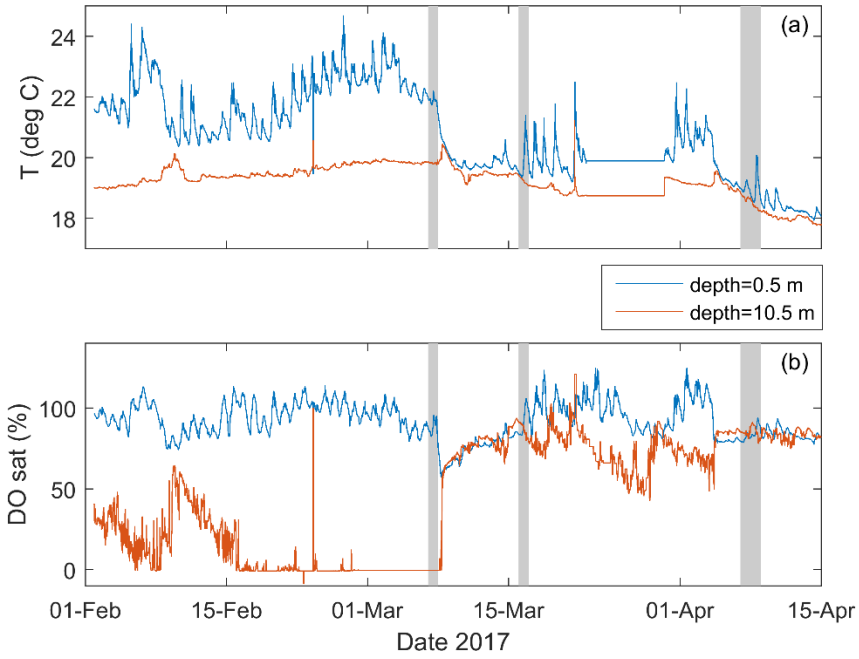

Figure 3.6. Data from the Lake Rotoehu monitoring buoy over the period of 01/02/17-15/04/17. (a) water temperature and (b) dissolved oxygen saturation (%) at the surface (depth=0.5 m, blue line) and bottom (depth=10.5 m, orange line). Measurements were taken every 15 min. Grey shading indicates dates over which additional water sampling occurred (07/03/17, 16/03/17, 07/04/17).

Kayak transects captured sharp horizontal temperature gradients within Te Wairoa Bay surface waters on both monitoring occasions 07/03/17 and 16/03/17, owing to the influence of the relatively warm geothermal Waitangi Springs plume entering Te Wairoa Bay (Figure 3.7). During 07/03/17 with low base flow and low lake level, the spatial footprint of the Waitangi Springs plume (~27 °C) was smaller than on 16/03/17, which had higher base flow and higher lake level. Visible within the interpolations are temperature differentiations (Figure 3.7a) due to *C. demersum* macrophyte beds (Figure 3.8). During increased discharge on 16/03/17 the spreading of the plume appeared to be inhibited by the presence of floating rafts of *C. demersum* around site 3 (region of strong temperature gradients, Figure 3.7b).

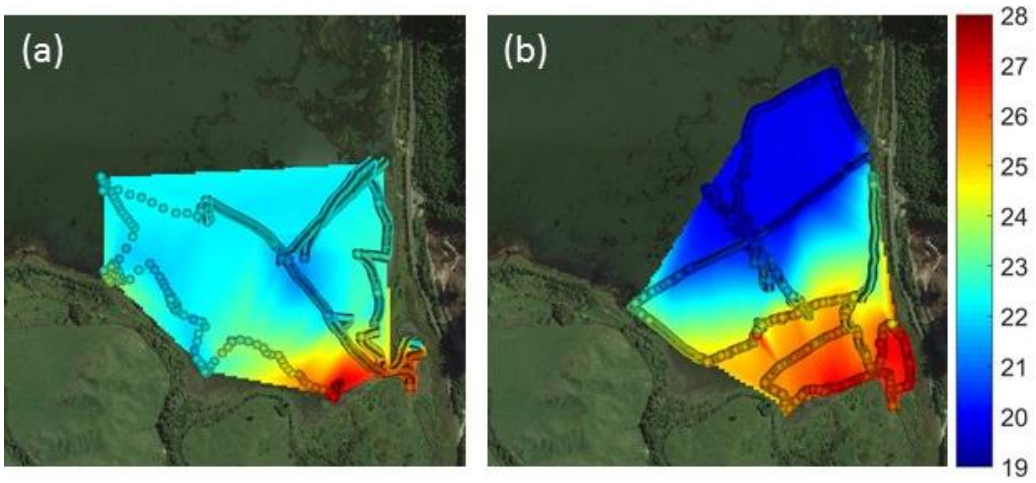

Figure 3.7. Surface temperatures (°C) measured by kayak mounted Sonde from (a) 07/03/17 and (b) 16/03/17. Tracks indicate path travelled with interpolated surface values underlain. The sampling frequency varied between 1/2 and 1/30 Hz (i.e. measurements were taken every 2 or 30 s) and is visible in tracks. The colour bar indicates °C.

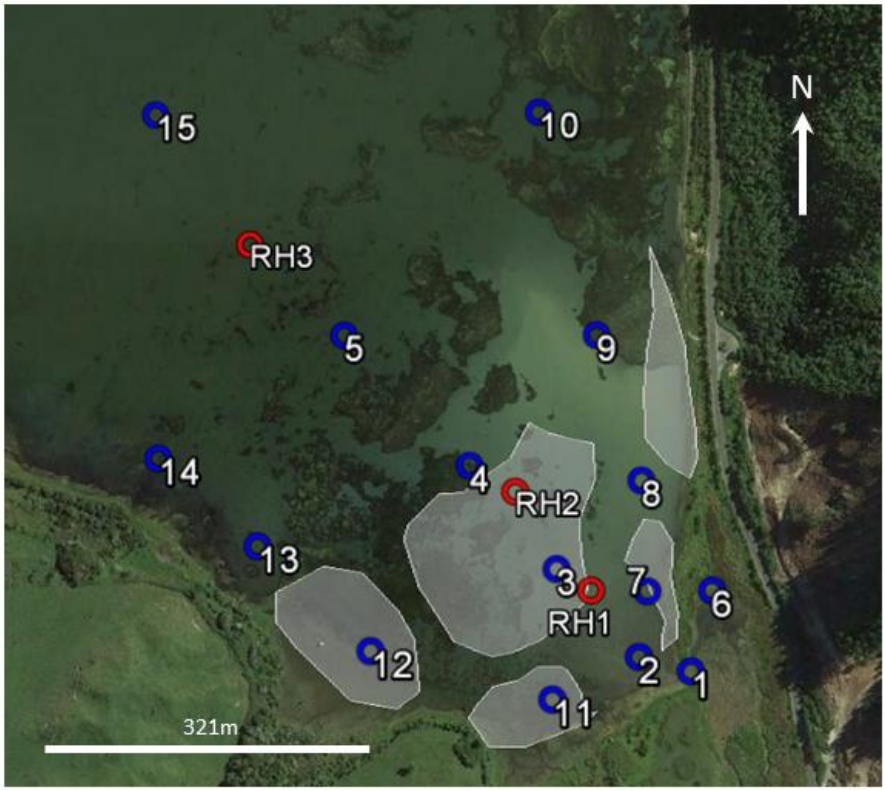

Figure 3.8. Surface reaching macrophyte *C. demersum* distribution patches (grey polygons), estimated based on GPS points during kayak transects in Te Wairoa Bay. Blue circles represent water sample sites, and red circles represent sediment core sites.

Water pH and specific conductance

pH and specific conductance distributions within Te Wairoa Bay were measured and interpolated from kayak transect data. Surface plots indicated

that the pH values from both 07/03/17 and 16/03/17 increased with distance from the Waitangi Springs outlet (Figure 3.9). However, the pH distribution within the bay became increasingly alkaline by 16/03/17 (Table 3.1). This increase in pH, was partly attributed to greater mixing with the higher-pH lake water due to the higher lake level (Figure 3.3c) and stronger stream outflow, but was also likely to be influenced by the increased photosynthesis in dense *C. demersum* beds and algal productivity within the outer portion of the bay. Similar to the temperature signal, there exists a sharp pH gradient between the inner and outer portion of the bay at of the location of the *C. demersum* beds (Figures 3.8, 3.9), which passively block the hydrodynamic flow both into and out of the outer bay.

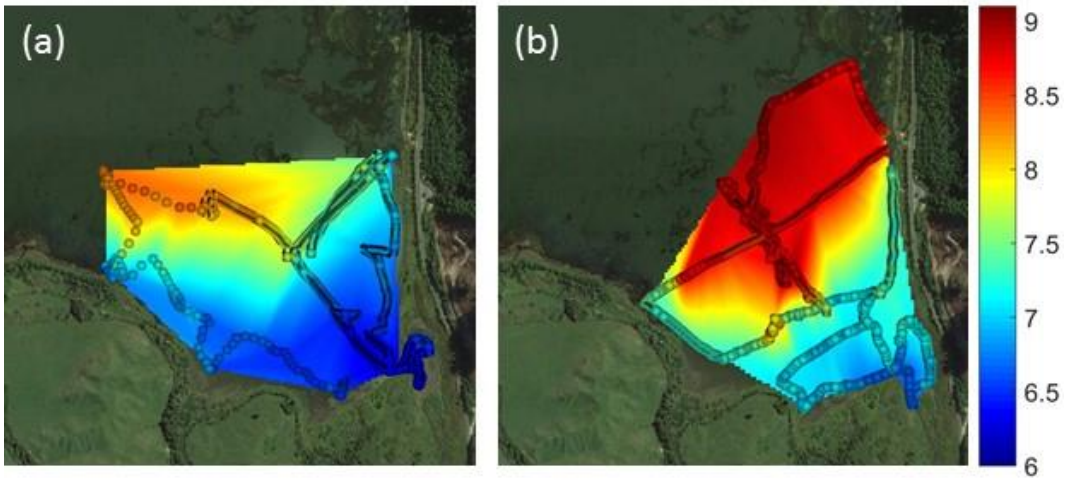

Figure 3.9. Surface pH measured by kayak mounted Sonde from (a) 07/03/17 and (b) 16/03/17. Tracks indicate path travelled with interpolated surface values underlain. Measurements were taken every 2 or 30 s, with the frequency of sampling (1/2 or 1/30 Hz) visible from the tracks. The colour bar shows pH values.

Table 3.1. Range and minimum and maximum values of surface pH from the two sampling dates.

Date	Min pH	Max pH	Range of pH
07/03/17	6.2	8.45	2.25
16/03/17	6.61	9.09	2.48

An increase in cyanobacteria within the lake on the 16/03/17 was captured by the lake monitoring buoy phycocyanin sensor, and confirmed from photos and samples as *Microcystis sp.* taken several days after the onset of the bloom (Figure 3.10). Levels of *Microcystis sp* reached red alert status

with recorded biovolumes of 14.6mm^3 L^{-1} on 20/03/17 (BOPRC data). Unfortunately, during the experimental period, the monitoring buoy pH sensor was not functioning and therefore sampled pH values were unable to be cross-referenced with the buoy.

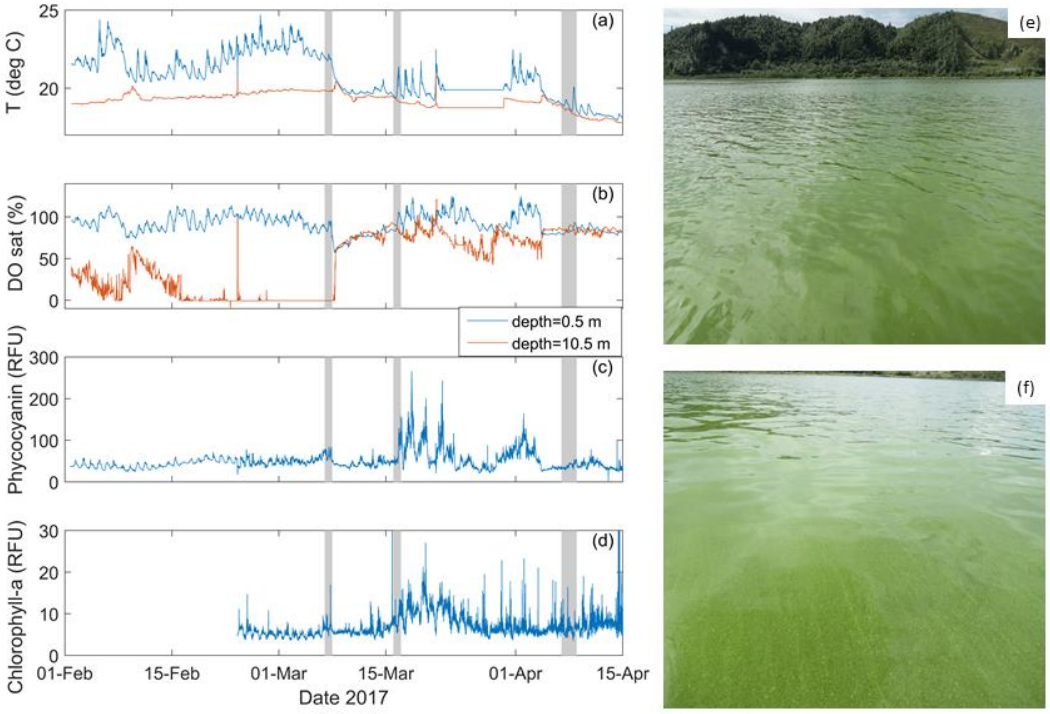

Figure 3.10. Data from the Lake Rotoehu monitoring buoy for the period of 01/02/17-15/04/17. (a) water temperature and (b) dissolved oxygen saturation (%) at the surface (depth=0.5 m, blue line) and bottom (depth=10.5 m, red line). Surface phycocyanin (RFU) (c) and Chl-a (RFU) (d) are also displayed. Photos from 24/03/17 showing *Microcystis sp.* blooms in (e) outer Te Wairoa Bay and (f) central Lake Rotoehu (photos provided by BOPRC). Grey shading indicates dates over which sampling took place (07/03/17, 16/03/17, 07/04/17).

Specific conductivity values showed a decrease in concentration between Waitangi spring outlet (800 µS/cm) and the lake (500 µS/cm) (Figure 3.11). The larger conductivity values are attributed to the increased ionic activities of the geothermal waters (Na^+, Ca^{2+}, K^+, Mg^{2+}, Cl^-, SO_4^{2-}). Again, rainfall events which occurred between sampling campaigns acted to dilute the specific conductivity in the Waitangi spring outlet and the increased discharge resulted in greater mixing of waters within Te Wairoa Bay (Figure 3.11).

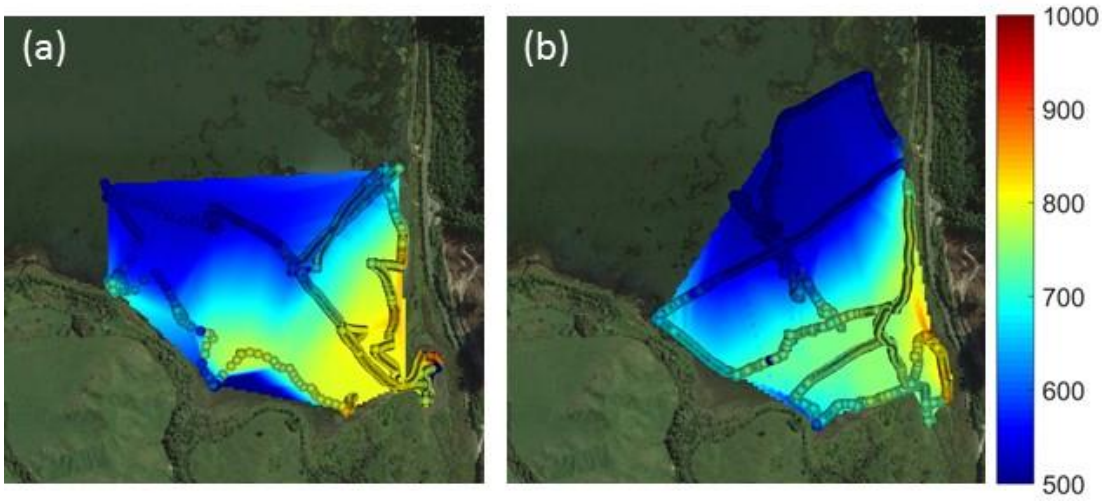

Figure 3.11. Specific conductance (μS/cm) measured by kayak mounted Sonde from (a) 07/03/17 and (b) 16/03/17. Tracks indicate path travelled with interpolated surface values underlain. Measurements were taken every 2 or 30 s, with the frequency of sampling (1/2 or 1/30 Hz) visible from the tracks. The colour bar shows specific conductance in μS/cm.

Dissolved Oxygen

Dissolved oxygen within the Waitangi Springs/ Te Wairoa Bay displayed supersaturated conditions during daytime sampling on both 07/03/17 and 16/03/17 (Figure 3.12). Saturated conditions were particularly elevated on 07/03/17 (150-350% sat), and the areas of high oxygen saturation were correlated with the density and location of the *Ceratophyllum demersum* beds (Fig 3.8). Similarly, on 16/03/17 the DO levels were also elevated (100-250% sat); however, the levels were lower than 07/03/16 possibly due to dilution and the increased volumetric change in the bay. The Sonde sensors were re-checked for calibration after deployment and standard procedures displayed the appropriate oxygen levels (100 % sat). Such high levels of oxygen are highly relevant for the speciation, transformation, and availability of redox sensitive ions within the water column and at the sediment water interface.

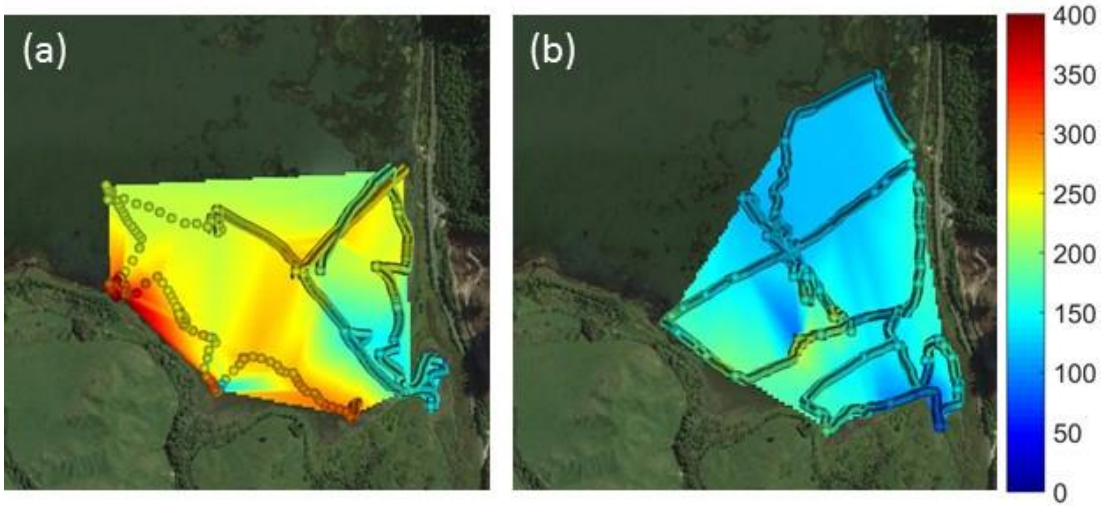

Figure 3.12. Dissolved Oxygen (% Sat) measured by kayak mounted Sonde from (a) 07/03/17 and (b) 16/03/17. Tracks indicate path travelled with interpolated surface values underlain. Measurements were taken every 2 or 30 s, with the frequency of sampling (1/2 or 1/30 Hz) visible from the tracks. The colour bar shows saturation values in %.

3.3.2 Major Ion Concentrations

ICP-MS, IC, alkalinity, and FIA results for major ion concentrations (in mg L^{-1}) and associated charge balance from the 07/03/17 and 16/03/17 sampling campaigns for all sites sampled are included in the appendix tables A1-A2 and A3-A4, respectively. These data or subsets of the data were used in the PHREEQC package for inorganic chemical speciation modelling (Parkhurst & Appelo 2013). Given the significant geothermal influence on the Waitangi spring waters, many major ions present in the bicarbonate-chloride waters (Na^+, Ca^{2+}, K^+, Mg^{2+}, B, Cl^-, Si, SO_4^{2-}) displayed elevated concentrations when compared to both background lake waters and natural freshwater systems in general (background lake waters are identified by higher pH values, Figure 3.13a). The highest concentration levels for reported ions were found at and upstream of the Alum dosing point in the primary geothermal stream input (sites 17 and 18). However, many of these ions displayed a shift in concentration with the onset of the rapid lake level increase (differences between symbols Figure 3.13). These changes are likely to be attributed to pH fluctuations associated with both increased stream discharge from the Waitangi Springs (sites 17,18) and the Manawahe Rd tributary (site 16) (Figure 3.3b), and the enhanced lake water interaction (volumetric increase) with the geothermal plume.

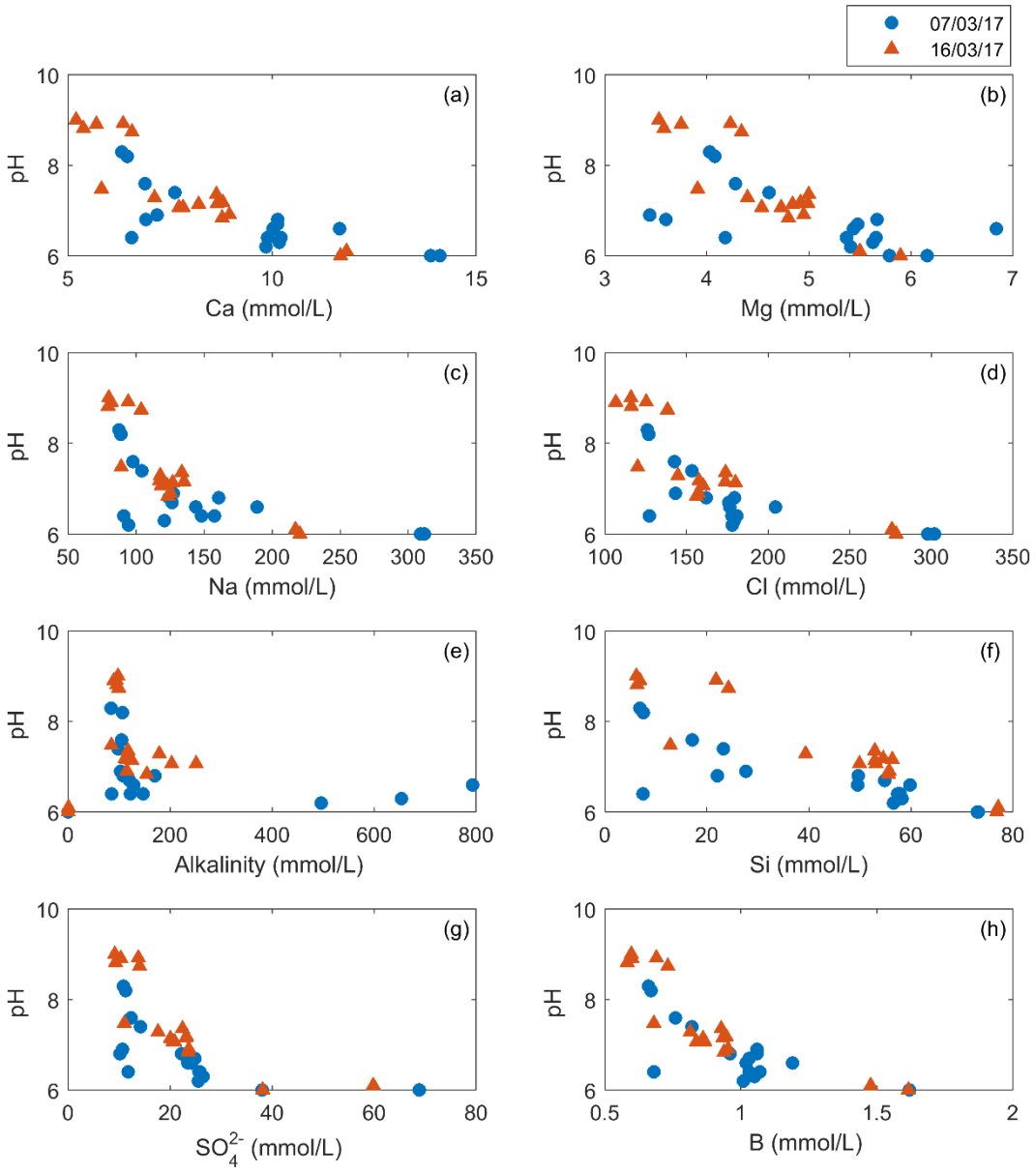

Figure 3.13. Major ion concentrations plotted against pH for all sites, except site 16. This site was excluded as it was not collected on both sampling occasions. Measurements from 07/03/17 (blue circles) and 16/03/16 (orange triangles). Note pH acts as a proxy for distance into the lake as in general, high pH values correspond to a longer distance from the stream outlet.

Aluminium, Iron, and Phosphorus Concentrations

Dissolved Al (Al_{dis}), dissolved Fe (Fe_{dis}), and DRP concentrations all displayed non-conservative behaviour across the stream-lake transition zone in Te Wairoa Bay. The increased pH on 16/03/17 (relative to 07/3/17, noting difference in colour scale) was likely an important factor contributing to the distribution of dissolved Al, Fe, and P within the bay (Figure 3.14a and Figure 3.15a). Fe_{dis} concentrations within the bay were an order of magnitude larger

than Al_{dis} and DRP concentrations on both sampling occasions (Figure 3.14b and Figure 3.15b). Fe_{dis} concentrations appeared to be highest at the stream outlet on both occasions, with decreasing concentrations moving out into the bay (Figure 3.14b and 3.15b). The macrophyte beds in the central portion of the bay appear to be associated with larger values of Al_{dis}, and DRP (Figure 3.13c,d and Figure 3.14c,d). Furthermore, DRP values appeared to be particularly elevated within the outer portion of the bay on the 16/03/17 sampling day in comparison to 07/03/17 (Figure 3.14d and 3.15d). It should be noted that site 6 on 07/03/17 appears as an outlier and skews the range of values, therefore, direct inter-comparison should be undertaken with caution.

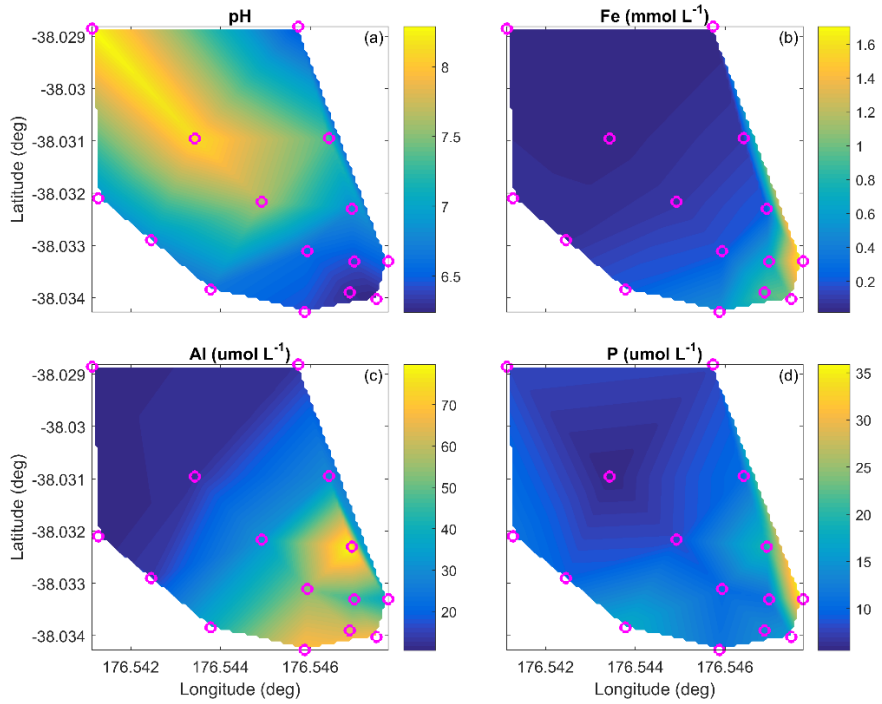

Figure 3.14. Surface water measurements from Te Wairoa Bay sample sites 1 to 15 (pink circles) from 07/03/17. (a) Field pH, (b) dissolved Al, (c) Fe and, (d) P. Concentrations units are shown above each plot. The colour map shows values interpolated between sampling sites. Waitangi springs outlet is located at the bottom right of each surface plot with Lake Rotoehu in the upper left.

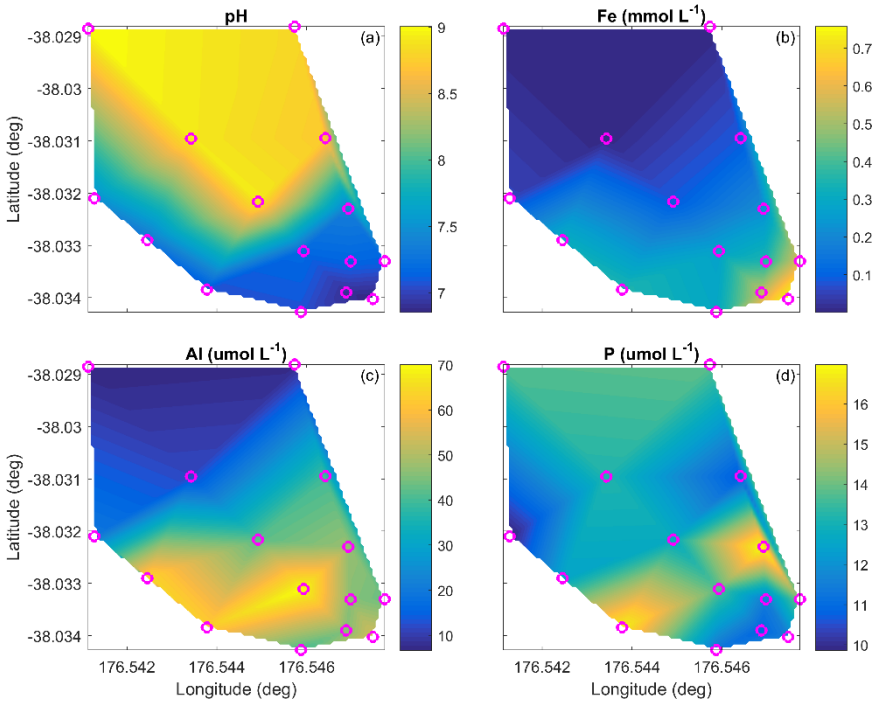

Figure 3.15. Surface water measurements from Te Wairoa Bay sample sites 1 to 15 (pink circles) from 16/03/17. (a) Field pH, (b) dissolved Al, (c) Fe and, (d) P. Concentrations units are shown above each plot. The colour map shows values interpolated between sampling sites. Waitangi springs outlet is located at the bottom right of each surface plot with Lake Rotoehu in the upper left.

3.3.3 Dissolved Aluminium and Iron Speciation

Aluminium, iron, and phosphorus speciation were calculated using geochemical modelling package PHREEQC based on analytically derived concentrations from the water samples.

Aluminium Speciation

Fractional contributions of the major inorganic aluminium hydroxide species and monomeric soluble Al^{3+} were plotted by site and then interpolated to show their spatial distribution within Te Wairoa Bay on both 07/03/17 and 16/03/17 (Figure 3.16 and 3.17). Results from both 07/03/17 and 16/03/17 indicated the greatest concentrations of the dissolved fraction of aluminium were primarily the soluble $Al(OH)_4^-$ (high pH) within the outer portion of the plume and $Al(OH)_2^+$ (low pH) nearest the springs outlet (Figure 3.16 a,d and 3.17 a,d). The dissolved component of the $Al(OH)_{3(aq)}$ species, which is the species likely to contribute to the amorphous $Al(OH)_{3(am)}$ floc (ranging in size between colloidal and particulate) was an order of magnitude lower in

concentration in comparison to $Al(OH)_4^-$ and $Al(OH)_2^+$, and its spatial distribution was primarily focused within the initial exit and inner portion of the bay (Figure 3.16b and 3.17b). It should be noted that the total dissolved $Al(OH)_3$ fraction, which would be inclusive of the $Al(OH)_{3(aq)}$, $Al(OH)_{3(am)}$, and gibbsite fractions was likely to be found in particulate form and may be why $Al(OH)_3$ displayed such low concentrations (i.e. being excluded by filtration at 0.45 μm). Soluble Al^{3+} represented the smallest fraction of the Al_{dis} species and was an order of magnitude lower in concentration. The Al^{3+} distribution was found almost exclusively at the stream outlet. Overall there was a decline in $Al(OH)_3$, $Al(OH)_2^+$, and Al^{3+} concentrations, and an increase in $Al(OH)_4^-$ concentrations between the 07/03/17 and 16/03/17 sampling dates (Figure 3.16 and 3.17).

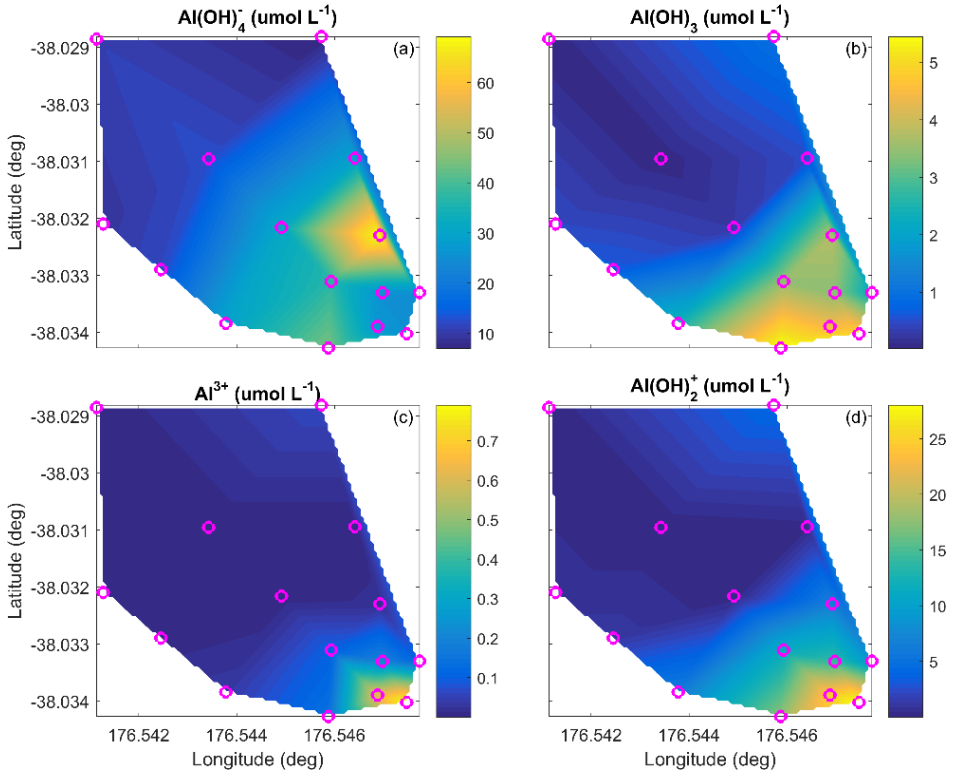

Figure 3.16. Interpolated major dissolved Aluminium species distributions based on PHREEQC geochemical model outputs of surface water measurements from sites 1-15 (pink circles) in Te Wairoa Bay 07/03/17. (a) $Al(OH)_4^-$, (b) $Al(OH)_3$, (c) Al^{3+}, (d) $Al(OH)_2^+$. Concentrations are in *u*mol L^{-1}. The underlying colour map shows interpolated surface values. Waitangi springs outlet is located at the bottom right of each surface plot with Lake Rotoehu in the upper left.

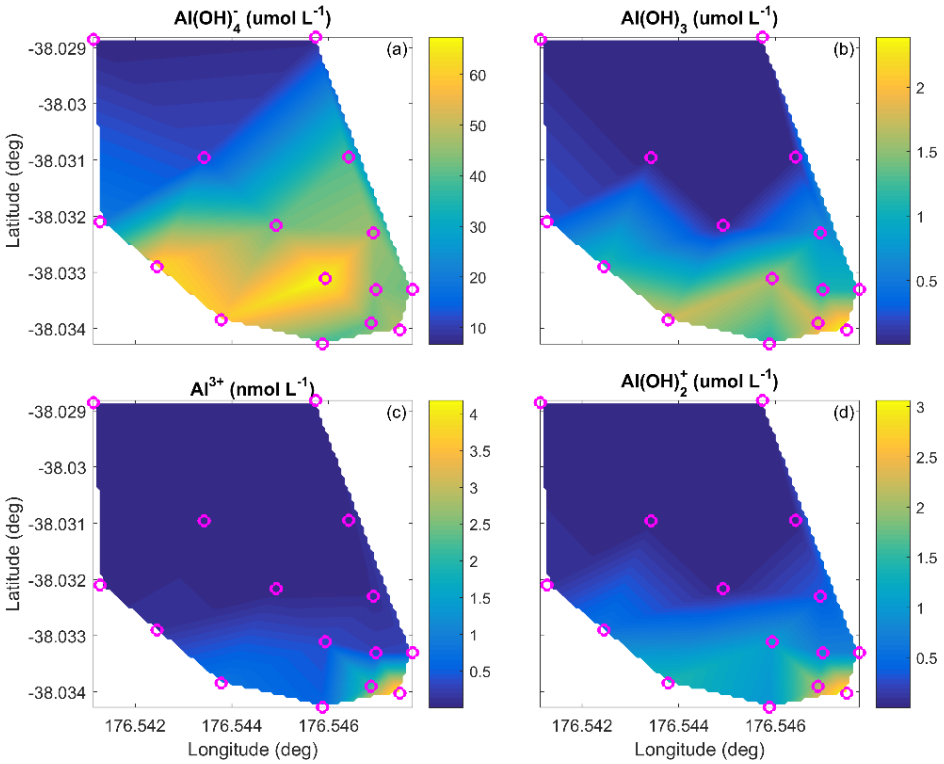

Figure 3.17. Interpolated major dissolved Aluminium species distributions based on PHREEQC geochemical model outputs of surface water measurements from sites 1-15 (pink circles) in Te Wairoa Bay 16/03/17. (a) $Al(OH)_4^-$, (b) $Al(OH)_3$, (c) Al^{3+}, (d) $Al(OH)_2^+$. Concentrations are in *u*mol L^{-1}. The underlying colour map shows interpolated surface values. Waitangi springs outlet is located at the bottom right of each surface plot with Lake Rotoehu in the upper left.

Iron Speciation

Dissolved Iron (Fe_{dis}) speciation was plotted with respect to the major Fe hydroxide species and the soluble Fe^{3+} ion. Given the supersaturated DO levels within the bay (Figure 3.12), any reduction of Fe^{3+}/Fe^{2+} was considered negligible over the sampling time period (i.e. during daytime hours). Overall there appeared to be an increase in Fe_{dis} species concentrations between the 07/03/17 and 16/03/17 sampling days (Figures 3.18 and 3.19). The concentrations of soluble Fe^{2+}/Fe^{3+} were modelled to be below detection limits and this agreed with DGT measurements. Furthermore, calculated $Fe(OH)_3$ showed the largest fractional concentrations during both sampling days, indicating that the system was close to thermodynamic equilibrium with respect to the Fe-oxyhydroxide species (Figures 3.18b and 3.19b). Distributions of the other hydroxide species $Fe(OH)_4^-$, and $Fe(OH)_2^+$ changed across the transition zone (sites 3 and 4), with large concentrations of $Fe(OH)_4^-$

and $Fe(OH)_2^+$ in the outer lake, corresponding to high and low pH values, respectively.

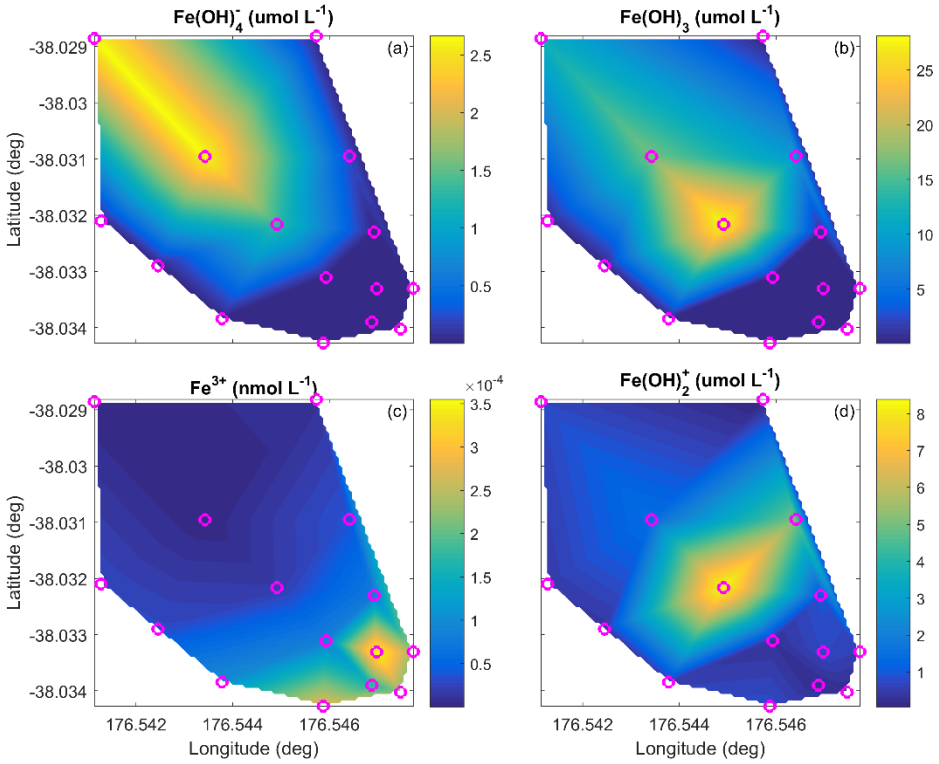

Figure 3.18. Interpolated major dissolved Aluminium species distributions based on PHREEQC geochemical model outputs of surface water measurements from sites 1-15 (pink circles) in Te Wairoa Bay 07/03/17. (a) $Fe(OH)_4^-$, (b) $Fe(OH)_3$, (c) Fe^{3+}, (d) $Fe(OH)_2^+$. Concentrations are in *u*mol L^{-1} (a,b,d) and nmol L^{-1} (c). The underlying colour map shows interpolated surface values. Waitangi springs outlet is located at the bottom right of each surface plot with Lake Rotoehu in the upper left.

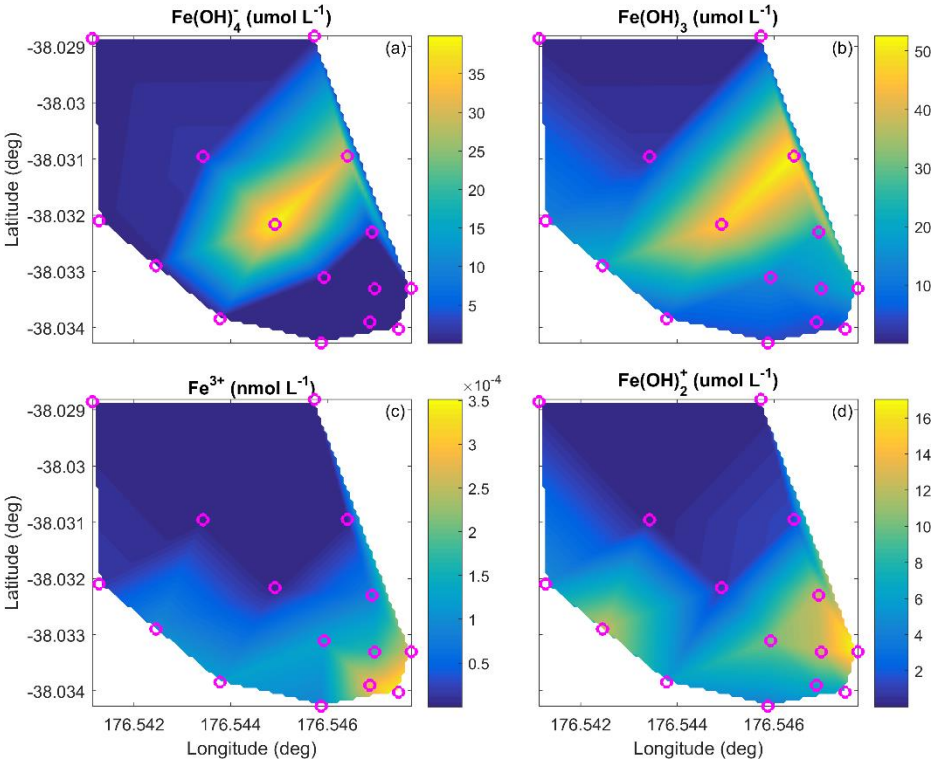

Figure 3.19. Interpolated major dissolved Aluminium species distributions based on PHREEQC geochemical model outputs of surface water measurements from sites 1-15 (pink circles) in Te Wairoa Bay 16/03/17. (a) $Fe(OH)_4^-$, (b) $Fe(OH)_3$, (c) Fe^{3+}, (d) $Fe(OH)_2^+$. Concentrations are in *u*mol L^{-1} (a,b,d) and nmol L^{-1} (c). The underlying colour map shows interpolated surface values. Waitangi springs outlet is located at the bottom right of each surface plot with Lake Rotoehu in the upper left.

Diffusive Gradients in Thin films (DGT)

DGT-derived concentrations of labile Al, Mn and Fe from a 24-hr deployment are shown in Table 3.2. These concentrations represent freely diffusible ionic forms of these elements and therefore represents the concentrations of the dissolved metal species in solution integrated over time. Higher concentrations of dissolved Al species were found close to the spring outlet (site 1) likely corresponding to Al^{3+} and $Al(OH)_2^+$, and in the macrophyte beds (site 3), associated with $Al(OH)_4^-$. These measurements lend support to the modelling results shown in Figure 3.17 by displaying similar distributions. However, it is prudent to consider the dynamic effects of $Al(OH)_3$ and pH when considering Al speciation. It is likely that a large component of total aluminium is precipitated out from solution in spontaneous reactions as gibbsite or other Al polymorphic minerals and would not be represented in the dissolved fraction measured by the DGTs.

Fe DGT measurements showed zero concentration of labile-Fe^{3+}, in agreement with the corresponding modelled concentrations, which were ~10^{-13} mol L^{-1} (i.e. below DGT detection levels). Although Fe speciation results indicate high molar concentrations (Figure 3.17), due to super saturated dissolved oxygen values (Figure 3.12), all the data support the interpretation that Fe is primarily in colloidal or particulate form under these conditions.

DGTs also showed concentrations of Mn which decreased with distance from the stream outlet. The cause of this concentration gradient are liukely to be associated with the control of $Mn^{2+}/^{3+}$ by equilibrium with MnO_2 at the higher pH conditions found in lake water, Mn is known to have a much slower oxidation kinetics than Fe (Davison 1993), and Mn provides an interesting counter point to the geochemical behaviour of Fe in this system.

Table 3.2. Results from DGT deployment, showing cDGT concentrations in nmol L^{-1} of Al, Mn and Fe in solution from sites 1-5. DGTs were deployed for 24 h from 15/03/17 to 16/03/17.

Chelex DGT concentrations nmol L^{-1}			
Location	**$cDGT_{Al}$**	**$cDGT_{Mn}$**	**$cDGT_{Fe}$**
Site 1	152.04	309.32	0
Site 2	37.78	193.48	0
Site 3	258.29	123.97	0
Site 4	42.78	7.98	0
Site 5	33.02	2.62	0

3.3.4 Mineral Saturation Indices

Mineral saturation indices (SI) for major Al ($Al(OH)_{3(am)}$, gibbsite) and Fe ($Fe(OH)_{3(am)}$, goethite) P binding minerals were calculated in PHREEQC based on thermodynamic PHREEQC equilibrium modelling. An adjusted redox equilibrium of 4 was used, given the bay was vertically well-mixed and supersaturated with respect to O_2. Results suggest that both pH and elemental concentrations were the primary drivers of the horizontal distributions of mineral saturation. Comparing both the gibbsite and amorphous $Al(OH)_{3(am)}$ mineral phases (Figure 3.20a,c and Figure 3.21a,c), it is clear the upwards shift in pH between the 07/03/17 and 16/03/7 sampling dates results in a decrease in the SI for these minerals phases. $Al(OH)_{3(am)}$ is primarily in equilibrium near

the vicinity of the stream outlet and the lower portion of the bay, but becomes under-saturated when moving out into the lake (Figure 3.20c and Figure 3.21c). gibbsite shows a similar spatial pattern to $Al(OH)_{3(am)}$ although waters are primarily super saturated with respect to gibbsite formation. Fe minerals goethite and $Fe(OH)_{3(am)}$ display opposite spatial patterns in mineral saturation compared to Al mineral saturation on the 07/03/17 (lower pH) sampling date, with supersaturated conditions in the lake and equilibrium conditions near the stream outlet (Figure 3.20 b,d). However, with an increase in pH 16/03/17 the SI of these minerals became super-saturated throughout the bay (Figure 3.21b,d).

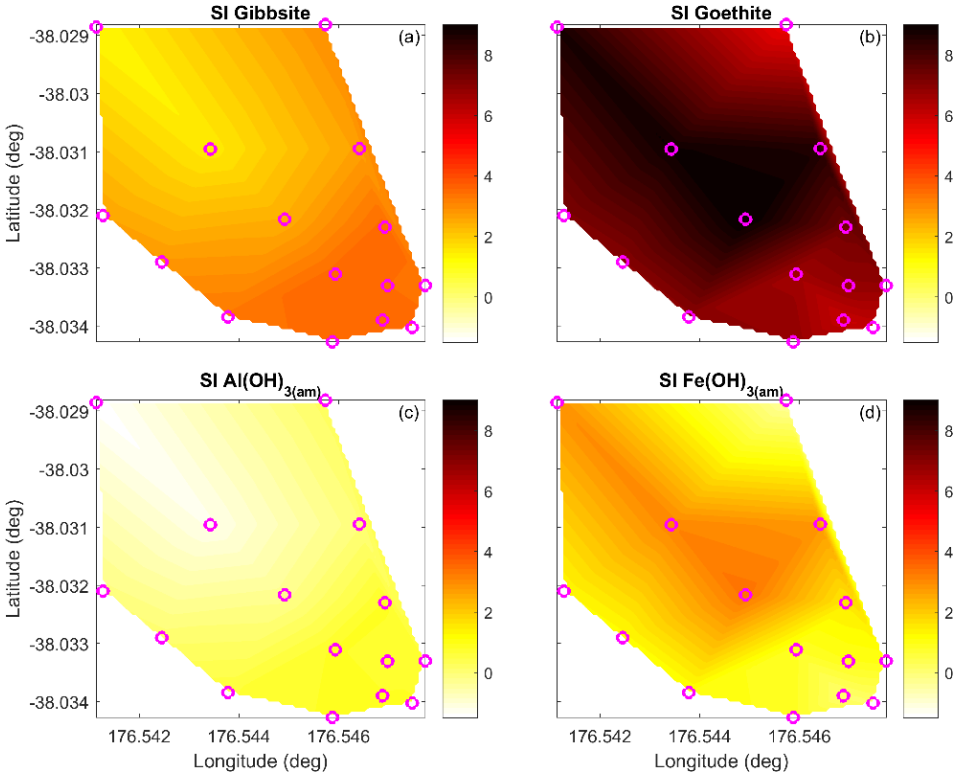

Figure 3.20. Mineral Saturation Indices (SI) for major Al and Fe mineral assemblages associated with P binding from sites 1-15 (pink circles) in Te Wairoa Bay from 07/03/17. SI distributions are based on modelled PHREEQC geochemical equilibrium speciation). The underlying colour map shows interpolated surface values. Positive values >0 indicate mineral saturation whereas negative values <0 indicate under-saturation. Waitangi springs outlet is located at the bottom right of each surface plot with Lake Rotoehu in the upper left.

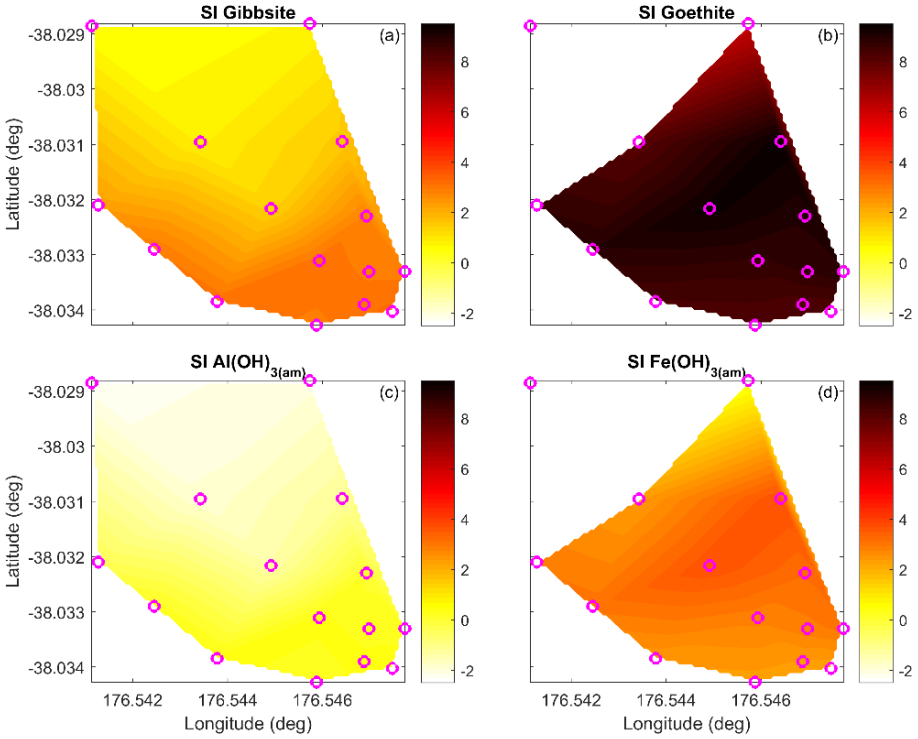

Figure 3.21. Mineral Saturation Indices (SI) for major Al and Fe mineral assemblages associated with P binding from sites 1-15 (pink circles) in Te Wairoa Bay from 16/03/17. SI distributions are based on modelled PHREEQC geochemical equilibrium speciation). The underlying colour map shows interpolated surface values. Positive values >0 indicate mineral saturation whereas negative values <0 indicate under-saturation. Waitangi springs outlet is located at the bottom right of each surface plot with Lake Rotoehu in the upper left.

3.3.5 Distribution of Aluminium, Iron, and Phosphorus in Lake Sediments

Sediment cores were collected at seven sites (RH1-RH7) from within Te Wairoa Bay out into the lake (Figure 3.1). The geochemical analysis showed a distinct separation between cores with respect to site location and the total concentrations of major sediment ions (Al, Fe, Mn, P). Sediment cores RH1 and RH2 corresponded to locations within the inferred deposition zone of the Waitangi springs outlet and showed elevated levels of Al, Fe, and P compared to the remaining cores (RH3-RH7), which were taken within the main lake basin (Figure 3.22).

The depth profiles from Te Wairoa Bay sediments (RH1, RH2) displayed a decrease in total Al (Al_{tot}) with depth, with and a significant drop in Al_{tot} concentration at ~10 cm below the sediment water interface. This decrease in Al is interpreted as the accumulation of the $Al(OH)_{3(am)}$ floc and/or

redeposited or mineralised Al minerals such as gibbsite (Figure 3.22a). Similarly, concentrations of Fe from the cores from the inner sites were also large and elevated relative to more distal sites. However, these cores showed a less stable pattern, implying the decreased stability of Fe minerals likely coupled to biological/redox assisted transformations (Figure 3.22b). P distributions were also higher in cores RH1 and RH2 when compared to cores from within the main lake basin (Figure 3.22c). However, unlike the Al and Fe vs depth profile in RH1, P concentrations increased with depth, indicating the possible diffusion of mobile-P fractions within this area of Te Wairoa Bay. Given that this core (RH1) also contained the highest concentrations of Fe, it is likely that the dynamic changes in water levels and redox sensitivity of Fe-bound labile P are associated with the negative trend in P with depth. Measurements from core RH2 showed a slight increase in P with depth, indicating a higher retention of P within the sediments at this location. Manganese profiles also showed clear separation between cores found within the bay versus those associated with lake sediments. In general Mn concentrations were higher in lake sediments, except in the surface of RH2 where a depletion of Mn can be seen in the upper portion of the sediments (Figure 3.22d), possibly being attributed to redox cycling within these compartments.

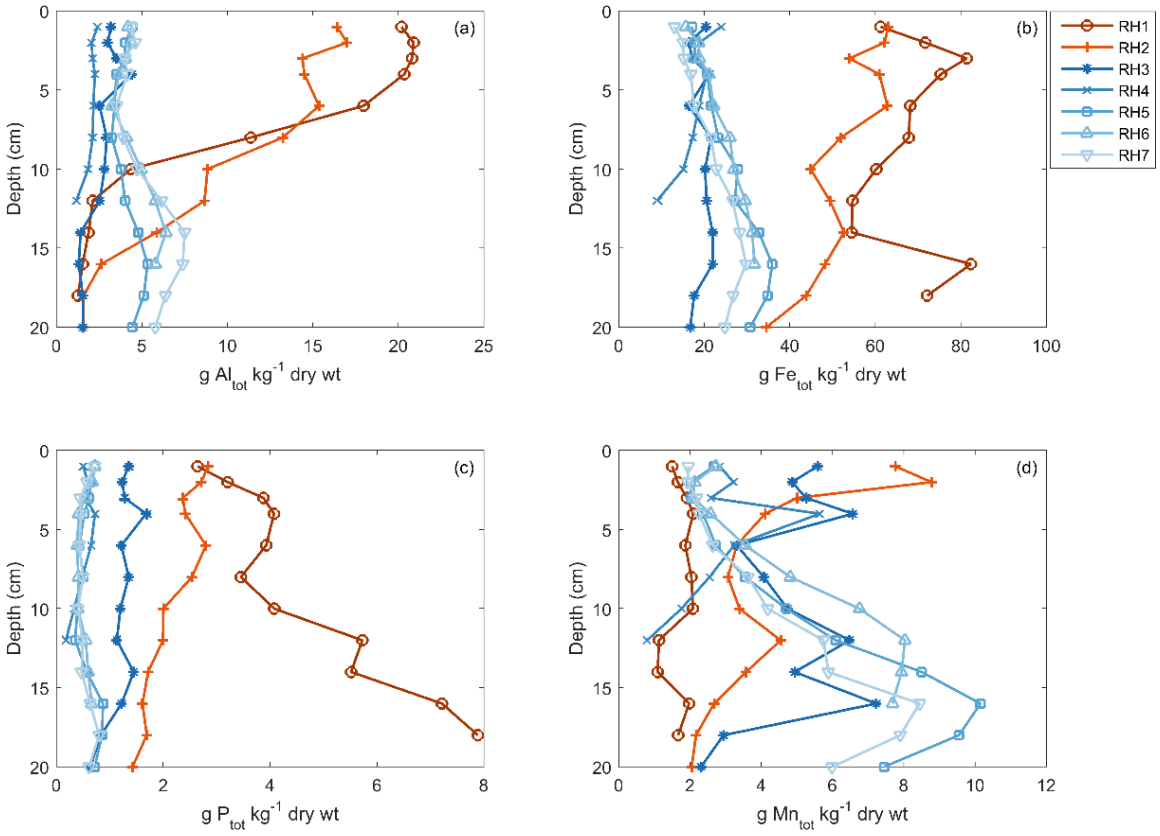

Figure 3.22. Depth profiles of elemental concentrations (dry wt) from sediment cores from within Te Wairoa Bay/Lake Rotoehu. Concentrations of (a) aluminium, (b) iron, (c) phosphorus, and (d) manganese taken. Sites correspond to those shown in Figure 3.1, orange and blue colours indicate sites within the inner and outer portions of the bay, respectively.

3.3.6 Long Term Nutrient Analysis of Lake Rotoehu

An analysis of a 15-year (2001-2016) dataset of surface water samples (TN,TP, Chl-*a*) collected from Lake Rotoehu, from two sites WU site 2 (2011-2015) and BOPRC site 3 (2001-2016) was undertaken. TP displayed a relatively stable trend between 2001-2011, although there appeared to be an increase in TP spikes during the period of (2005-2011) (Figure 3.23a). Upon the initiation of alum dosing (vertical dashed line) of the Waitangi Springs in 2011, there was a significant drop in the overall mean TP value and decreased variability over the 2011-2014 period, followed by a general upward trend in TP values (2014-2016). TN displayed a pronounced reduction over the 2001-2005 timespan with what appears to be a further response to the initiation of alum dosing (Figure 3.23b). However, there does appear to be a significant upward trend in TN over the timeframe of 2014-2016 (Figure 3.23b). Chl-*a* levels have also declined over the measured timeframe, and, as with TP and

TN, showed a further reduction with the initiation of alum dosing (Figure 3.23c), but an upward trend from 2014, including several large peaks over the 2015-2016 period.

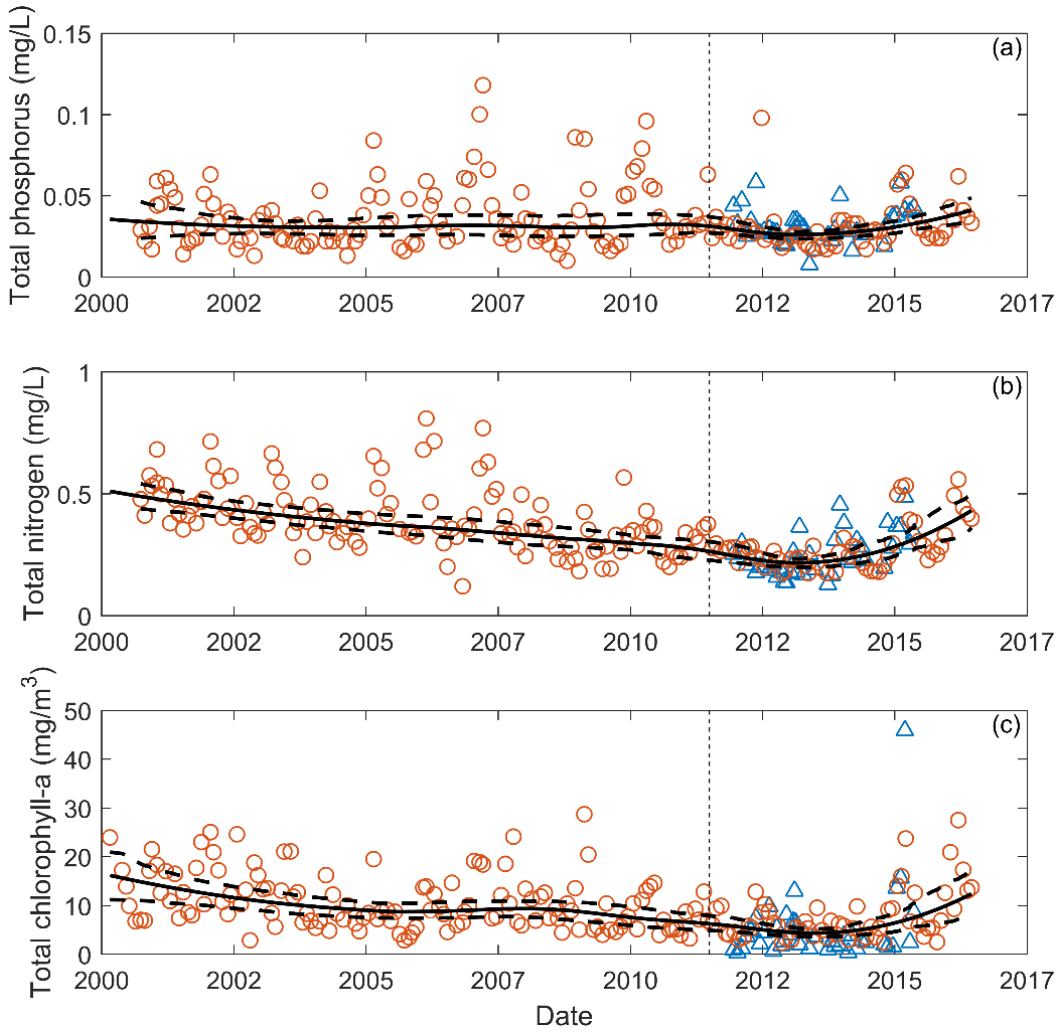

Figure 3.23. Long-term (2001-2016) surface water sampling data from Lake Rotoehu. Blue triangles denote surface samples from WU-site 2 and red circles are surface samples from BOPRC site 3 (Figure 3.1). Measurements of (a) total phosphorus (mg L^{-1}), (b) total nitrogen (mg L^{-1}), and (c) chlorophyll-*a* (mg m^{-3}). The thick solid lines are robust-loess-smoothed local polynomial regression fits, and the dashed thick lines are pointwise bootstrapped 95% confidence intervals of the fitted data using 2000 bootstrap samples. The vertical dashed line indicates commencement of Alum dosing in mid-2011.

The long-term TP, TN, and Chl-*a* values were also plotted against month of year to show seasonal variation (Figure 3.24). Peaks in TP and TN appeared to be related to austral summer months (Nov-May), and the confidence bounds indicated increased variability over these months versus winter months (Figure 3.24). Seasonal Chl-*a* data displayed the highest variability in summer

months (Nov-Apr), although high values were sometimes also measured in winter months. Interestingly, the shoulder months of May and Sept-Oct appeared to have the smallest variation in Chl-*a*; the times likely correspond to the transition in thermal regime of the lake, and the subsequent changes in phytoplankton species dominance.

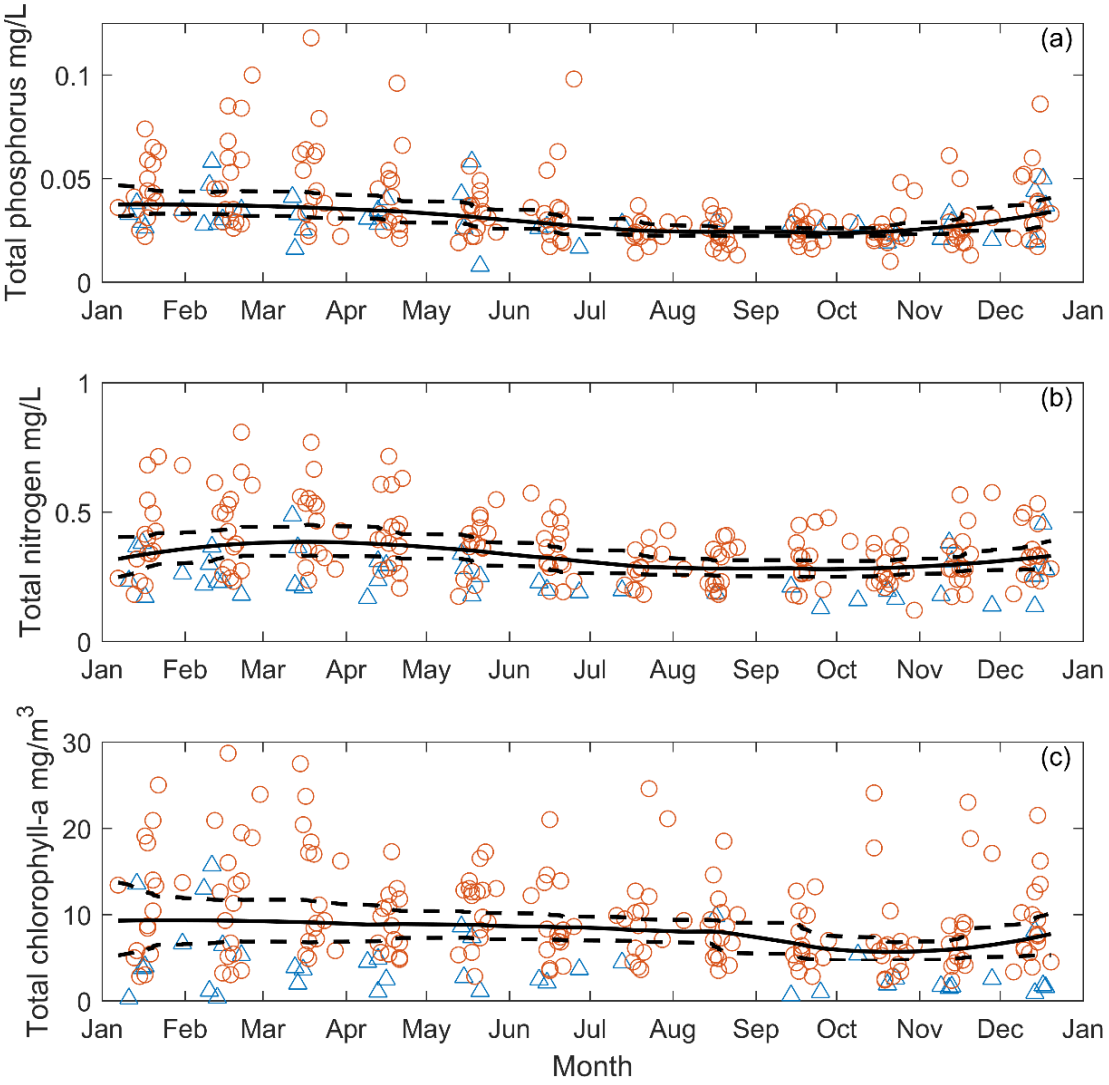

Figure 3.24. Seasonal long-term (2001-2016) water sampling data from Lake Rotoehu Blue triangles denote surface samples from WU-site 2 and red circles are surface samples from BOPRC site 3 (Figure 3.1). Measurements of (a) total phosphorus (mg L^{-1}), (b) total nitrogen (mg L^{-1}), and (c) chlorophyll-*a* (mg m^{-3}). The thick solid lines are robust-loess-smoothed local polynomial regression fits, and the dashed thick lines are pointwise bootstrapped 95% confidence intervals of the fitted data using 2000 bootstrap samples. Fitted line is a robust-loess-smoothed local polynomial regression, and the highlighted boundaries are 95% confidence intervals of the fitted data.

Regression plots of surface Chl-a values against nutrient concentrations show a significant and positive relationship between phytoplankton concentrations and both TN and TP (Figure 3.25), with more of the variance in Chl-a explained by TN (R^2=0.244) than TP (R^2=0.103). The difference between

the two-correlation coefficients was significant (using a two-tailed Fisher's z-transformation of R, z=2.16, p=0.03). Time series of TN:TP ratios showed that from 2000 to 2007 the lake was predominantly P-limited or N and P co-limited (Figure 3.26). After 2007, until commencement of alum dosing in 2011, the lake exhibited variable states of N-limitation and N and P co-limitation, possibly due to N-limitation remediation methods being undertaken in the lake (which began around 2007). Following the initiation of alum dosing (2011), the lake was almost entirely N and P co-limited at site 3, and a combination of N limited and N and P co-limited at site 2.

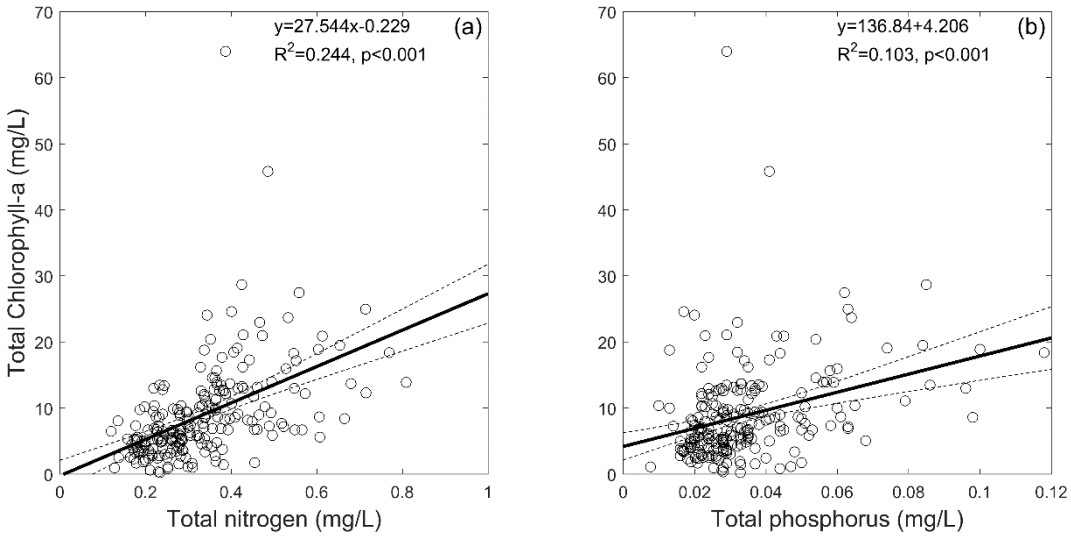

Figure 3.25. Relationships of chlorophyll-a vs. (a) total nitrogen, (b) total phosphorus from long term (2001-2016) Lake Rotoehu surface water sampling, Waikato University (WU-site 2) and BOPRC (site 3). Linear regression model fits are shown (black lines) with accompanying R^2 and p-values and 95% confidence intervals (dashed lines).

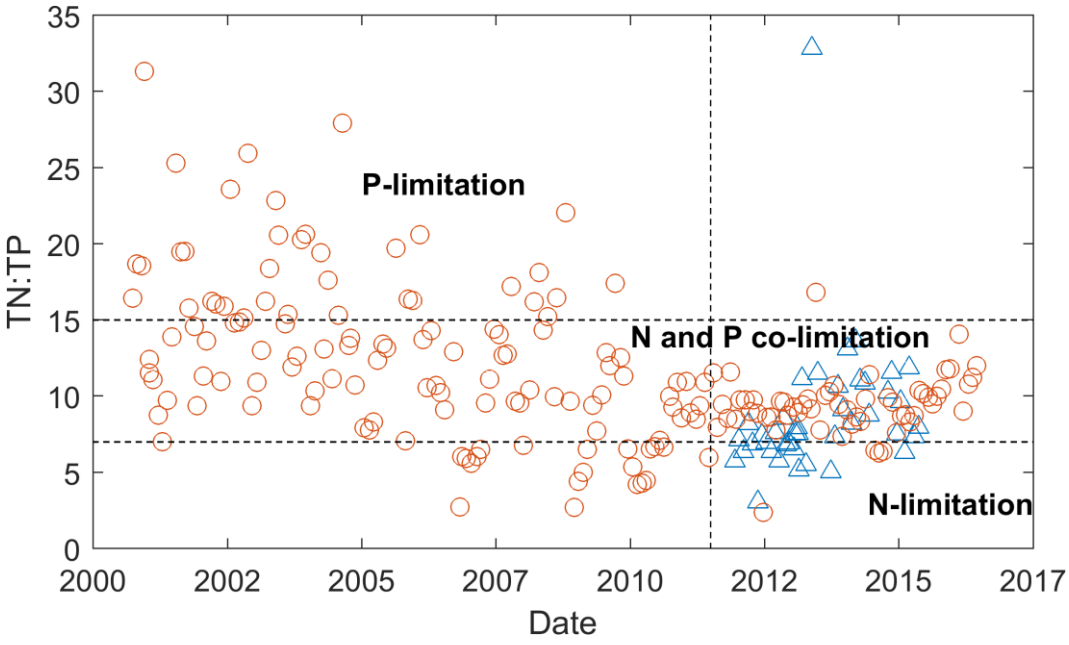

Figure 3.26. Ratios of TN:TP from the long-term surface water sampling (2001-2016) program in Lake Rotoehu showing data from Waikato University (site 2, blue triangles) and BOPRC (site 3, orange circles). Horizontal dashed lines indicate TN:TP values from Abell *et al.* (2010) for N, N+P, and P limitation. The vertical dashed line indicates commencement of Alum dosing in mid-2011.

3.4 Discussion

The water chemistry associated with the influence of geothermal inputs to Lake Rotoehu has been studied and quantified in the past by both McColl (1975) and Timperley & Vigor-Brown (1986). According to Timperley & Vigor-Brown (1986), Lake Rotoehu exhibits a high concentration of total dissolved salts (336 mg L^{-1}) of which 69 % were shown to originate from geothermally derived sources. Additionally, in a comparison of 32 lakes within the TVZ from the Timperley study, Lake Rotoehu was ranked 7th based on total dissolved salts, and 2nd based on proportion of geothermal influence. However, unlike many other geothermally influenced lakes within the TVZ, Lake Rotoehu displays a reduced contribution of sulfuric acid (H_2SO_4) within the system, and a moderate level of carbonic acid (H_2CO_3), which is likely to be an important factor in the overall chemical behaviour of the lake.

In order to better illustrate how geothermal contributions to Lake Rotoehu can affect the biogeochemical behaviour of the lake, it is helpful to compare the Waitangi Spring/Rotoehu case study with the alum-dosed geothermally influenced Puarenga stream which discharges to Lake Rotorua.

Drawing a comparison between Lake Rotoehu and Lake Rotorua, it is apparent that the contribution of H_2SO_4 in Lake Rotorua is much higher and the H_2CO_3 values are lower than in Lake Rotoehu (Table 3.3). Such a difference in the elemental proportion of acid contributions to lake water is reflected in both the mean alkalinity and pH of these respective lakes. Furthermore, Lake Rotorua contains far fewer total dissolved salts as well as specific major ions (Na, Ca, K, Cl, HCO_3,) which contribute to the alkalinity and ANC capacity of the lake. These contributions are reflected in the proportion of ions attributed to geothermal waters, and which are corroborated (for Lake Rotoehu) by the measurements in this study (Table 3.4). Conversely, Lake Rotoehu displays much higher values of ANC buffering ions as well as increased Si and B which may also contribute to the ANC of the lake (Evans *et al.* 2004). Given the high proportion of geothermal input attributed to both lakes Rotorua (43 %) and Rotoehu (69 %), the geochemistry of geothermal inputs is clearly an important mechanism which influences the biogeochemical conditions within the lakes.

Table 3.3. Values of mean pH and Alkalinity for Lake Rotoehu and Rotorua (Tempero et. al. 2015), and proportional contribution of total dissolved salts (Precipitation, H_2CO_3, H_2SO_4, and Geothermal waters) from Timperley (1986).

			Proportional				
Lake	**pH**	**Precip.**	**H_2CO_3**	**H_2SO_4**	**Geothermal water**	**Alkalinity (mg L^{-1}as $CaCO_3$)**	**Total dissolved salts (mg L^{-1})**
Lake Rotoehu	7.8±0.06	2	26	3	69	67±1.71	336
Lake Rotorua	7.0±0.07	6	12	38	43	8.3±0.37	107

Table 3.4. Values of major ions for Lake Rotoehu and Rotorua (Timperley, 1986) and from this study. Values are expressed in mg L^{-1}.

Lake	**Na**	**K**	**Ca**	**Mg**	**Cl**	**HCO_3**	**Si**	**SO_4**	**B**
Lake Rotoehu (Site 15 07/03/17)	87.49	8.31	6.32	4.03	126.01	84.5	6.91	10.86	0.66
Lake Rotoehu (Timperley, 1986)	92	17.1	5.2	3.4	123	84.2		11	
Lake Rotorua (Timperley, 1986)	28.5	4.4	3.2	1.4	26.6	12.5		30.5	

Comparing the two alum-dosed geothermal streams, reveals they are geochemically distinct. The Waitangi Springs is classified as bicarbonate-neutral-chloride waters (Chapter 2.1.2), while the main geothermal input to Lake Rotorua, the Puarenga stream is heavily influenced by the high sulfur geothermal inputs from the Whakarewarewa and Sulfur Bay areas (pH of ~3)

(Bioresearches 2003; Browne & Evans 2004; Simpson & Bignall 2015). It has also been noted by Ling (2014) that colloidal sulphur and a low pH transitional plume is dispersed into lake Rotorua from the Puarenga stream/Sulphur Bay on its eastern side. Such a low pH would have a marked effect on the speciation of Fe, and Al within the transition zone to the lake, favouring dissolved, highly charged cationic species. These dissolved species would influence the lability of such cations until physicochemical conditions within the lake-favoured hydroxide complexation and P binding. Such a scenario could perhaps assist in the dispersal of Al and P binding capacity to Lake Rotorua and potentially influence the response of the lake to such remediation measures (Ling 2014; Smith *et al.* 2016). The Waitangi Springs system, in comparison displays higher pH, lower sulfur, high HCO_3^- conditions, which primarily favour amorphous or solid Fe and Al (oxy)hydroxide species (Figures 3.17-3.19 and 3.20-3.21). Interestingly, increased dissolved Si has been associated with both amorphous HFO formation and decreased Al-P binding efficiency within the literature (Davison 1993; de Vicente *et al.* 2008b), conditions which have been observed within the Waitangi Springs system, and in lake Nordborg in Denmark (Egemose *et al.* 2011). Additionally, increased concentrations of major ions (e.g Ca, Na, K) from the Waitangi spring and their overall contribution to the alkalinity and ANC within Lake Rotoehu are likely to contribute to the increased mean pH (7.8) of the lake. Additionally, the larger quantities of H_2CO_3 would contribute more heavily to primary production and gaseous exchange to the atmosphere given many lakes act as sources of CO_2, whereas the H_2SO_4 in Lake Rotorua would be more prone to sedimentation as part of organic and inorganic particulate matter (Cole *et al.* 1994; Couture *et al.* 2016b). Furthermore, H_2SO_4 may contribute heavily to the coupled phosphorus-iron-sulfur interactions within lacustrine sediments, and could potentially influence P availability. Thus, it is possible that geothermally derived S may be an important contribution to P dynamics within geothermally influenced lakes within the TVZ.

3.4.1 Transition zone dynamics

The geothermal stream-lake transition zone in Te Wairoa Bay is a dynamic and variable physicochemical feature. Based on data from in-situ monitoring platforms and kayak transects, physicochemical conditions throughout the bay changed substantially over the nine-day experimental period. The large rainfall events which occurred during the experimental timeframe and the resulting lake de-stratification appeared to be the primary drivers in the observed dynamic changes in environmental conditions. Comparison of the stream-lake transition zone, which fluctuated from low base flow/ low lake level to higher base flow/higher lake level conditions provided key insights into the near and far field mixing of the geothermal plume, and how submerged aquatic vegetation may alter the local hydrodynamic and biogeochemical conditions within the littoral lacustrine environment.

The lake destratification which occurred during the first rainfall event, resulted in enhanced vertical mixing of waters within Te Wairoa Bay decreasing the in-lake temperature by ~4 ^{o}C (Figure 3.6a). Water temperatures from temperature logger moorings characterised the dispersal and mixing of the geothermal inflow demonstrating that it was generally well-mixed with respect to depth (Figure 3.5). A geothermal inflow such as the Waitangi Spring is analogous to warm water inflows from thermal power station cooling discharges (Rutherford 1981). These discharges are often characterised by plume dispersal which have been shown to mix across near, mid, and far fields differently depending on the temperature differential, density differences, and interacting currents within the water column (Abell & Hamilton 2015; Kalinowska & Rowiński 2015). The strength of the stream flow discharge affects the dispersal of the geothermal stream plume and therefore also its capacity to transport dissolved and particulate matter (Jones *et al.* 2007). Additionally, differential thermal gradients between littoral and pelagic waters can influence the mixing and transport of nutrients between such water masses in lakes. The interaction of flow with submerged macrophytes such as in Te Wairoa Bay may however reduce mixing dependent on the vegetation density and configuration (James & Barko, 1991; Monismith,

Imberger, & Morison, 1990). Changes in stream flow velocities between 07/03/17 and 16/03/17 were captured by both the Waitangi Springs stage height and the extent of thermal dispersion within the interior of Te Wairoa Bay (Figures 3.3b and 3.7). Based on the lateral distribution from both temperature and specific conductivity results, the dispersal plume would be classified as a free jet with increasing lateral mixing with distance from the stream outlet according to Jones et. al (2007). The patterns of temperature, pH, and specific conductivity interpolations indicated that a definitive mixing boundary existed between the stream outlet/inner bay waters and the outer bay/lake waters regardless of the magnitude of stream discharge. This boundary was attributed to the presence of extremely dense submerged *C. demersum* rafts within the middle section of the bay (approximately site 3) and their ability the control hydrodynamic flow paths. The configuration of the *C. demersum* rafts allowed significant lateral channels to develop where stream flow was preferentially routed within the bay. This flow routing is demonstrated by increased temperature, specific conductivity values and decreased pH values along the lateral nearshore arms within the bay (Figures 3.7, 3.9, 3.11). The transition in pH values at the mid bay *C. demersum* mixing boundary are also a key driver of the behaviour of Al, Fe, and P dynamics within this zone, due to thermodynamic dissolution. The temperature gradient is also corroborated in the temperature mooring values (Figure 3.5) based on the behaviour of temperature profiles from both the inner (warmer) and outer bay (cooler). The physical behaviour demonstrated from these measurements represent a key mechanism in the transport of both dissolved and particulate matter into and out of the bay.

Previous remote sensing work by Allan et al. (2016) demonstrated that temperature gradients within Te Wairoa Bay were capable of being resolved using LANDSAT-satellite-derived lake surface skin temperatures. Subsequent 3D hydrodynamic modelling revealed that the plume dynamics showed much variability in flow paths when compared to remote sensing measurements even when considering the effects of windspeed. Local scale hydrodynamics, submerged vegetation density and configuration, stream discharge, and lake level are likely to have a significant effect on the plume dynamics entering Te

Wairoa Bay, and such variability could be inferred from the discharge-dependent changes in stream plume dispersion found in the present study.

3.4.2 Spatial P binding efficiency of continuous Alum dosing

Results from the water samples and geochemical analyses allowed for the distribution of major ions, Fe_{dis}, $Al_{dis,}$ and DRP, to be spatially interpolated within the bay. Within the Waitangi springs/ Te Wairoa system the increased ionic strength of the water and geothermally derived particulate HFO were striking features (Figure 2.2). Fe_{dis} concentrations were primarily associated with areas of decreased pH (Figures 3.14 and 3.15), given O_2 values were supersaturated throughout the bay on both sampling occasions (Figure 3.12). Although Fe_{dis} values were in the mmol range, cDGT values indicated that there was no freely exchangeable Fe_{dis} and therefore the primary fraction of Fe_{dis} within the system was interpreted as being in colloidal form. Such conditions have been described in previous work in which colloidal forms of Fe_{dis} have been associated with increased ionic strength in freshwater systems and in concert with high O_2 values and increased organic matter (Lofts *et al.* 2008; Dol Hamid *et al.* 2011). However, these results do not preclude the large potential P binding capacity from the colloidal Fe_{dis} fraction. Unpublished data collected by Shirley and Hartland from Waitangi stream sediments have indicated that the greatest fraction of P within the sediments near the geothermal alum dose point was bound to the Fe mobile P fraction. Therefore, both particulate and dissolved fractions of Fe are likely to represent a significant sink for P cycling within the Waitangi/Lake Rotoehu system.

Both Al_{dis} and DRP displayed higher concentration values in areas where pH values were elevated, and appeared to be associated with the *C. demersum* mixing boundary within the central portion of the bay (Figures 3.14 and 3.15). The dynamics of Al-P within areas of high density submerged macrophyte growth has been identified in previous work by Barko & James (1998), in which heightened levels of pH led to the mobilisation of P from Fe and Al (oxy)hydroxides from both the sediment and the water column (Carter *et al.* 1988; Boers 1991; Jeppesen *et al.* 1997). Such geochemical dynamics are

likely to be occurring within Te Wairoa Bay due to the increased photosynthesis, O_2 production, and inorganic C drawdown associated with the high-density *C. demersum* beds (Maberly & Spence 1983). Additionally, *C. demersum* is known to uptake DRP directly through the water column which could explain the depletion of DRP moving into the lake (Figure 3.14 before lake overturn). Another potential explanation of this gradient of DRP is the interception through phytoplankton uptake, although *C. demersum* is known to inhibit phytoplankton growth through allelopathy as well as through nutrient uptake inhibition, and light inhibition (Lombardo & Dennis Cooke 2003; Hilt & Gross 2008; Pełechata & Pełechaty 2010). Variability of DRP across the transition zone also demonstrates the inadequacy in relying on a single sample for estimating lake-wide variations in nutrient values as these variables often vary over small spatial and short temporal scales in response to numerous forcing processes (Mackay *et al.* 2011a; Abell & Hamilton 2015). Overall, results indicate that at lower pH levels (pH~6) near the stream outlet concentrations of DRP and Al_{dis} are lower and are likely to be in particulate form with DRP adsorbed to $Al(OH)_{3(am)}$. However, as the pH values increase further out into Te Wairoa Bay, Al_{dis} and DRP concentrations increase as Al bound P is desorbed from $Al(OH)_{3(am)}$, and appears to be highest in areas where *C. demersum* interacts with the stream flow.

Furthermore, the elevated levels of DRP observed on 16/03/17 (Figure 3.15d) are likely to be associated with the lake destratification event, which homogenised the water column and led to increased DRP concentrations within the lake (Figure 3.6). Such conditions would likely favour P desorption from the mobile-P (Fe bound) fraction within lake sediments, and could be responsible for the large *Microcystis* sp. bloom which occurred approximately a week after the destratification. Similar conditions have previously been reported to have triggered bloom events (Oliver & Ganf 2000; Paerl & Otten 2013) .

Major ions may also be responsible for the extended growth of *C. demersum* within Te Wairoa Bay. K and Ca have been identified as critical nutrients which are taken up directly from the water column and which can

influence macrophyte growth (Barko *et al.* 1991). Given the high K (see Appendix), inorganic C, and Ca concentrations present within the transition zone (Figure 3.13), the reduced limitation of these nutrients could promote the increased abundance of *C. demersum* within the lake. *C. demersum* has also been shown to uptake NH_4^+ and NO_3^- directly from the water column and the naturally elevated levels of NH_4^+present within the Waitangi spring could therefore influence both macrophyte growth and N cycling within the lake Rotoehu (Toetz 1971). Other factors aside from nutrients which could promote such dense vegetation within the Te Wairoa Bay are the high water temperatures and high light availability due to increased particle coagulation from the alum dosing (Best & Visser 1987).

Results from PHREEQC speciation modelling indicated that $Al(OH)_4^-$ and $Al(OH)_2^+$ constituted the largest fractions of aluminium species (Figures 3.16 and 3.17). In particular, the largest values of $Al(OH)_4^-$ appeared around the locations of the *C. demersum* beds (and associated high pH values). The modelled fractions of $Al(OH)_3$ were around 10 times smaller, which could be attributed to its particulate form at the observed pH values. Modelled values of dissolved Fe^{3+} fractions were extremely small ($< 1 \times 10^{-3}$ nmol L^{-1}) which explains the inability to resolve them in cDGT measurements. $Fe(OH)_3$ displayed the largest fraction as it was likely to be in colloidal form (Figures 3.18 and 3.19).

3.4.3 Accumulation of Al and Fe in sediments

Al, Fe and P concentrations within the sediment cores collected close to the Waitangi Springs outlet were elevated relative to the outer portion of the lake. Several processes likely contribute to this area of enhanced sediment deposition and high elemental concentrations within this region. We list them below although the current work does not ascertain the relative importance of each process. As flow exits the stream outlet constriction, the plume can spread, velocities decrease and the flow loses its sediment carrying capacity. Also the presence of the submerged vegetation increases drag within the flow, and promotes sediment deposition (Madsen *et al.* 2001). Additionally, the

alum-dosing promotes flocculation of organic and inorganic particles, increasing sediment size and settling velocity, thus enhancing the deposition rates.

In the main body of the lake, the concentrations of Al are relatively close to depth-uniform within the sediment. However, in the vicinity of the stream outlet, the cores show a substantially larger Al content close to the surface (> 10 g Al_{tot} kg^{-1} dry weight in the top 10 cm of sediment). These results indicate that Al is in particulate form and settling out as $Al(OH)_{3(am)}$ and potentially transitioning to gibbsite.

The Fe levels measured in the main lake body in the present work are consistent with those obtained by Trolle et al. (2010) (~25 000 mg Fe kg^{-1} and net sedimentation rates of 2.6 mm y^{-1}). Trolle's work also found that these values (of Fe) for Lake Rotoehu are relatively high compared to most of the other Rotorua lakes. The current results coupled with these previous results indicate that the potential for Fe bound P cycling from sediments would be relatively high in Lake Rotoehu when compared to other lakes in the TVZ. However, in the study of Trolle et al. (2010) no significant linear correlation between Fe and TP was found among TVZ lakes, perhaps due to the limited spatial coverage of their study.

The release of P within lake sediments is dependent on several factors including the concentration gradients between the sediment and the sediment water interface, the Fe:S ratio, microbial reduction, and the redox conditions (Caraco et al., 1989; Reddy & DeLaune, 2008). Although the current study presents no S values from lake sediments, it is known that the geothermally derived inputs of S can be high in geothermal waters and variations in S levels from Te Wairoa Bay water samples are significantly higher than background concentrations. Therefore, S could be an important component in the coupled P-Fe-S cycle within sediments in Lake Rotoehu. Fe:S ratios in sediments >3:2 may be indicative of the formation of P-locking minerals such as vivianite and goethite and thus lead to P burial within sediments. Fe:S ratios <3:2 may lead to the formation of pyrite and thus remove P binding capacity of Fe from the sediment leading to P dissolution and potential release back to the water

column (noting this process is possibly supported by the gradient in P with depth observed in the core at site RH1, Figure 3.22c). Such Fe:S ratios within sediments could present specific management challenges within geothermally influenced lakes such as Lake Rotoehu as well as other lakes within the TVZ.

3.4.4 Conceptual Model

Figure 3.27 summarises the key results and processes within the Waitangi Springs/Te Wairoa Bay system. Immediately after the Alum dosing inputs at the geothermal Waitangi Springs, DRP is reduced from ~0.30 μg L^{-1} to 0.10 μg L^{-1} through $Al(OH)_3$ formation and DRP adsorption. High background Fe and Al inputs preferentially form particulate oxyhydroxides at pH 6 at the dosing point. After exiting the stream outlet, particulate Fe-bound P and Al-bound P are both deposited to the sediment. This deposition may lead to P-cycling via redox-controlled adsorption-desorption from Fe-bound P, under the appropriate conditions (anoxia or pyrite formation). Al-bound P deposited at the stream outlet accumulates as $Al(OH)_{3(am)}$ or gibbsite, acting to lock P within sediments in solid mineral form.

As waters from the Waitangi Springs outlet mix with the high-pH lake water, pH-controlled dissolution-speciation of Fe and Al bound minerals in suspension may lead to additional DRP release. Furthermore, localised areas of *C. demersum* appear to result in DRP-release due to diel fluxes in pH, driven by photosynthesis. DRP released to the water column may be taken up by *C. demersum* or phytoplankton within the water column. Organic P settles to and is incorporated into sediments through the processes of vegetation senescence or phytoplankton sedimentation. During times of thermal stratification, anoxia may occur at the sediment-water interface leading to a return of P to the water column from Fe-bound P.

The processes described within Figure 3.27 are consistent with the observed values obtained from water and sediment geochemical analyses as well as geochemical speciation modelling. Longer-term analyses of water column properties (Section 3.3.6) indicate that since the inception of alum

dosing in 2011, TP within the lake has been reduced overall. From around 2014, the data shows an increasing trend in TP values. However, the precise causes of this recent trend are not yet known as it is difficult to separate the effects of multiple influences such as climatic conditions, changes in remediation methods which may affect biological P pools, or shifts in nutrient limitations (nitrogen, see Figures 3.24 and 3.26).

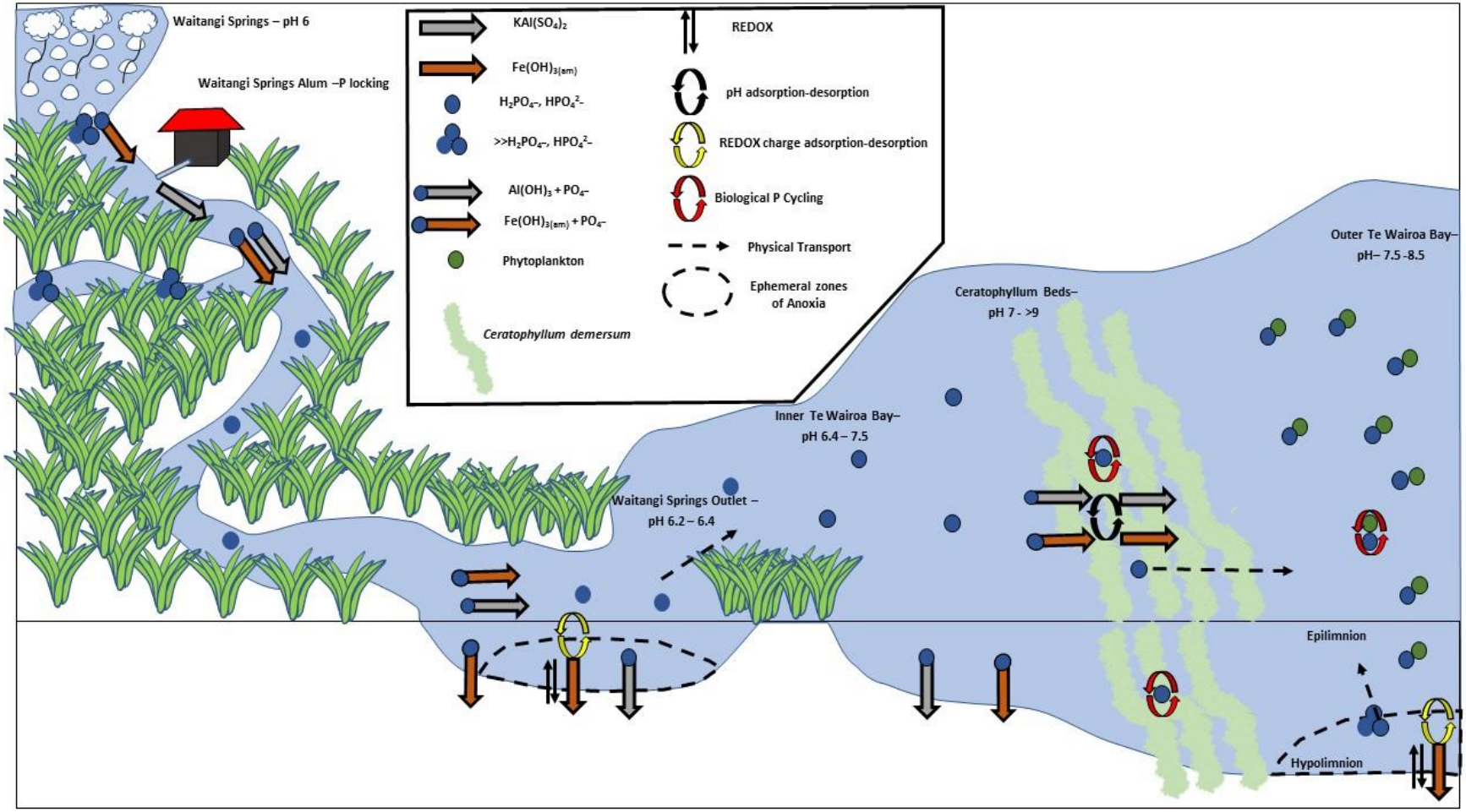

Figure 3.27. Conceptual summary of the biogeochemical processes operating in Te Wairoa Bay in Lake Rotoehu. In particular, the diagram shows the observed pH values and illustrates the interactions of Al, Fe and P with primary producers and environmental processes.

CHAPTER FOUR

DIEL GEOCHEMICAL FLUXES WITHIN A SUBMERGED MACROPHYTE BED: IMPLICATIONS FOR ALUMINIUM, IRON, AND PHOSPHORUS IN ALUM-TREATED LAKES

4.1 Introduction

Aquatic macrophytes are integral components within freshwater ecosystems and comprise emergent, free-floating and submerged aquatic vegetation (SAV). In particular SAV plays a crucial role in the development of structural heterogeneity in aquatic environments. Indeed, the transition from low productivity oligotrophic to eutrophic highly productive lake ecosystems, is often defined in part by the reduction in aquatic vegetation and the ecosystem services that they provide (Scheffer et al., 1993). Many of the ecosystem services provided by SAV are directly linked to their ability to eco-engineer their aquatic environment (Caraco, Cole, Findlay, & Wigand, 2006; Marion et al., 2014). Through the development of three-dimensional structure within the water column, many SAV species are able to control the exchange of biologically limiting parameters including light availability (Barko *et al.* 1986). These species also control the exchange of macro-nutrients (N,P) (van Donk *et al.* 1993; Kufel & Kufel 2002; Lombardo & Dennis Cooke 2003), micro-nutrients (Ca, K, Zn) (Barko *et al.* 1991), and metals (As, Al, Mercury), (Maessen *et al.* 1992; Robinson *et al.* 2006). Furthermore, diel photosynthesis/respiration cycles within SAV, strongly control the availability of dissolved inorganic C and O_2. This regulation of dissolved gasses can in turn alter localized environmental physicochemical conditions such as pH and REDOX potential, which can fundamentally alter chemical availability and speciation within the aquatic environment (Maberly 1996; Nimick *et al.* 2011).

SAV has a three dimensional structure which provides a sheltering habitat for other aquatic organisms such as epiphytic microorganisms, invertebrates, and fish (Bogut *et al.* 2010). Additionally, this habitat structure creates hydrodynamic drag, which reduces water velocities and promotes the settling of particulate matter and sediments, and can also promote the maintenance of water column clarity (Madsen *et al.* 2001; Downing-Kunz &

Stacey 2012). SAV may also exert significant control on the extent of phytoplankton productivity within lakes via the production of allelopathic chemicals which can inhibit nutrient uptake of phytoplankton species (Gross *et al.* 2003; Hilt & Gross 2008).

Although SAV are often associated with aquatic ecosystem health, in New Zealand many invasive SAV species have been introduced to freshwater aquatic ecosystems and are responsible for over-proliferation and loss of native SAV species (Vant *et al.* 1986). Due to nutrient enrichment of N and P, as well as increased light availability, invasive SAV species such as *Ceratophyllum demersum*, *Egeria densa*, and *Logarisphon major* are responsible for the clogging of waterbodies, including many of the Te Arawa Rotorua lakes (Burton & Clayton 2015). Increased biomass of SAV within lakes can be detrimental to ecosystem health, as the senescence of large quantities of SAV biomass can introduce C, N, and P to lake sediments fuelling heterotrophic decomposition and promoting reduced/anoxic conditions within lake sediments and water column (Welch & Cooke 1999). Within shallow lakes the availability of suitable habitat is increased due to the shallow mean water depth and substantial light availability. Furthermore, ample nutrient supply in both the sediments and in the water column of eutrophic lakes allow SAV to thrive. In particular, within Lake Rotoehu, *C. demersum* or hornwort has proliferated to the point where active intervention has been required. High density *C. demersum* beds are removed with an aquatic weed harvester as a remediation measure for the reduction of N and P (BOPRC 2007).

C. demersum is a cosmopolitan SAV species which has been intensively studied. Unlike many submerged macrophytes which have roots which anchor themselves into lake sediments, *C. demersum* has rhizoid structures which allow it to subsist both at the sediment surface and within the water column (Best & Visser 1987). Such a life strategy lends itself as an adaptive trait which can allow rapid dispersal and colonization under favourable conditions. Additionally, *C. demersum* is capable of obtaining nutrients N and P directly from the water column (Lombardo & Dennis Cooke 2003).

This study was undertaken in the transition zone of a lacustrine embayment influenced by a geothermal stream outlet within the medium sized polymictic Lake Rotoehu. Here, we seek to identify the dynamics of Al, Fe, and P cycling within Te Wairoa Bay over a diel cycle. Given the ability of SAV to significantly alter the local physicochemical conditions, we hypothesized that under conditions favouring increased photosynthesis (i.e. summer time conditions), high density *C. demersum* would control the availability of DRP, and dissolved Al and Fe within the water column.

4.2 Methods

4.2.1 Study Site: Te Wairoa Bay

The study site was Te Wairoa Bay (-38.032161°, 176.544915°), previously introduced in section 3.2.2. Figure 4.1a shows an example of one of the large high-density beds of *C. demersum* close to sampling site 3 (Figure 4.2). At this site, the *C. demersum* extended over the full depth of the water column and produced a large surface canopy. The locations of macrophyte beds were easily discerned as the lake surface above the beds was much smoother than in the adjacent channels (Figure 4.1b).

Figure 4.1. Photographs of the *C. demersum* bed close to sampling site 3: (a) close up showing the vegetation canopy at the surface and (b) overall photo showing the smooth water surface above the macrophyte beds.

4.2.2 Sampling and Monitoring

The experiment took place over a 24 h period during April, 2017, near the end of the austral summer. Intensive water sampling began at 14:00 on 07/04/17 and ended at 15:00 on 08/04/17, representing a diel cycle. High frequency temperature moorings (sites 1-5, Figure 4.2), a Nortek Acoustic Doppler Current Profiler (ADCP) (site 1), as well as real-time lake monitoring data wind speed and direction (BOPRC buoy) spanned the duration of the experiment. The ADCP was deployed in ~0.75 m water depth and measured flow speeds (*u, v, w*) in 3 dimensions (east/west, north/south and vertical, respectively), at the stream outlet under high resolution sampling frequency settings of 4 Hz.

Physicochemical (Sonde: pH, DO saturation, temperature, conductivity, and depth) and biogeochemical (TA, ICPMS, IC, FIA) variables were measured at both surface and bottom waters across a 5-site transect within Te Wairoa Bay. Sites 1-2 and 4-5 were sampled approximately every 6 h, while site 3 (*C. demersum* bed) was sampled every 2 h. Furthermore sites 15-18 were sampled at the end of the experiment in order to ascertain the upstream and lake water concentrations of all geochemical components.

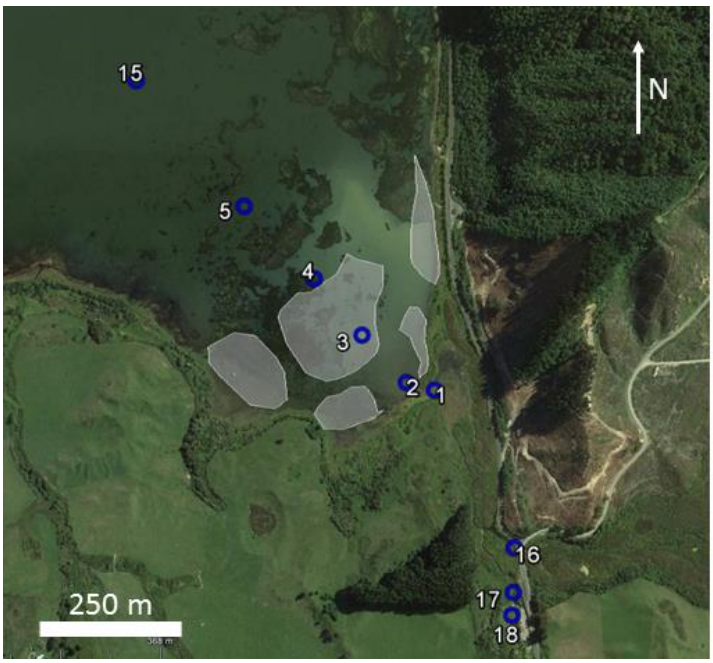

Figure 4.2. Sampling sites (blue circles) for the 24-h experiment. Site numbers correspond to those from Chapter 3. The white shaded regions show the approximate locations and extent of the *C. demersum* beds. Site 3 was sampled regularly at ~2 h intervals. Sites 1, 2, 4 and 5 were sampled approximately every 6 h. Sites 15-18 were sampled once at the completion of the experiment.

Time series of temperature were recorded at sites 1-5 using Onset Hobo Tidbit dataloggers at various depths within the water column. At sites 1 and 2, there were sensors at the top and bottom; at sites 4 and 5, temperatures were recorded at 3 depth levels and at site 3, there were 7 loggers at roughly equal spacing over the water depth. Measurements were taken every 30 s.

4.2.3 Data Analysis

Physicochemical Monitoring

Profiles of physicochemical data was obtained using the Sonde. Erroneous data points, such as samples taken above the surface, and when the sensor head was resting in the lake bottom, were removed. The data obtained were used to generate time-series plots in MATLAB.

Water Sampling - Geochemical Modelling

As with the analysis in chapter 3, data from the water sampling (ICPMS, IC, alkalinity, and pH) were compiled and analysed in Excel and MATLAB. Equilibrium and speciation models for water samples at each site (sites 1-5 and sites 15- 18) were obtained using Notepad++ PHREEQC (version 3.3) and the WATEQ4 database. The models provided output molar concentrations, molar speciation concentrations, and equilibrium charge balances.

ADCP Flow data and Windspeed

ADCP velocities were analysed using MATLAB scripts provided by the University of Waikato Coastal Marine Group. The depth-averaged and time-averaged flow speeds over the experiment and distance across the outlet channel (5 m) were used to provide an order-of-magnitude estimate of the volume flux ($m^3\ s^{-1}$) from the stream into the lake.

4.3 Results

4.3.1 Diel physicochemical conditions

The physicochemical conditions measured across the stream-lake transition zone within Te Wairoa Bay exhibited significant changes over the course of the experimental period from 07/04/17 to 08/04/17. These changes are described within the following sections.

Environmental Conditions

Preceding the experimental period, a sizeable precipitation event delivered an accumulated rainfall total of 277.5 mm (4-6/04/17), (Figure 4.3a), which resulted in very rapid changes in the Waitangi Springs stage height which increased from 0.4 to 0.8 m eventually subsiding to a baseflow of ~0.6-0.5 m (Figure 4.3b). Lake Rotoehu surface elevation level increased 0.4 m in height from 294.7 m to 295.1 m during the single rain event (Figure 4.3c). Conditions from 07/04/17-08/04/17 were representative of the post rapid rise in stream and lake water levels and the subsequent decreasing limb in the hydrograph. Meteorological conditions comprised an atmospheric high with low cloud cover throughout the experiment. Therefore, high solar radiation influencing photosynthesis and large fluxes in air temperatures were observed (data not shown). As noted in Chapter 3, the previous months were characterised by several large rainfall events and associated increases in stream and lake water levels; therefore, these measurements are representative of the relaxation after near-flood conditions in which overland flow would have likely been an important component of the runoff given the saturated soil conditions.

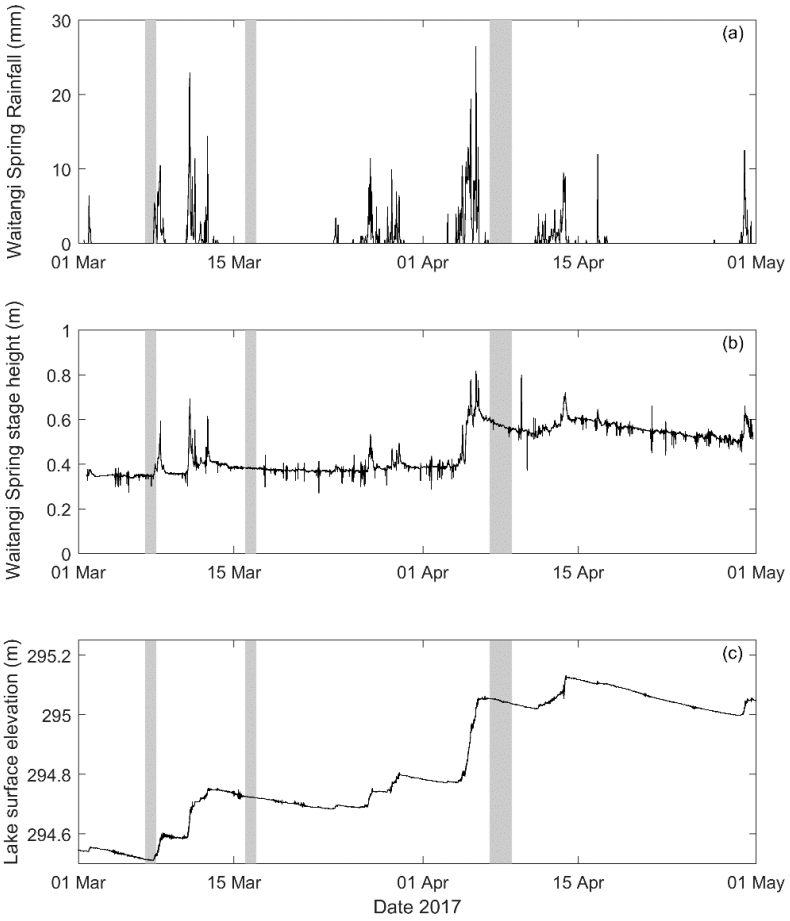

Figure 4.3. Conditions covering the experimental periods 7/04/17 – 16/03/17 (Chapter 3) and 07/04/17 - 08/04/17 (Chapter 4). Data is from BOPRC website and provided at 15 min intervals. (a) Rainfall measured at Waitangi Springs. (b) Waitangi Springs stage height. (c) Lake Rotoehu surface elevation. Grey shading indicates times of additional water sampling.

Wind speed and direction were measured within the lake at the location of the BOPRC monitoring buoy (Chapter 3, Figure 3.1a). Wind speed was variable ranging between very light and 7 ms^{-1} (Figure 4.4). Wind direction was primarily from the ESE, which also coincided with the strongest windspeeds. This wind direction therefore favoured offshore winds within Te Wairoa Bay. Winds observed during daylight hours were light, with the faster wind speeds primarily occurring overnight.

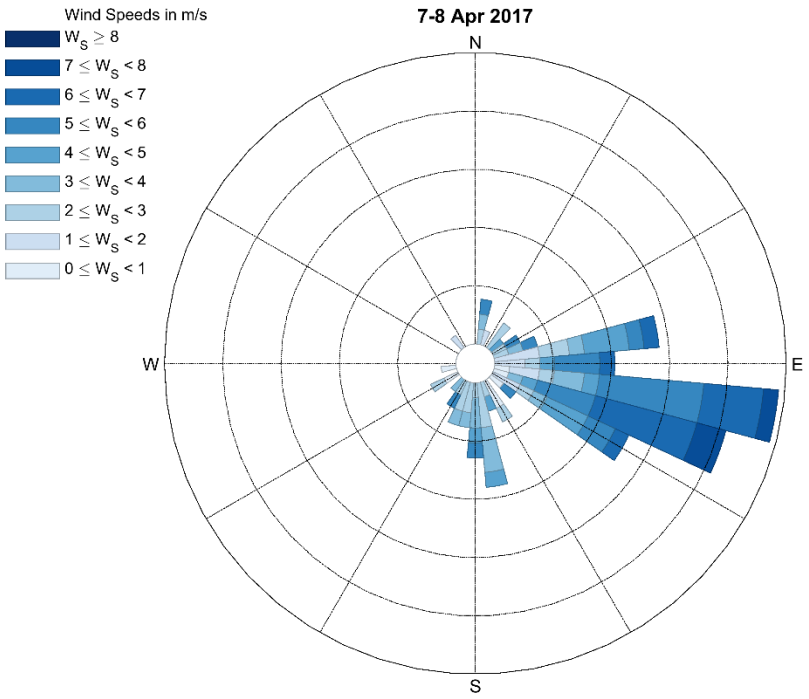

Figure 4.4. Wind conditions during the full experimental period 07/04/17 – 08/04/17. Bar lengths show the frequency of winds from each direction and colours indicate wind speeds.

Water Flow Speeds

Water flow speeds measured using the ADCP at the stream outlet (to the main lake) were largest in the (E/W) along-channel direction with values reaching up to ~0.09 m s^{-1} towards the west (i.e. into the lake) (Figure 4.5c). Flow speeds in the N/S (Figure 4.5b) and vertical (Figure 4.5c) directions were much smaller. Therefore, an estimate for water discharge (Q) was simply calculated by multiplying the depth-mean time-average of the westward flow speed (0.067 m s^{-1}), with the average depth across the channel (0.75 m) and width of the outlet channel (6 m). The estimate derived was ~300 L s^{-1}.

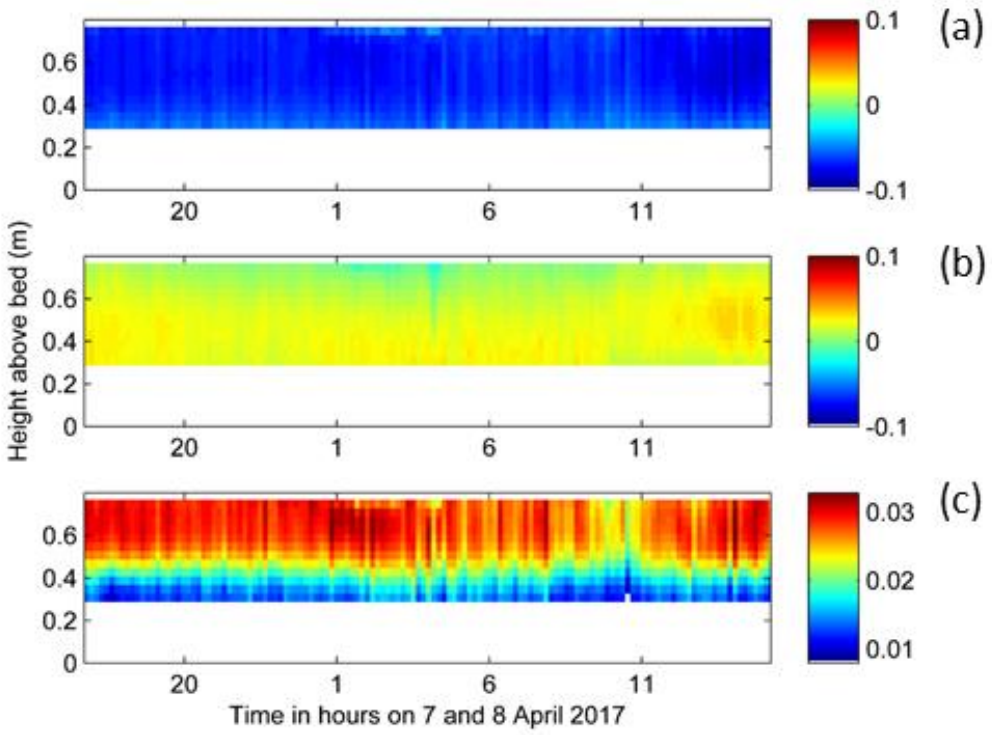

Figure 4.5. Waitangi Springs outlet current velocities in m/s during the 07 - 08/04/17, deployment. (a) E/W, (b) N/S and (c) vertical components. The sampling frequency was 4 Hz and values were averaged over ~10 min to reduce noise.

Diel Water Temperature, pH, and Alkalinity

Time series of temperature measurements from the moorings at sites 1-5 are shown in Figure 4.6. Overall, measurements nearest the surface at all sites showed the greatest variability in temperature with a decrease in temperature variability with depth. Due to the shallow depths and the influence of geothermal waters at sites 1-2, temperatures there generally exhibited a smaller top to bottom difference than the other sites. However, there appeared to be a temperature inversion at site 1 between 17:00 and 02:00 h. At all sites, the surface temperatures were the most variable. Throughout the night, temperatures at all sites became more depth-uniform until approximately 08:00 h when solar radiation at the water surface began to increase surface temperatures again. Furthermore, the effect of shading by *C. demersum* on water temperatures at site 3 is readily apparent with temperatures at depth showing very little change in temperature while surface

temperatures changed markedly (Figure 4.6c), leading to the largest surface to bottom difference over all sites (>7 °C by the end of the experiment).

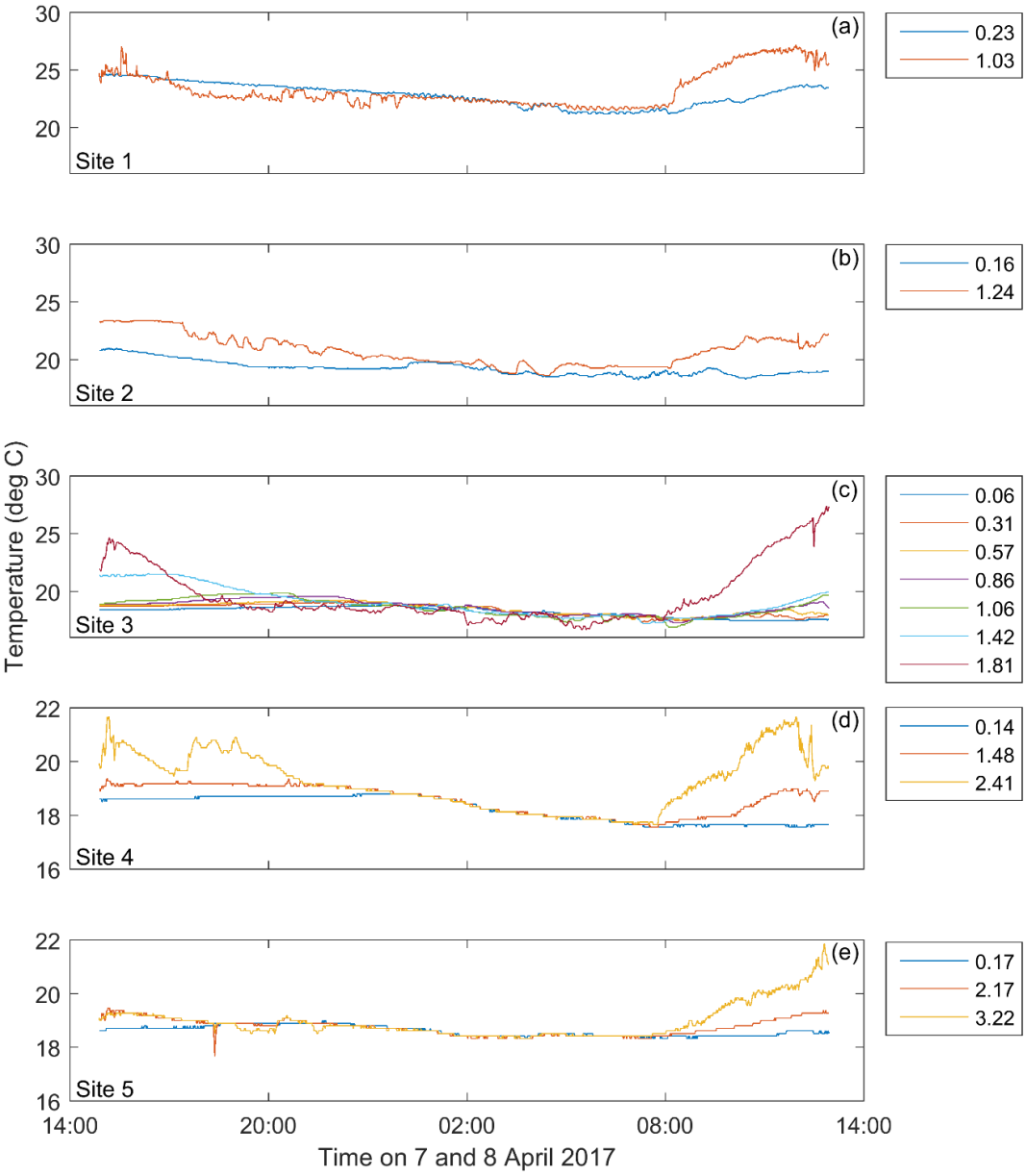

Figure 4.6. Diel temperature time-series from water column moorings at sites 1 to 5 (a-e). Heights above the bed are marked in figure boxes next to the corresponding plot. The sampling frequency was 1/30 Hz.

A time series of pH measurements at the surface and bottom of the water column were extracted from the Sonde profiles. Generally, pH increased with distance from the stream outlet into the lake (Figure 4.7). Overall the pH in surfaces waters appeared to vary more than in the bottom waters (Figure 4.7a,b). Site 3 (in *C. demersum* beds) showed the most variation in pH, especially in the surface waters where pH values demonstrated large

fluctuations between high daytime values of pH~9 to night-time values of ~ 7, whereas in-lake values and sites near the stream outlet remained relatively stable (sites 1-2 and 5). However, open-water site 4 also showed quite large changes (from pH 6.6 to 8) in surface water values.

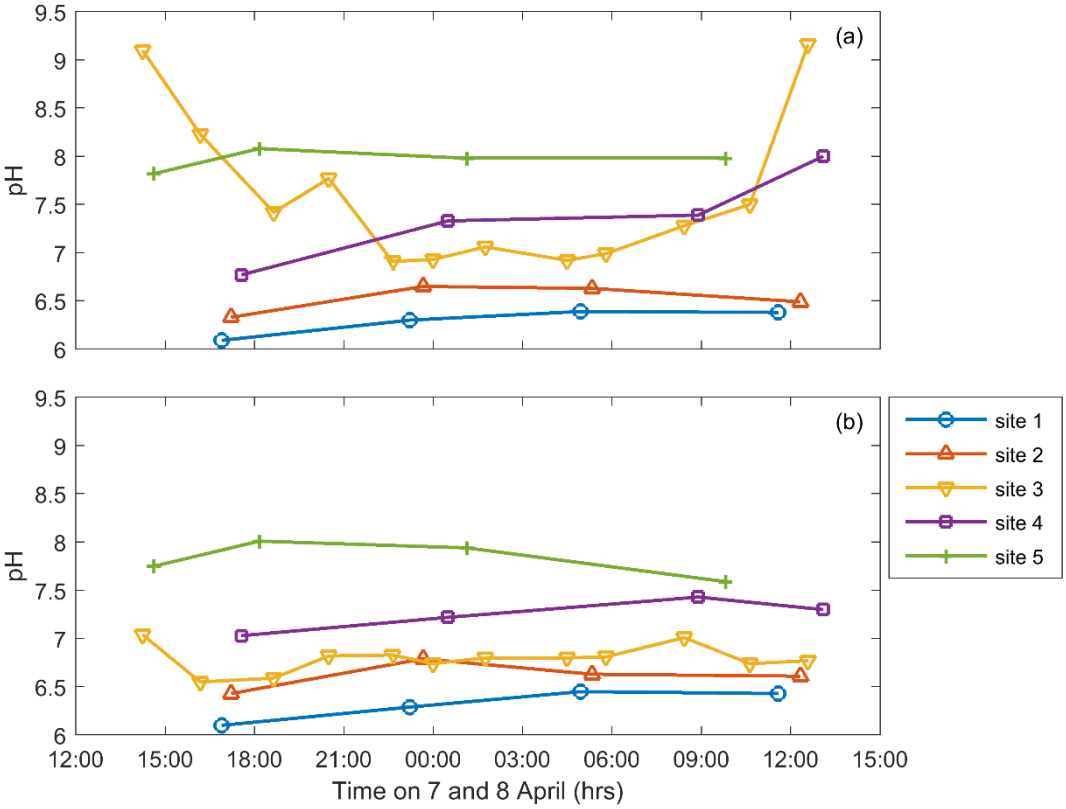

Figure 4.7. Diel pH time-series measurements (extracted from Sonde profile data) at sites 1-5 for (a) surface values and (b) bottom water values, during the 07-08/04/17 sampling period. The sampling frequency was 0.5 Hz.

Alkalinity values were relatively time-uniform across all sites, with the exception of the surface and bottom waters at site 3 and the bottom waters of site 5 (Figure 4.8). Of particular note, at site 3, alkalinity was larger at the bottom than the surface over the 18:00-01:00 h time period, after which values rapidly stabilised to be similar to those observed values at the other sites.

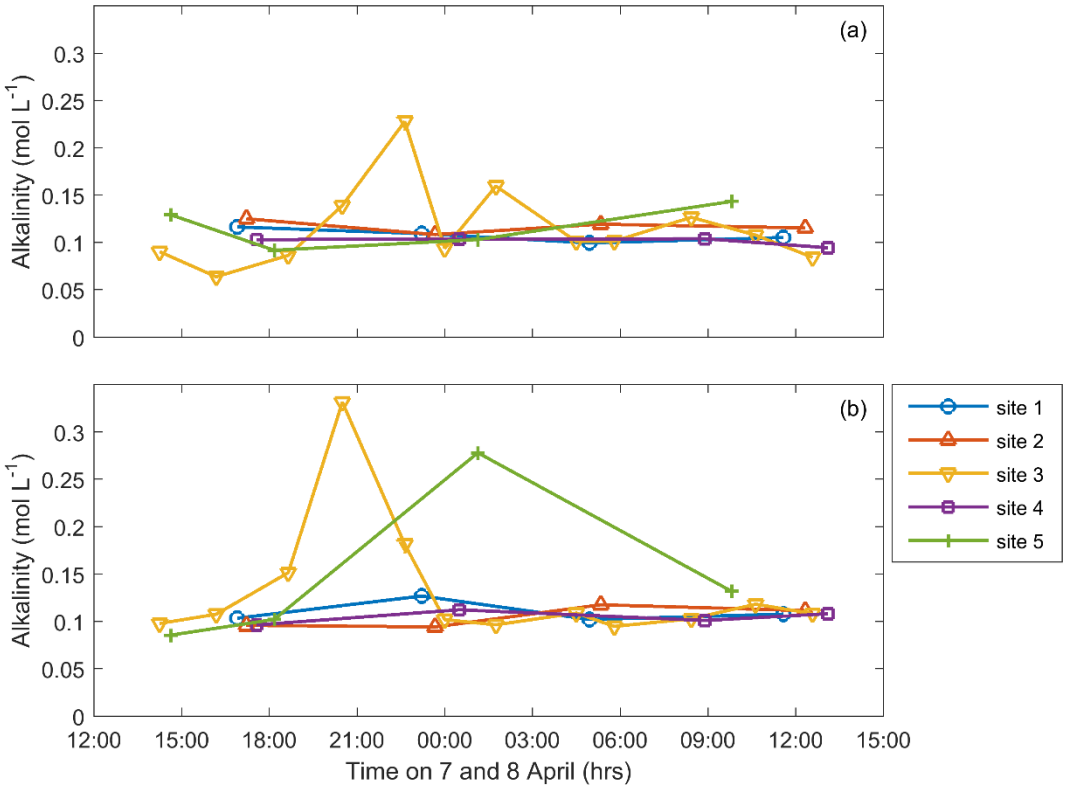

Figure 4.8. Time-series measurements of Alkalinity expressed as (HCO_3^-), obtained from 0.45 µm filtered water samples at sites 1-5 for (a) surface values and (b) bottom water values, during the 07 - 08/04/17 sampling period. Sampling times varied between sites (indicated by markers and colours).

Water Column Profiles (pH, Temperature, Conductivity, Dissolved Oxygen)

Water column profiles taken using the Sonde also supported previous results showing differences between site 3 and other sites. Profiles of pH, DO saturation, temperature and conductivity demonstrated that these parameters at site 3 varied significantly over depth and time (Figure 4.9 a-d). In contrast, sites 1-2 and 4-5 displayed closer to uniform profiles (Figures 4.10 – 4.12). Interestingly, the DO at site 3 dropped significantly overnight to below the DO values for all other sites; whereas during the daytime hours, DO values at site 3 were the highest recorded but had a steep gradient decreasing with depth, again indicating the strong biological controls imposed at this site (Figures 4.9, 4.10-4.12b). Conductivity and temperature values at site 3 appeared to be more similar to values from sites 4-5 than sites 1-2 (Figures 4.10-4.12c,d). Furthermore, site 2 was the most stratified in conductivity and temperature (Figures 4.10-4.12c-d), indicating it was a site of mixing between the stream outlet and lake waters.

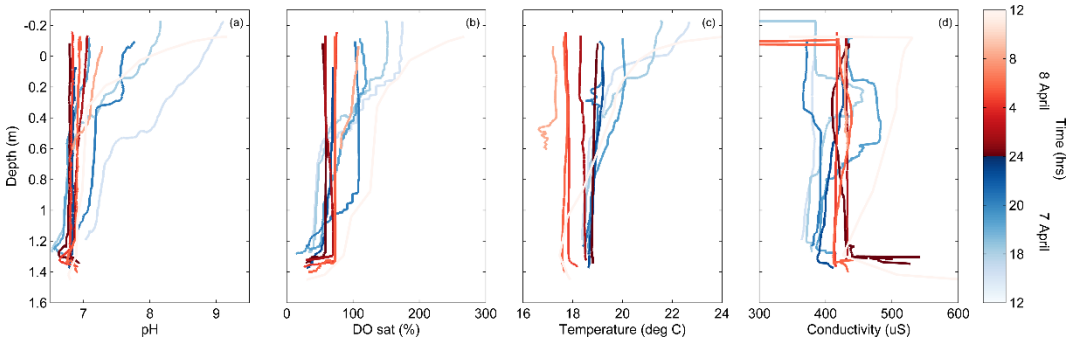

Figure 4.9. Site 3 (*C. demersum* bed), Sonde depth profiles of (a) pH, (b), DO % sat, (c) temperature, and (d) conductivity throughout the full 7/04/17- 8/04/17 sampling period. Y axis is depth and the colorbar denotes the time at which the profile was taken. The sampling frequency was 0.5 Hz.

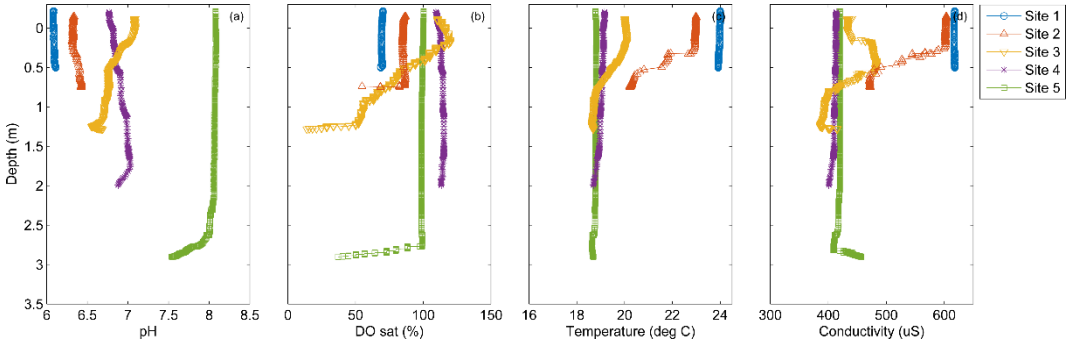

Figure 4.10. Sonde profiles of (a) pH, (b), DO % sat, (c) temperature, and (d) conductivity at sites 1-5 between 4:45 PM and 6:45 PM on 7/04/17. Y axis is depth (m) and sites are represented by colour and marker. The sampling frequency was 0.5 Hz.

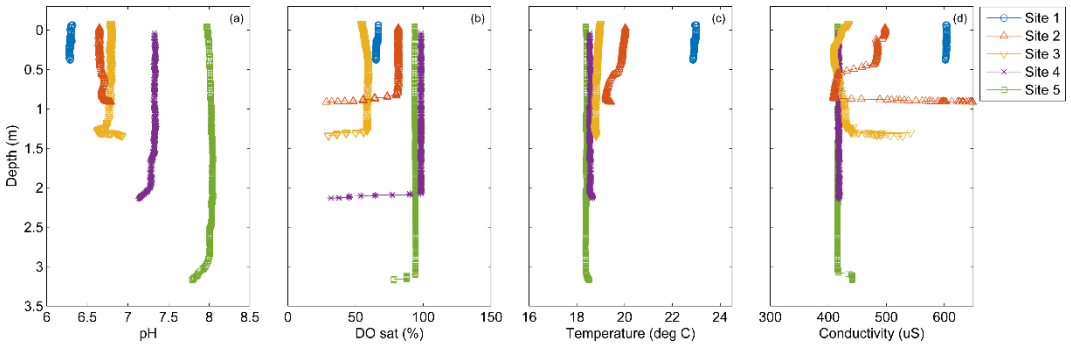

Figure 4.11. Sonde profiles of (a) pH, (b), DO % sat, (c) temperature, and (d) conductivity at sites 1-5 between 11:15 PM and 1:15 AM on 7/04/17 and 8/04/17. Y axis is depth (m) and sites are represented by colour and marker. The sampling frequency was 0.5 Hz.

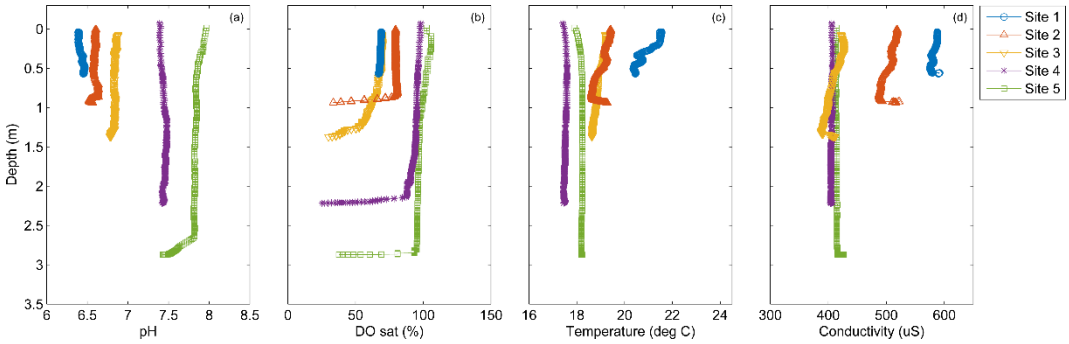

Figure 4.12. Sonde profiles of (a) pH, (b), DO % sat, (c) temperature, and (d) conductivity at sites 1-5 between 4:45 AM and 9:45 AM on 8/04/17on 7/04/17 and 8/04/17. Y axis is depth (m) and sites are represented by colour and marker. The sampling frequency was 0.5 Hz.

4.3.2 Diel Aluminium, Iron, and Phosphorus Concentrations

The physicochemical measurements undertaken and described in the preceding section were also associated with geochemical measurements of Al_{dis}, Fe_{dis} and DRP, at each site within the bay. In general, most sites displayed relatively stable values over the 24 h period, except for site 3, which exhibited substantial variability. At this site, dissolved Al_{dis} within the surface waters reached values as high as 140 μmol L^{-1}, followed by a rapid reduction in Al_{dis} over the night time hours (Figure 4.13a). At site 1 Al_{dis}, concentrations were lower than at site 2, and the lowest concentrations were observed at sites 4 and 5 (Figure 4.13).

Surface Fe_{dis} at site 3 also demonstrated a similar pattern to Al_{dis}, with lower values during night time hours (Figure 4.14a), noting the orders of magnitude difference in concentrations between Fe_{dis} and Al_{dis}. However, unlike Al_{dis}, Fe_{dis} concentration values decreased with distance from the stream outlet (i.e. from sites 1-5).

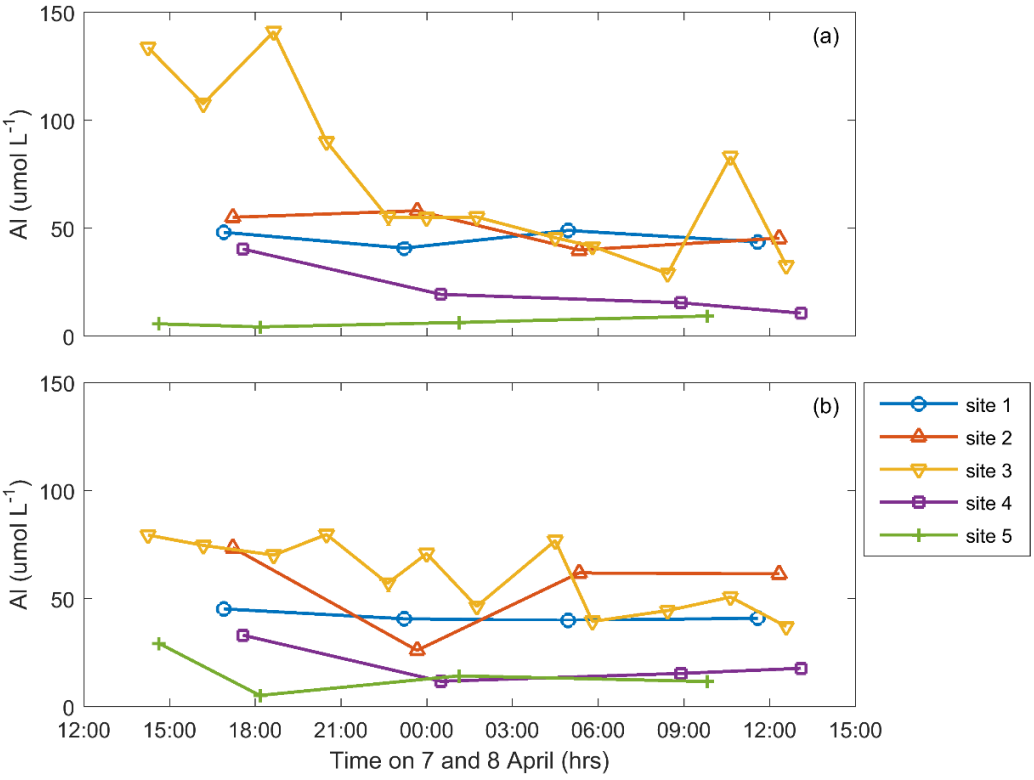

Figure 4.13. Diel dissolved Aluminium (Al_{dis}) time-series measurements obtained from 0.45 μm filtered water samples at sites 1-5 for (a) surface values and (b) bottom water values, during the 07-08/04/17 sampling period. Sampling times varied between sites.

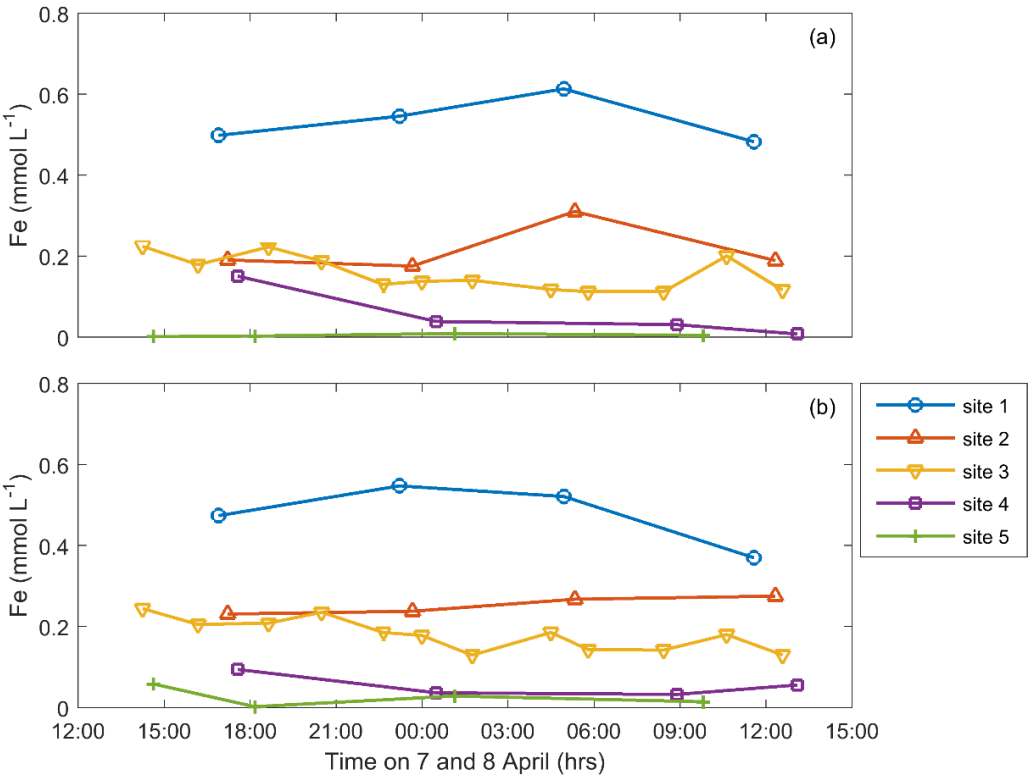

Figure 4.14. Diel dissolved Iron (Fe_{dis}) time-series measurements obtained from 0.45 μm filtered samples at sites 1-5 for (a) surface values and (b) bottom water values, during the 07-08/04/17 sampling period. Sampling times varied between sites.

Patterns of DRP were not as clear cut. In general concentrations at the open water sites declined from site 1 through to site 5 (i.e. with increasing distance from the stream outlet), (Figure 4.15). Differences between surface and bottom waters were minimal. Site 3 had the highest concentrations overall in both surface and bottom waters, and as with the metals, the concentrations decreased during the night time hours. Indeed, maximum surface concentrations were twice those measured around 05:00 (Figure 4.15a).

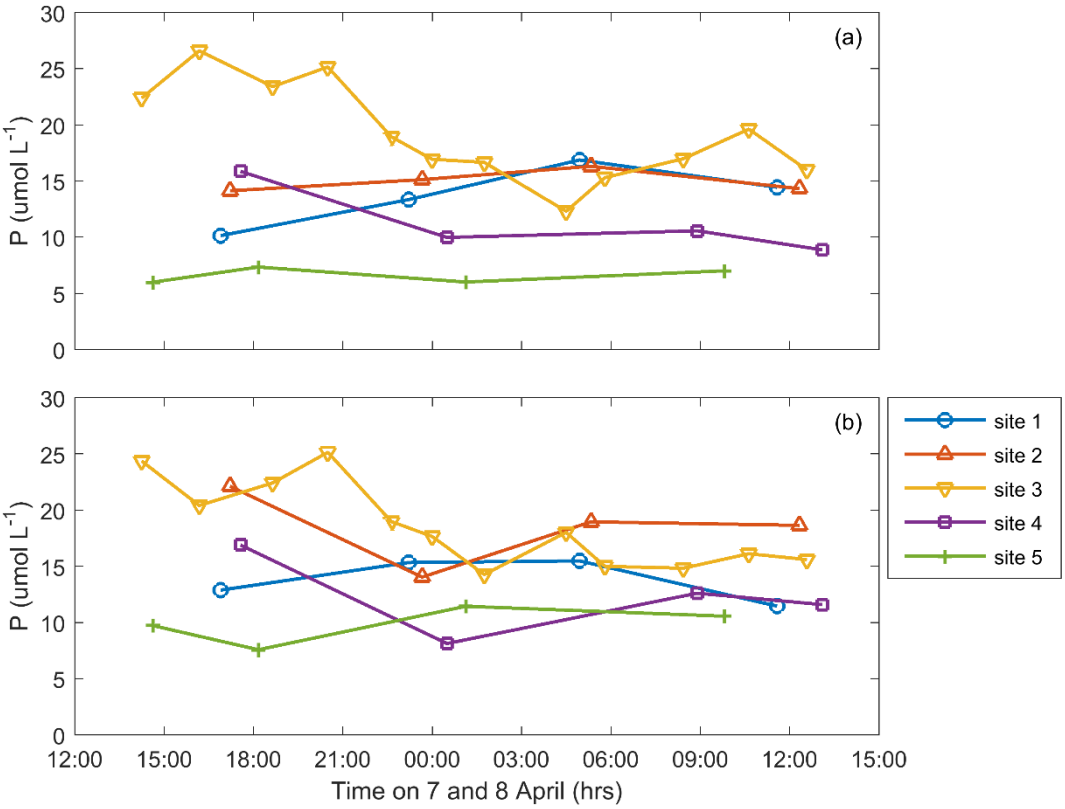

Figure 4.15. Diel dissolved Phosphorus (DRP) time-series measurements obtained from 0.45 μm filtered water samples at sites 1-5 for (a) surface values and (b) bottom water values, during the 07-08/04/17 sampling period. Sampling times varied between sites.

4.3.3 Diel site 3 Aluminium Speciation

PHREEQC speciation modelling indicated that αAl or the fractional dissolved species was primarily in the form of $Al(OH)_4^-$ under conditions present at the site 3 (*C. demersum* beds). pH conditions at this site range between pH of 9 during the daytime to a pH of 7 overnight in surface waters (Figure 4.7a), while in bottom waters pH conditions remained approximately at pH 7 (Figure 4.7b). The differences in pH in both surface and bottom waters is reflected in the relative contributions of $Al(OH)_3$, $Al(OH)^{2+}$, $AlOH^{2+}$, and Al^{3+}

(Figure 4.16a-b). $Al(OH)_{4-}$ contributed the largest proportion of dissolved Al species in both surface and bottom waters (50-150 and 30-70 μmol L^{-1}, respectively), with largest proportions at the surface. At the surface, contributions from other species were at least an order of magnitude smaller; whereas in the bottom waters non-negligible contributions were modelled for $Al(OH)^{2+}$ and $Al(OH)_3$ (Figure 4.16b).

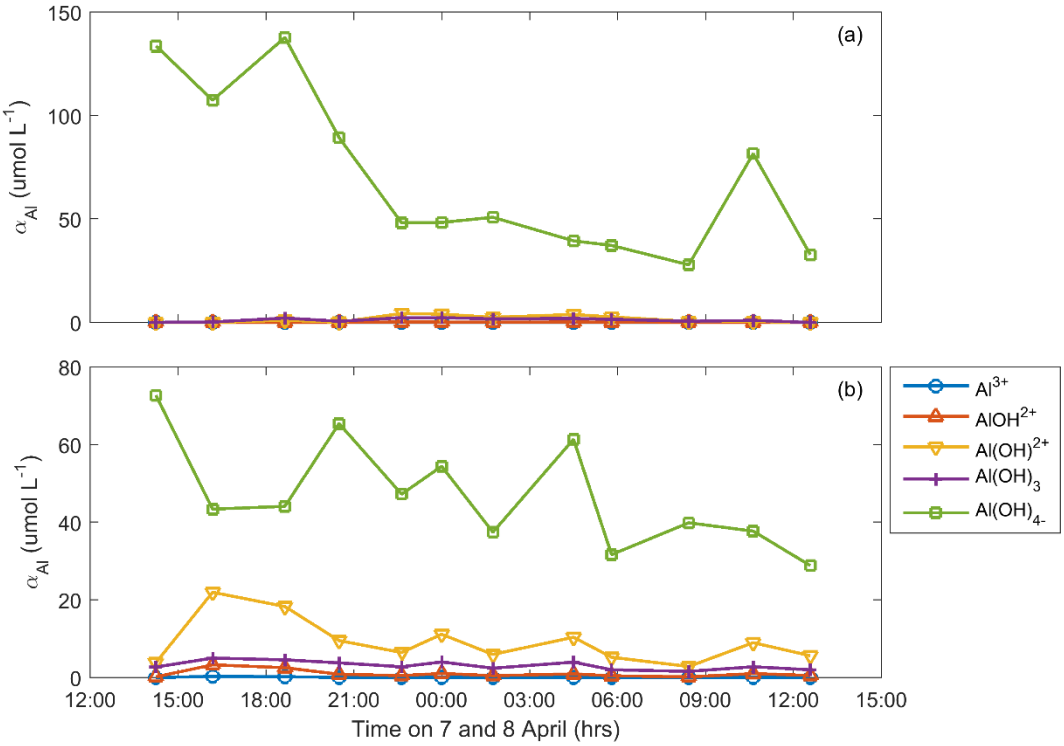

Figure 4.16. Time series of dissolved Aluminium speciation (αAl) based on PHREEQC model output using Al_{dis} data obtained from 0.45 μm filtered water samples at site 3 for (a) surface values and (b) bottom water values, during the 07-08/04/17 sampling period.

4.4 Discussion

4.4.1 Diel physicochemical conditions

A comparison of results from the different sites within Te Wairoa Bay demonstrates the strength of the biogeochemical controls exerted by the beds of submerged aquatic vegetation (*C. demersum*) on the physicochemical conditions within the water column. Overall, physicochemical conditions (pH, temperature, conductivity and DO) at sites 1,4,5 were well mixed in the vertical dimension, and values did not fluctuate substantially over the sampling period, as these sites were in relatively unvegetated water. However, sites 2 and 3 displayed substantial variation with depth and over time (Figures

4.9-4.12). When examining site 3, it is apparent that pH, DO and temperature displayed similar patterns with time (Figure 4.9): bottom waters maintained relatively constant values whereas the properties of the surface waters showed far greater fluctuations.

During daytime hours, the *C. demersum* beds photosynthesize taking up HCO_{3^-} producing O_2 and OH^-. At site 3, within a thin surface layer (~10 cm), high rates of photosynthesis during daytime hours, led to substantial increases in OH^- activity which results in large changes in pH (from ~7 to 9) (Figure 4.7 a,b). pH showed much greater variation in the surface waters than in the bottom waters. Conversely, sampling sites 1,2 and 5 which were generally free of SAV, displayed very little variation in pH throughout the sampling timeframe. However, pH at site 4 also varied (from 6.8 to 8), which could have been due to the water from site 3 and the areas of substantial *C. demersum* coverage being transported into the bay. The phenomenon of pH driven changes from SAV within natural waters is a well-studied process and can lead to conditions which are able to influence water column structure, changes in local geochemical conditions such as the pH driven dissolution of many elemental species, as well as influence biogeochemical spatial heterogeneity within lakes (James & Barko 1991; Jeppesen *et al.* 1997; Mackay *et al.* 2011b).

Alkalinity at site 3 also exhibited large fluctuations: values increased rapidly in the later afternoon/early evening and decreasing rapidly thereafter. Such a large change in alkalinity values could potentially be linked to DIC drawdown and calcium carbonate precipitation under high pH conditions followed by dissolution and biological respiration which contribute to the lower pH values at night (Figures 4.7 and 4.8) (Mook 2000; Nimick *et al.* 2011). Sporadic increases in HCO_3^- during the early evening (Figure 4.8) could be related to the dissolution of $CaCO_3$ thereby buffering some of the pH change.

Site 3 also appears to represent the trailing edge of a physical mixing region between the stream outlet water and lake water with profiles of temperature and conductivity generally showing values between sites 1,2 and sites 4,5, but much closer to the lake values (sites 4 and 5). These results are

perhaps unsurprising as vegetation beds slow flow and remove momentum and energy available for mixing (Nepf 2012b).

4.4.2 Diel Al_{dis}, Fe_{dis}, and DRP concentrations

The diel coupled cycling of O_2 and DIC played an important role in the thermodynamic geochemical behaviour of site 3 primarily through the large shifts in pH, and such conditions are often observed within lakes over these timescales (Maberly 1996; Nimick *et al.* 2011). Geochemical measurements at this site displayed markedly higher concentrations (particularly at the surface) and more variability of $Al_{dis,}$ Fe_{dis} and DRP (Figures 4.13 to 4.15). These large variations are likely to be due to thermodynamic phase transitions and adsorption-desorption reactions on account of shifts in pH (Warren & Haack 2001; Xue *et al.* 2012). Amorphous particulate fractions of Al and Fe as well as colloidal Fe, much of which undoubtedly carries adsorbed P, are transported from the stream outlet (sites 1 and 2) to site 3, where the *C. demersum* beds provide a three- dimensional surface which can trap sediments and particles in addition to reducing flow velocities (Madsen *et al.* 2001). During daytime hours, the photosynthetically driven increases in pH leads to physicochemical conditions which favour dissolution of particulate $Al(OH)_3$ and $Fe(OH)_3$. This dissolution causes Al and Fe bound P to be released to the water column (Eisenreich & Armstrong 1978; Lijklema 1980; Karamalidis & Dzombak 2010). Although, Fe_{dis} values were an order of magnitude higher than Al_{dis} values, it could be argued that increased DRP concentrations were more closely coupled to Al than to Fe, as increased Fe dissolution coupled to P desorption would result in much larger DRP values (Shirley & Hartland, unpublished data).

Conversely, at night, the respiration-driven decreases in pH lead to decreases in Al_{dis}, Fe_{dis} and DRP, particularly in the surface waters at site 3. SAV driven respiration also removes O_2 explaining the change to a more uniform profile (Figure 4.9b). Although diel changes in DO in the bottom waters were relatively small in comparison to those at the surface, they could nonetheless potentially lead to anoxic conditions which could also result in DRP release from redox labile Fe bound P from the sediment. The trapping of particulates

in the *C. demersum* beds at and around site 3 also appears to result in a reduction in Al_{dis} at sites 4 and 5. At site 1 Al_{dis}, concentrations were lower than at site 2 (Figure 4.13) reflecting the likely phase transition from particulate form to dissolved form as pH values increased at the stream outlet (Figure 4.13). This increased solubility is attributed to the higher fraction of the soluble $Al(OH)_{4^-}$ species which is favoured under increased pH and is synonymous with the modelled Al_{dis} speciation seen at site 3 (Figure 4.16) as pH values changed over the diel cycle.

Modelled speciation indicated that the primary Al species present at site 3 was the dissolved $Al(OH)_4^-$ anion. Although these results do not consider the fraction of amorphous or solid $Al(OH)_3$, this result gives credence to the desorption of DRP binding at site 3. It is evident that the dynamic changes in in both Al and P are likely to be associated with the changes in Al species and the effects that charge has on the desorption of P when amorphous $Al(OH)_3$ transitions to $Al(OH)_4^-$ (Dzombak & Morel 1990; Karamalidis & Dzombak 2010). ANZECC guidelines state that a level of 0.055 mg L^{-1} is the trigger value for ecotoxicity of Al_{dis} in natural waters. At site 3, values of Al_{dis} were in exceedance during the day times coinciding with high pH values (see Appendix). Lake Rotoehu is characterised by large patches of *C. demersum*, and therefore such conditions could be common over much of Te Wairoa Bay. Furthermore, the prevalence of phytoplankton blooms within Lake Rotoehu and their ability to increase pH is a well-known process, thus the interaction of high Al concentrations with phytoplankton blooms could also present conditions which would favour high dissolved Al concentrations.

The key processes within the *C. demersum* beds are summarised in the conceptual diagram in Figure 4.17, which highlights the relevant biogeochemical changes throughout the diel cycle. Longer-term variations (seasonal etc.) are not considered here.

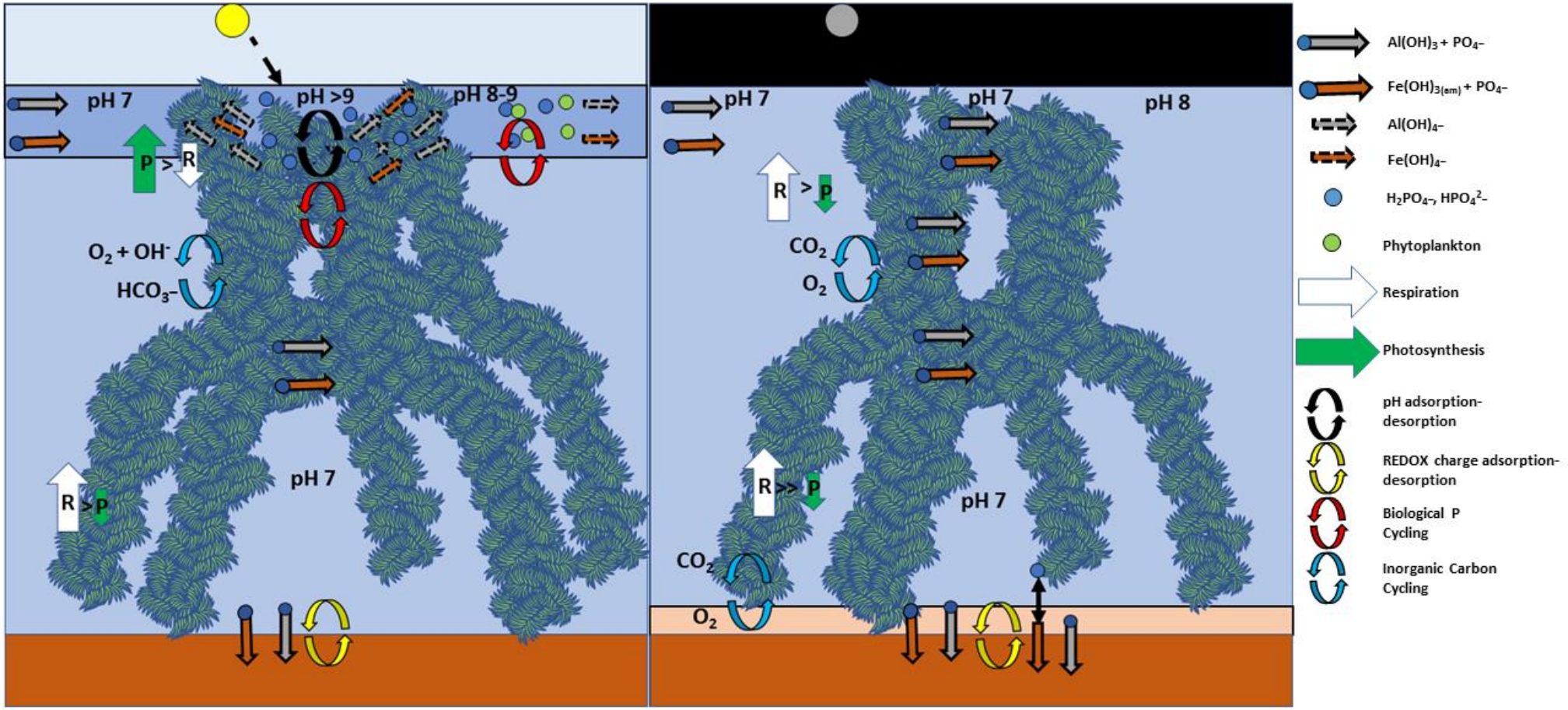

Figure 4.17. Conceptual summary of the biogeochemical processes operating in the *C. demersum* beds in Te Wairoa Bay in Lake Rotoehu, based on measurements from site 3. (a) and (b) show day and night time conditions, respectively.

CHAPTER FIVE

CONCLUSIONS

5.1 Thesis summary

This thesis examined physicochemical and biogeochemical processes within the Waitangi Springs/Te Wairoa Bay system in Lake Rotoehu, New Zealand. In particular, it examined how physicochemical conditions influenced the concentrations and phase transformations of Al, Fe and P within the water column. A major aim of this thesis was to assess the effects of alum dosing across the stream/lake interface. The major findings of this thesis were:

1. Overall, pH, O_2 and DRP values increased with distance from the Waitangi Springs outlet into the Bay, although some patchiness was observed. Conversely, temperature, major ion concentrations and conductivity all decreased with distance into the bay.
2. The ecogeomorphological setting of the Waitangi springs affects the transportation of sediments and geochemical particulate matter into the bay. In particular, dense vegetation within the stream and the stream-lake interface increases hydrodynamic drag, reduces flow velocities and promotes the deposition of such sediments and particulate matter. Sediment cores indicated that Al and Fe deposition was highest at the stream outlet.
3. Dense *C. demersum* beds also played a critical role in altering water column properties and mixing. During day time hours, when rates of photosynthesis were high, high pH and O_2 levels locally influenced the concentrations and speciation of Al, Fe and DRP. These processes control the availability of limiting nutrients within Lake Rotoehu.
4. An analysis of the longer-term trends (since 2001) indicated a reduction in total nitrogen, total phosphorus and Chl-*a* until the alum-dosing commenced in 2011. After the start of alum dosing, concentrations continued to decrease until around 2014 since

which time, levels have been sharply increasing. Over these last few years, the system appears to be predominantly N and P co-limited.

5. Alum dosing is an effective method in reducing DRP within the Waitangi Springs and the receiving Te Wairoa Bay. Although dosing is effective, high colloidal and particulate Fe is likely to be a major sink for DRP within the system. Furthermore, it appears that several physicochemical and biogeochemical processes (pH and diel biological respiration) are key factors influencing the spatial heterogeneity and control Al-P and Fe-P dynamics. In particular DRP is sequestered through adsorption, and incorporated into the lake bed by flocculation and deposition at the Waitangi Springs outlet (see conceptual model Figure 3.27). A longer term strategy for the continued use of in-stream alum-dosing should be explored, in order to maximise the effectiveness of this remediation method moving into the future.

5.2 Implications for management of Lake Rotoehu and recommendations for future research

The results obtained here have several implications which should be considered as part of the overall management of Lake Rotoehu. While alum dosing appears to be an effective method for DRP removal, the formation of alum flocs at the outlet appears to promote sediment deposition. This deposition, combined with effects from recent clearcutting within the catchment may lead to infilling and potentially also heightened P loads in Te Wairoa Bay. The local nature of this deposition and limited dispersal capabilities of the stream implies that alum is not reaching a great distance into the lake, and therefore its P-binding capabilities are restricted to Te Wairoa Bay.

Results indicate that TP, TN and Chl-*a* levels have increased over the past few years. The mechanisms responsible for this shift are not yet known, but could be related to climatic shifts, changes in nutrient pools, or the use of lake remediation methods other than alum-dosing (e.g. such as vegetation

removal or nitrogen control). However, such an increase in levels should be monitored closely and be investigated further. Measurements also demonstrated considerable heterogeneity over the relatively small spatial scales of Te Wairoa Bay and over a single diel cycle. Further spatio-temporal high-resolution measurements would be required to more carefully quantify the dynamics within the lake.

From a lake-wide perspective, further work should focus on the spatial geochemical characteristics of the sediments at the lake bed, see James (2011). In particular, the coupled iron-sulfur-phosphorus dynamics (pyrite formation) should be examined in order to ascertain the potential for binding P and P-cycling. Moreover, Lake Rotoehu is characterised by a number of smaller arms and embayments, and these areas could be used as sites in which to explore alternative alum-dosing techniques in search of an improvement in the P-locking capabilities of the sediments.

REFERENCES

Abell JM, Hamilton DP (2015) Biogeochemical processes and phytoplankton nutrient limitation in the inflow transition zone of a large eutrophic lake during a summer rain event. *Ecohydrology*, **8**, 243–262.

Abell JM, Özkundakci D, Hamilton DP (2010) Nitrogen and phosphorus limitation of phytoplankton growth in New Zealand lakes: Implications for eutrophication control. *Ecosystems*, **13**, 966–977.

Adrian R, O'Reilly CM, Zagarese H *et al.* (2009) Lakes as sentinels of climate change. *Limnology and Oceanography*, **54**, 2283–2297.

Allan MG, Hamilton DP, Trolle D, Muraoka K, McBride C (2016) Spatial heterogeneity in geothermally-influenced lakes derived from atmospherically corrected Landsat thermal imagery and three-dimensional hydrodynamic modelling. *International Journal of Applied Earth Observation and Geoinformation*, **50**, 106–116.

Andersen DT, Sumner DY, Hawes I, Webster-Brown J, Mckay CP (2011) Discovery of large conical stromatolites in Lake Untersee, Antarctica. *Geobiology*, **9**, 280–293.

Anderson D, Glibert P, Burkholder J (2002) Harmful algal blooms and eutrophication: nutrient sources, compositions, and consequences. *Estuaries*, **25**, 704–726.

Anderson G, Taylor M (2008) *Denitrification in a Rotoehu Stream, 2nd installation. Report LC0809/149 for Environment Bay of Plenty.* Landcare Research, Hamilton, New Zealand.

Aufdenkampe AK, Mayorga E, Raymond PA *et al.* (2011) Riverine coupling of biogeochemical cycles between land, oceans, and atmosphere. *Frontiers in Ecology and the Environment*, **9**, 53–60.

Ballantine DJ, Tanner CC (2010) Substrate and filter materials to enhance phosphorus removal in constructed wetlands treating diffuse farm runoff: a review. *New Zealand Journal of Agricultural Research*, **53**, 71–95.

Barbiero R, Carlson RE, Cooke GD, Beals AW (1988) The Effects of a Continuous Application of Aluminum Sulfate on Lotic Benthic Invertebrates. *Lake and Reservoir Management*, **4**, 63–72.

Barko JW, Adams MS, Clesceri NL (1986) Environmental factors and their consideration in the management of submersed aquatic vegetation: a review. *Journal of Aquatic Plant Management*, **24**, 1–10.

Barko JW, Gunnison D, Carpenter SR (1991) Sediment interactions with submersed macrophyte growth and community dynamics. *Aquatic Botany*, **41**, 41–65.

Barko JW, James WF (1998) Effects of submerged aquatic macrophytes on nutrient dynamics, sedimentation, and resuspension. In: *The structuring role of submerged macrophytes in lakes* (eds Jeppesen E, Søndergaard M, Søndergaard M, Christoffersen K), pp. 197–214. Springer, New York, NY, U.S.A.

Berg U, Neumann T, Donnert D, Nüesch R, Stüben D (2004) Sediment capping in eutrophic lakes - efficiency of undisturbed calcite barriers to immobilize phosphorus. *Applied Geochemistry*, **19**, 1759–1771.

Bernhardt H (1980) Reservoir protection by in-river nutrient reduction. In: *Restoration of Lakes and Inland Waters*, pp. 272–277. USEPA 440/5-81-010.

Best EPH, Visser HWC (1987) Seasonal growth of the submerged macrophyte *Ceratophyllum demersum* L. in mesotrophic Lake Vechten in relation to insolation, temperature and reserve carbohydrates. *Hydrobiologia*, **148**, 231–243.

Bioresearches (2003) *Estimate of the geothermal nutrient inputs to twelve rotorua lakes. Report for Environment Bay of Plenty*.

Boano F, Harvey JW, Marion A *et al.* (2014) Hyporheic flow and transport processes: Mechanisms, models, and biogeochemical implications. *Reviews of Geophysics*, 1–77.

Boers PCM (1991) The influence of pH on phosphate release from lake sediments. *Water Research*, **25**, 309–311.

Bogut I, Čerba D, Vidaković J, Gvozdić V (2010) Interactions of weed-bed invertebrates and *Ceratophyllum demersum* stands in a floodplain lake. *Biologia*, **65**, 113–121.

BOPRC (2007) *Lake Rotoehu Action Plan. Environmental Publication 2007/19*. Bay of Plenty Regional Council.

Boström B, Andersen JM, Fleischer S, Jansson M (1988) Exchange of phosphorus across the sediment-water interface. *Hydrobiologia*, **170**, 229–244.

Bromley CJ, Bottomley JJ, Pearson CF (1988) Geophysical exploration for prospective geothermal resources in the Tarawera Forest. In: *Proceedings 10th New Zealand Geothermal Workshop*, pp. 123–128.

Browman M, Harris R, Armstrong D, Chesters G (1977) *Interaction of soluble phosphate with aluminum hydroxide in lakes. Technical Report No. 77-05*. Water Resources Center, University of Wisconsin, Madison, Wisc.

Browne P, Evans M (2004) *Second stage phosphorus removal for Rotorua lakes / streams. Report for Environment Bay of Plenty*. URS New Zealand Limited, Auckland, New Zealand.

Burger DF, Hamilton DP, Pilditch CA, Gibbs MM (2007) Benthic nutrient fluxes in a eutrophic, polymictic lake. *Hydrobiologia*, **584**, 13–25.

Burns N, McIntosh J, Scholes P (2009) Managing the lakes of the Rotorua District, New Zealand. *Lake and Reservoir Management*, **25**, 284–296.

Burton T, Clayton J (2015) *Assessment of the Rotorua Te Arawa lakes using LakeSPI - 2015. Report HAM2015-091 for Bay of Plenty Regional Council*. NIWA, Hamilton, New Zealand.

Canfield DE, Kristensen E, Thamdrup B (2005) *Aquatic Geomicrobiology*. Elsevier, San Diego, California, U.S.A.

Caraco N, Cole J, Findlay S, Wigand C (2006) Vascular plants as engineers of oxygen in aquatic systems. *BioScience*, **56**, 219.

Caraco NF, Cole JJ, Likens GE (1989) Evidence for sulphate-controlled phosphorus release from sediments of aquatic systems. *Nature*, **341**, 316–318.

Carpenter SR, Benson BJ, Biggs R *et al.* (2007) Understanding Regional Change: A Comparison of Two Lake Districts. *BioScience*, **57**, 323–335.

Carpenter S, Caraco N, Correll D *et al.* (1998) Nonpoint pollution of surface waters with phosphorus and nitrogen. *Ecological Application*, **8**, 559–568.

Carter D (1973) A preliminary investigation of the location and general ecology of mat plants in the Rotorua Lake District. *Tane*, **19**, 233–242.

Carter V, Barko JW, Godshalk GL, Rybicki NB (1988) Effects of submersed macrophytes on water quality in the tidal Potomac River, Maryland. *Journal of Freshwater Ecology*, **4**, 493–501.

Cassie V (1978) Seasonal changes in phytoplankton densities in four North Island lakes, 1973-74. *Journal of Marine and Freshwater Research*, **12**, 153–66.

Cole JJ, Caraco NF, Kling GW *et al.* (1994) Carbon Dioxide Supersaturation in the Surface Waters of Lakes. *Science*, **265**, 1568–1570.

Conley DJ, Paerl HW, Howarth RW *et al.* (2009) Controlling eutrophication: nitrogen and phosphorus. *Science*, **323**, 1014–1015.

Cooke GD, Carlson RE (1986) Water quality management in a drinking water reservoir. *Lake and Reservoir Management*, **2**, 363–371.

Cooke GD, Welch EB, Martin AB *et al.* (1993) Effectiveness of Al, Ca, and Fe salts for control of internal phosphorus loading in shallow and deep lakes. *Hydrobiologia*, **253**, 323–335.

Cooke GD, Welch EB, Peterson SA, Nichols SA (2005) *Restoration and management of lakes and reservoirs*. Taylor & Francis, New York, NY, U.S.A.

Correll DL (1998) The role of phosphorus in the eutrophication of receiving waters: A review. *Journal of Environment Quality*, **27**, 261.

Couture RM, Fischer R, Van Cappellen P, Gobeil C (2016a) Non-steady state diagenesis of organic and inorganic sulfur in lake sediments. *Geochimica et Cosmochimica Acta*, **194**, 15–33.

Couture RM, Fischer R, Van Cappellen P, Gobeil C (2016b) Non-steady state diagenesis of organic and inorganic sulfur in lake sediments. *Geochimica et Cosmochimica Acta*, **194**, 15–33.

Cullen P, Forsberg C (1988) Experiences with reducing point sources of phosphorus to lakes. *Hydrobiologia*, **170**, 321–336.

Das SK, Routh J, Roychoudhury AN, Val Klump J, Ranjan RK (2009) Phosphorus dynamics in shallow eutrophic lakes: An example from Zeekoevlei, South Africa. *Hydrobiologia*, **619**, 55–66.

Davison W (1993) Iron and manganese in lakes. *Earth-Science Reviews*, **34**, 119–163.

Davison W (2016) *Diffusive gradients in thin-films for environmental measurements*. Cambridge University Press, Cambridge, U.K.

Dodds WK, Bouska WW, Eitzmann JL *et al.* (2009) Eutrophication of U. S. freshwaters: Analysis of potential economic damages. *Environmental Science and Technology*, **43**, 12–19.

Dol Hamid R, Swedlund PJ, Song Y, Miskelly GM (2011) Ionic strength effects on silicic acid (H_4SiO_4) sorption and oligomerization on an iron oxide surface: An interesting interplay between electrostatic and chemical forces. *Langmuir*, **27**, 12930–12937.

van Donk E, Gulati RD, Iedema A, Meulemans JT (1993) Macrophyte-related shifts in the nitrogen and phosphorus contents of the different trophic levels in a biomanipulated shallow lake. *Hydrobiologia*, **251**, 19–26.

Douglas GB (2002) Remediation material and remediation process for sediment, Patent No.: US 6,350,383 B1, 26 February 2002.

Douglas GB, Hamilton DP, Robb MS *et al.* (2016a) Guiding principles for the development and application of solid-phase phosphorus adsorbents for freshwater ecosystems. *Aquatic Ecology*, **50**, 385–405.

Douglas GB, Lurling M, Spears BM (2016b) Assessment of changes in potential nutrient limitation in an impounded river after application of lanthanum-modified bentonite. *Water Research*, **97**, 47–54.

Downing-Kunz MA, Stacey MT (2012) Observations of mean and turbulent flow structure in a free-floating macrophyte root canopy. *Limnology and Oceanography: Fluids and Environments*, **2**, 67–79.

Driscoll CT, Schecher WD (1990) The chemistry of aluminum in the environment. *Environmental Geochemistry and Health*, **12**, 28–49.

Dzombak DA, Morel F (1990) *Surface complexation modeling: Hydrous ferric oxide*. Wiley, New York.

Egemose S, Reitzel K, Andersen F, Flindt MR (2010) Chemical lake restoration products: Sediment stability and phosphorus dynamics. *Environmental Science and Technology*, **44**, 985–991.

Egemose S, Reitzel K, Andersen F, Jensen HS (2013) Resuspension-mediated aluminium and phosphorus distribution in lake sediments after aluminium treatment. *Hydrobiologia*, **701**, 79–88.

Egemose S, Sønderup MJ, Beinthin M V. *et al.* (2012) Crushed concrete as a phosphate binding material: A potential new management tool. *Journal of Environmental Quality*, **41**, 647–653.

Egemose S, de Vicente I, Reitzel K *et al.* (2011) Changed cycling of P, N, Si, and DOC in Danish Lake Nordborg after aluminum treatment. *Canadian Journal of Fisheries and Aquatic Sciences*, **68**, 842–856.

Egemose S, Wauer G, Kleeberg A (2009) Resuspension behaviour of aluminium treated lake sediments: Effects of ageing and pH. *Hydrobiologia*, **636**, 203–207.

Eisenreich SJ, Armstrong DE (1978) Adsorption of inorganic and organic phosphorus by amorphous aluminum hydroxide. *Journal of Environmental Science and Health Part A: Environmental Science and Engineering: Toxic/Hazardous Substances and Environmental Engineering*, **13**, 337–364.

Elder JF (1989) *Metal biogeochemistry in surface-water systems — A review of principles and concepts*. United States Geological Survey, Denver, Colorado, U.S.A.

Emerson S (1976) Early diagenesis in anaerobic lake sediments: Chemical equilibria in interstitial waters. *Geochimica et Cosmochimica Acta*, **40**, 925–934.

Emerson S, Widmer G (1978) Early diagenesis in anaerobic lake sediments-II. Thermodynamic and kinetic factors controlling the formation of iron phosphate. *Geochimica et Cosmochimica Acta*, **42**, 1307–1316.

European Parliament and the Council of the European Union (2000) Directive 2000/60/EC of the European Parliament and of the Council of 23 October 2000 establishing a framework for Community action in the field of water policy. *Official Journal of the European Communities*, **L327**, 1–82.

Evans MJ, Deny LA, France-Lanord C (2004) Geothermal fluxes of alkalinity in the Narayani river system of central Nepal. *Geochemistry, Geophysics, Geosystems*, **5**.

Fastner J, Abella S, Litt A *et al.* (2016) Combating cyanobacterial proliferation by avoiding or treating inflows with high P load—experiences from eight case studies. *Aquatic Ecology*, **50**, 367–383.

Fee EJ (1979) A relation between lake morphometry and primary productivity and its use in interpreting whole lake eutrophication experiments. *Limnology and Oceanography*, **24**, 401–416.

Fischer HB, List EJ, Koh RCY, Imberger J, Brooks NH (1979) *Mixing in inland and coastal waters*. Academic Press, London, U.K.

Fish GR (1970) A limnological study of four lakes near Rotorua. *New Zealand Journal of Marine and Freshwater Research*, **4**, 165–194.

Flynn Jr. CM (1984) Hydrolysis of inorganic iron(III) salts. *Chemical Reviews*, **84**, 31–41.

Foley JA, DeFries R, Asner GP *et al.* (2005) Global Consequences of Land Use. *Science*, **8**, 570–575.

Froelich PN (1988) Kinetic control of dissolved phosphate in natural rivers and estuaries: A primer on the phosphate buffer mechanism. *Limnology and Oceanography*, **33**.

Gächter R, Meyer JS (1993) The role of microorganisms in mobilization and fixation of phosphorus in sediments. *Hydrobiologia*, **253**, 103–121.

Gächter R, Müller B (2003) Why the phosphorus retention of lakes does not necessarily depend on the oxygen supply to their sediment surface. *Limnology and Oceanography*, **48**, 929–933.

Garrison PJ, Knauer DR (1984) Long-term evaluation of three alum treated lakes. *Lake and Reservoir Management*, **1**, 513–517.

Gensemer RW, Playle RC (1999) The bioavailability and toxicity of aluminum in aquatic environments. *Critical Reviews in Environmental Science and Technology*, **29**, 315–450.

Gibbs MM, Hickey CW, Özkundakci D (2011a) Sustainability assessment and comparison of efficacy of four P-inactivation agents for managing internal phosphorus loads in lakes: Sediment incubations. *Hydrobiologia*, **658**, 253–275.

Gibbs MM, Stephens S, Wright-Stow A, Edhouse S (2011b) *Current measurements in Lakes Rotorua and Rotoehu 2010 and 2011. Report for Bay of Plenty Regional Council*. NIWA, Hamilton, New Zealand.

Glibert PM, Wilkerson FP, Dugdale RC *et al.* (2016) Pluses and minuses of ammonium and nitrate uptake and assimilation by phytoplankton and implications for productivity and community composition, with emphasis on nitrogen-enriched conditions. *Limnology and Oceanography*, **61**, 165–197.

Goldberg S, Davis JA, Hem JD (1996) The surface chemistry of aluminum oxides and hydroxides. In: *The environmental chemistry of aluminum* (ed Sposito G), pp. 272–318. CRC Press, Boca Raton, Florida, U.S.A.

Government of New Zealand (2014) *National Policy Statement for Freshwater Management 2014*.

Gran G (1952) Determination of the equivalence point in potentiometric titrations. Part II. *The Analyst*, **77**, 661.

Gran G (1988) Equivalence volumes in potentiometric titrations. *Analytica Chimica Acta*, **206**, 111–123.

Greensberg AE, Eaton AD, Franson MAH (1998) *APHA: Standard Methods for the Examination of Water and Wastewater* (MAH Franson, Ed,). American Public Health Association, Washington D.C., U.S.A.

Gross EM, Erhard D, Iványi E (2003) Allelopathic activity of *Ceratophyllum demersum* L. and *Najas marina* ssp. *intermedia* (Wolfgang) Casper. *Hydrobiologia*, **506–509**, 583–589.

Hamilton DP, Collier KJ, Howard-Williams C (2016) Lake restoration in New Zealand. *Ecological Management and Restoration*, **17**, 191–199.

Hamilton DP, Mcbride CG, Jones HFE (2015) *Assessing the effects of alum dosing of two inflows to Lake Rotorua against external nutrient load reductions : Model simulations for 2001-2012. ERI report 49 prepared for Bay of Plenty Regional Council*. University of Waikato, Hamilton, New Zealand.

Hamilton DP, Mitchell SF (1996) An empirical model for sediment resuspension in shallow lakes. *Hydrobiologia*, **317**, 209–220.

Han C, Yao L, Xu D, Xie X, Zhang C (2016) High-resolution imaging of pH in alkaline sediments and water based on a new rapid response fluorescent planar optode. *Scientific Reports*, **6**, 26417.

Harper H (1990) *Long-term performance evaluation of the alum stormwater treatment system at Lake Ella, Florida. Report for Florida Department of Environmental Regulation Project WM339*. Environmental Research and Design, Inc., Orlando, Florida, U.S.A.

Harper HH (2007) Current research and trends in alum treatment of stormwater runoff. In: *The 9th Biennial Conference on Stormwater Research*, pp. 1–14. Orlando, Florida, U.S.A.

Hartland A (2013) The environmental significance of natural nanoparticles. *Nature Education Knowledge*, **4**.

Hartland A, Andersen MS, Hamilton DP (2015a) Phosphorus and arsenic distributions in a seasonally stratified, iron-and manganese-rich lake: Microbiological and geochemical controls. *Environmental Chemistry*, **12**, 708–722.

Hartland A, Larsen JR, Andersen MS, Baalousha M, O'Carroll D (2015b) Association of arsenic and phosphorus with iron nanoparticles between streams and aquifers: Implications for arsenic mobility. *Environmental Science and Technology*, **49**, 14101–14109.

Heinzmann B (1998) Improvement of the surface water quality in the Berlin region. *Water Science and Technology*, **38**, 191–200.

Heinzmann B, Chorus I (1994) Restoration concept for Lake Tegel, a major drinking and bathing water resource in a densely populated area. *Environmental Science and Technology*, **28**, 1410–6.

Henley RW, Ellis AJ (1983) Geothermal systems ancient and modern: A geochemical review. *Earth Science Reviews*, **19**, 1–50.

Hickey CW, Gibbs MM (2009) Lake sediment phosphorus release management—Decision support and risk assessment framework. *New Zealand Journal of Marine and Freshwater Research*, **43**, 819–856.

Hilt S, Gross EM (2008) Can allelopathically active submerged macrophytes stabilise clear-water states in shallow lakes? *Basic and Applied Ecology*, **9**, 422–432.

Hodgson KA, Nairn IA (2004) *The sedimentation and drainage history of Haroharo Caldera and the Tarawera River system, Taupo Volcanic Zone, New Zealand. Environment Bay of Plenty Operations Publication 2004/3*. Environment Bay of Plenty, Whakatane, New Zealand.

Hoellein TJ, Bruesewitz DA, Hamilton DP (2012) Are geothermal streams important sites of nutrient uptake in an agricultural and urbanising landscape (Rotorua, New Zealand)? *Freshwater Biology*, **57**, 116–128.

Hurwitz S, Lowenstern J (2014) Dynamics of the Yellowstone hydrothermal system. *Reviews of Geophysics*, **52**, 522–555.

Huser BJ, Bajer PG, Chizinski CJ, Sorensen PW (2016a) Effects of common carp (*Cyprinus carpio*) on sediment mixing depth and mobile phosphorus mass in the active sediment layer of a shallow lake. *Hydrobiologia*, **763**, 23–33.

Huser B, Brezonik P, Newman R (2011) Effects of alum treatment on water quality and sediment in the Minneapolis Chain of Lakes, Minnesota, USA. *Lake and Reservoir Management*, **27**, 220–228.

Huser BJ, Egemose S, Harper H *et al.* (2016b) Longevity and effectiveness of aluminum addition to reduce sediment phosphorus release and restore lake water quality. *Water Research*, **97**, 122–132.

Huser BJ, Pilgrim KM (2014) A simple model for predicting aluminum bound phosphorus formation and internal loading reduction in lakes after aluminum addition to lake sediment. *Water Research*, **53**, 378–385.

Huser BJ, Rydin E (2005) Phosphorus inactivation by aluminum in Lakes Gårdsjön and Härsvatten sediment during the industrial acidification period in Sweden. *Canadian Journal of Fisheries and Aquatic Sciences*, **1709**, 1702–1709.

Hutton G, Haller L (2004) *Evaluation of the costs and benefits of water and sanitation improvements at the global level. Report WHO/SDE/WSH/04.04*. World Health Organization, Geneva, Switzerland.

Imberger J, Patterson JC (1989) Physical Limnology. In: *Advances in Applied Mechanics*, pp. 303–475. Academic Press, Boston, U.S.A.

Istvánovics V (2008) The Role of Biota in Shaping the Phosphorus Cycle in Lakes. *Freshwater Reviews*, **1**, 143–174.

Izydorczyk K, Skowron A, Wojtal A, Jurczak T (2008) The stream inlet to a shallow bay of a drinking water reservoir, a “hot-spot” for *Microcystis* blooms initiation. *International Review of Hydrobiology*, **93**, 257–268.

James WF (2011) Variations in the aluminum:phosphorus binding ratio and alum dosage considerations for Half Moon Lake, Wisconsin. *Lake and Reservoir Management*, **27**, 128–137.

James WF, Barko JW (1991) Littoral-pelagic phosphorus dynamics during nighttime convective circulation. *Limnology and Oceanography*, **36**, 949–960.

Jansson M, Olsson H, Pettersson K (1988) Phosphatases; origin, characteristics and function in lakes. *Hydrobiologia*, **170**, 157–175.

Jarvie HP, Sharpley AN, Spears B *et al.* (2013) Water quality remediation faces unprecedented challenges from "legacy phosphorus." *Environmental Science and Technology*, **47**, 8997–8998.

Jensen HS, Kristensen P, Jeppesen E, Skytthe A (1992) Iron:phosphorus ratio in surface sediment as an indicator of phosphate release from aerobic sediments in shallow lakes. *Hydrobiologia*, **235–236**, 731–743.

Jensen HS, Reitzel K, Egemose S (2015) Evaluation of aluminum treatment efficiency on water quality and internal phosphorus cycling in six Danish lakes. *Hydrobiologia*, **751**, 189–199.

Jeppesen E, Kristensen P, Jensen JP *et al.* (1991) Recovery resilience following a reduction in external phosphorus loading of shallow, eutrophic danish lakes. *Memorie dell'Istituto Italiano di Idrobiologia*, **48**, 127–148.

Jeppesen E, Søndergaard M, Jensen JP *et al.* (2005) Lake responses to reduced nutrient loading - an analysis of contemporary long-term data from 35 case studies. *Freshwater Biology*, **50**, 1747–1771.

Jeppesen E, Søndergaard M, Meerhoff M, Lauridsen TL, Jensen JP (2007) Shallow lake restoration by nutrient loading reduction - some recent findings and challenges ahead. *Hydrobiologia*, **584**, 239–252.

Jeppesen E, Søndergaard M, Søndergaard M, Christoffersen K (1997) *The Structuring Role of Submerged Macrophytes in Lakes*. Springer New York, New York, NY, U.S.A.

Jiang JQ, Graham NJD (1998) Pre-polymerised inorganic coagulants and phosphorus removal by coagulation - A review. *Water SA*, **24**, 237–244.

Jolly VH (1968) The comparative limnology of some New Zealand lakes. *New Zealand Journal of Marine and Freshwater Research*, **2**, 214–259.

Jolly VH, Brown MA (1975) *New Zealand lakes*. Auckland University Press.

Jolly VH, Chapman MA (1977) The comparative limnology of some New Zealand lakes. *New Zealand Journal of Marine and Freshwater Research*, **11**, 307–340.

Jones GR, Nash JD, Doneker RL, Jirka GH (2007) Buoyant surface discharges into water bodies. I : Flow classification and prediction methodology. *Journal of Hydraulic Engineering*, **133**, 1010–1021.

Kalinowska MB, Rowiński PM (2015) Thermal pollution in rivers—modelling of the spread of thermal plumes. In: *Rivers-Physical, Fluvial and Environmental Processes* (eds Rowiński PM, Radecki-Pawlik A), pp. 591–613. Springer, New York, NY, U.S.A.

Karamalidis AK, Dzombak DA (2010) *Surface complexation modeling: gibbsite*. Wiley, Hoboken, N.J., U.S.A.

Kennedy RH, Cooke GD (1982) Control of lake phosphorus with aluminum sulfate: Dose determination and application techniques. *Journal of the American Water Resources Association*, **18**, 389–395.

Kopáček J, Borovec J, Hejzlar J *et al.* (2005) Aluminum control of phosphorus sorption by lake sediments. *Environmental Science and Technology*, **39**, 8784–8789.

Kratz T, Macintyre S, Webster K (2005) Causes and consequences of spatial heterogeneity in lakes. In: *Ecosystem Function in Heterogeneous Landscapes* (eds Lovett GM, Turner MG, Jones CG, Weathers KC), pp. 329–346. Springer, New York, London.

Kufel L, Kufel I (2002) *Chara* beds acting as nutrient sinks in shallow lakes - a review. *Aquatic Botany*, **72**, 249–260.

Kumar E, Bhatnagar A, Hogland W, Marques M, Sillanpää M (2014) Interaction of anionic pollutants with Al-based adsorbents in aqueous media - a review. *Chemical Engineering Journal*, **241**, 443–456.

Lewis WM, Wurtsbaugh WA (2008) Control of lacustrine phytoplankton by nutrients: Erosion of the phosphorus paradigm. *International Review of Hydrobiology*, **93**, 446–465.

Lewis WM, Wurtsbaugh WA, Paerl HW (2011) Rationale for control of anthropogenic nitrogen and phosphorus to reduce eutrophication of inland waters. *Environmental Science and Technology*, **45**, 10300–10305.

Lijklema L (1980) Interaction of orthophosphate with iron (III) and aluminum hydroxides. *Environmental Science and Technology*, **14**, 537–541.

Likens GE (2009) *Encyclopedia of inland waters*. Elsevier, Amsterdam, the Netherlands.

Ling N (2014) *Puarenga Stream alum dosing – Summary of effects on lake biota 2013/2014. Report prepared for the Bay of Plenty Regional Council. University of Waikato, Hamilton.* Hamilton, New Zealand.

Liu J, Dietz T, Carpenter SR *et al.* (2007) Complexity of coupled human and natural systems. *Science*, **317**, 1513–1516.

Lofts S, Tipping E, Hamilton-Taylor J (2008) The chemical speciation of Fe(III) in freshwaters. *Aquatic Geochemistry*, **14**, 337–358.

Lohse KA, Brooks PD, McIntosh JC, Meixner T, Huxman TE (2009) Interactions between biogeochemistry and hydrologic systems. *Annual Review of Environment and Resources*, **34**, 65–96.

Lombardo P, Dennis Cooke G (2003) *Ceratophyllum demersum* - phosphorus interactions in nutrient enriched aquaria. *Hydrobiologia*, **497**, 79–90.

Lowe DJ, Green JD (1987) Origins and development of the lakes. In: *Inland Waters of New Zealand* (ed Viner AB), pp. 1–64. New Zealand Department of Scientific and Industrial Research, Wellington, New Zealand.

Lurling M, Mackay E, Reitzel K, Spears BM (2016) Editorial - a critical perspective on geo-engineering for eutrophication management in lakes. *Water Research*, **97**, 1–10.

Luther GW (2016) *Inorganic chemistry for geochemistry and environmental sciences: Fundamentals and applications*. Wiley, Chichester, U.K.

Maberly SC (1996) Diel, episodic and seasonal changes in pH and concentrations of inorganic carbon in a productive lake. *Freshwater Biology*, **35**, 579–598.

Maberly SC, Spence DHN (1983) Photosynthetic inorganic carbon use by freshwater plants. *Journal of Ecology*, **71**, 705–724.

Mackay EB, Jones ID, Folkard AM, Thackeray SJ (2011a) Transition zones in small lakes: The importance of dilution and biological uptake on lake-wide heterogeneity. *Hydrobiologia*, **678**, 85–97.

Mackay EB, Jones ID, Thackeray SJ, Folkard AM (2011b) Spatial heterogeneity in a small, temperate lake during archetypal weak forcing conditions. *Fundamental and Applied Limnology/Archiv für Hydrobiologie*, **179**, 27–40.

Mackay EB, Maberly SC, Pan G *et al.* (2014) Geoengineering in lakes: Welcome attraction or fatal distraction? *Inland Waters*, **4**, 349–356.

Madsen JD, Chambers PA, James WF, Koch EW, Westlake DF (2001) The interaction between water movement, sediment dynamics and submersed macrophytes. *Hydrobiologia*, **444**, 71–84.

Maessen M, Roelofs JGM, Bellemakers MJS, Verheggen GM (1992) The effects of aluminium, aluminium/calcium ratios and pH on aquatic plants from poorly buffered environments. *Aquatic Botany*, **43**, 115–127.

Marion A, Nikora V, Puijalon S *et al.* (2014) Aquatic interfaces: A hydrodynamic and ecological perspective. *Journal of Hydraulic Research*, **52**, 744–758.

Martell AE, Hancock RD, Smith RM, Motekaitis RJ (1996) Coordination of Al(III) in the environment and in biological systems. *Coordination Chemistry Reviews*, **149**, 311–328.

Marti CL, Mills R, Imberger J (2011) Pathways of multiple inflows into a stratified reservoir: Thomson Reservoir, Australia. *Advances in Water Resources*, **34**, 551–561.

Martin T, Creed J, Brockhoff C (1994) *Method 200.2, Revision 2.8: Sample: Sample preparation procedure for spectrochimical determination of total recoverable elements*. Cincinnati, Ohio, U.S.A.

Martinez WL, Martinez AR (2002) *Computational Statistics Handbook with Matlab*. Chapman and Hall/CRC, London, U.K.

McBride CG, Tempero GW, Hamilton DP *et al.* (2015) *Ecological Effects of Artificial Mixing in Lake Rotoehu May 2015. ERI Report 59 prepared for Bay of Plenty Regional Council*. University of Waikato, Hamilton, New Zealand.

McIntosh J (2012) *Alum Dosing of two stream discharges to Lake Rotorua. Bay of Plenty Regional Council internal report.* Whakatane, New Zealand.

Ministry for the Environment NZ (2017) *Clean Water*. Government of New Zealand, Wellington, New Zealand.

Monismith SG, Imberger J, Morison ML (1990) Convective motions in the sidearm of a small reservoir. *Limnology and Oceanography*, **35**, 1676–1702.

Mook WG (2000) Chemistry of carbonic acid in water. In: *Environmental Isotopes in the Hydrological Cycle Principles and Applications Vol 1*, pp. 143–166. International Atomic Energy Agency and United Nations Educational, Scientific and Cultural Organization, Paris, France.

Moore PA, Reddy KR (1994) Role of Eh and pH on phosphorus geochemistry in sediments of Lake Okeechobee, Florida. *Journal of Environment Quality*, **23**, 955–964.

Mortimer C (1941) The exchange of dissolved substances between mud and water in lakes. *Journal of Ecology*, **29**, 280–329.

Mueller H, Hamilton DP, Doole GJ (2016) Evaluating services and damage costs of degradation of a major lake ecosystem. *Ecosystem Services*, **22**, 370–380.

Murphy J, Riley JP (1962) A modified single solution method for the determination of phosphate in natural waters. *Analytica Chimica Acta*, **27**, 31–36.

Na EH, Park SS (2006) A hydrodynamic and water quality modeling study of spatial and temporal patterns of phytoplankton growth in a stratified lake with buoyant incoming flow. *Ecological Modelling*, **199**, 298–314.

Nairn IA (1992) The Te Rere and Okareka eruptive episodes - Okataina Volcanic Centre, Taupo Volcanic Zone, New Zealand. *New Zealand Journal of Geology and Geophysics*, **35**, 16.

Nepf HM (2012a) Flow and Transport in Regions with Aquatic Vegetation. *Annual Review of Fluid Mechanics*, **44**, 123–142.

Nepf HM (2012b) Hydrodynamics of vegetated channels. *Journal of Hydraulic Research*, **50**, 262–279.

Nimick DA, Gammons CH, Parker SR (2011) Diel biogeochemical processes and their effect on the aqueous chemistry of streams: A review. *Chemical Geology*, **283**, 3–17.

Norton SA, Coolidge K, Amirbahman A *et al.* (2008) Speciation of Al, Fe, and P in recent sediment from three lakes in Maine, USA. *Science of the Total Environment*, **404**, 276–283.

O'Reilly CM, Rowley RJ, Schneider P *et al.* (2015) Rapid and highly variable warming of lake surface waters around the globe. *Geophysical Research Letters*, 1–9.

Oelßner W, Schmid J, Guth U (2003) Determination of carbon dioxide dynamics in lakes. In: *Proceedings of ICGG7*, pp. 50–52.

Oliver RL, Ganf GG (2000) Freshwater Blooms. In: *The Ecology of Cyanobacteria*, pp. 149–194. Kluwer Academic Publishers, Dordrecht, Germany.

Orihel DM, Schindler DW, Ballard NC, Wilson LR, Vinebrooke RD (2016) Experimental iron amendment suppresses toxic cyanobacteria in a hypereutrophic lake. *Ecological Applications*, **26**, 1517–1534.

Özkundakci D, Hamilton DP, McDowell R, Hill S (2014a) Phosphorus dynamics in sediments of a eutrophic lake derived from 31P nuclear magnetic resonance spectroscopy. *Marine and Freshwater Research*, **65**, 70–80.

Özkundakci D, Hamilton DP, Scholes P (2010) Effect of intensive catchment and in-lake restoration procedures on phosphorus concentrations in a eutrophic lake. *Ecological Engineering*, **36**, 396–405.

Özkundakci D, Pearson L, Mcbride CG, Hamilton DP (2014b) *Lake Rotorua sediment survey. ERI report 41 for Bay of Plenty Regional Council*. University of Waikato, Hamilton, New Zealand.

Pacini N, Gachter R (1999) Speciation of riverine particulate phosphorus during rain events. *Biogeochemistry*, **47**, 87–109.

Paerl HW, Otten TG (2013) Harmful cyanobacterial blooms: Causes, consequences, and controls. *Microbial Ecology*, **65**, 995–1010.

Paludan C, Jensen HS (1995) Sequential extraction of phosphorus in freshwater wetland and lake sediment: Significance of humic acids. *Wetlands*, **15**, 365–373.

Panther JG, Bennett WW, Teasdale PR, Welsh DT, Zhao H (2012) DGT measurement of dissolved aluminum species in waters: Comparing chelex-100 and titanium dioxide-based adsorbents. *Environmental Science and Technology*, **46**, 2267–2275.

Parkhurst DL, Appelo CAJ (2013) *Description of input and examples for PHREEQC version 3—a computer program for speciation, batch-reaction, one-dimensional transport, and inverse geochemical calculations: U.S. Geological Survey Techniques and Methods, book 6*. United States Geological Survey.

Paul WJ, Hamilton DP (2008) Low-dose alum application trialled as a management tool for internal nutrient loads in Lake Okaro , New Zealand. *New Zealand Journal of Marine and Freshwater Research*, **42**, 207–217.

Pełechata A, Pełechaty M (2010) The in situ influence of *Ceratophyllum demersum* on a phytoplankton assemblage. *Oceanological and Hydrobiological Studies*, **39**, 95–101.

Penn M, Auer T, Orman E Van, Korienek J (1995) Phosphorus diagenesis in lake sediments: investigations using fractionation techniques. *Marine and Freshwater Research*, **46**, 89–99.

Peryer-Fursdon J, Abell JM, Clarke D *et al.* (2014) Spatial variability in sediment phosphorus characteristics along a hydrological gradient upstream of Lake Rotorua, New Zealand. *Environmental Earth Sciences*, **73**, 1573–1585.

Pilgrim KM, Brezonik PL (2005a) Treatment of lake inflows with alum for phosphorus removal. *Lake and Reservoir Management*, **21**, 1–9.

Pilgrim KM, Brezonik PL (2005b) Evaluation of the potential adverse effects of lake inflow treatment with alum. *Lake and Reservoir Management*, **21**, 78–88.

Pretty JN, Mason CF, Nedwell DB *et al.* (2003) Environmental costs of freshwater eutrophication in England and Wales. *Environmental Science and Technology*, **37**, 201–208.

Raiswell R, Canfield DE (2012) The iron biogeochemical cycle past and present. *Geochemical Perspectives*, **1**, 1–220.

Ratouis TMP, Zarrouk SJ (2016) Factors controlling large-scale convective geothermal in the Taupo Volcanic Zone (TVZ), New Zealand. *Geothermics*, **59**, 236–251.

Reddy KR, DeLaune RD (2008) *Biogeochemistry of wetlands : science and applications*. CRC Press, Boca Raton, Florida, U.S.A.

Reddy KR, Kadlec RH, Flaig E, Gale PM (1999) Phosphorus retention in streams and wetlands : A review. *Critical Reviews in Environmental Science and Technology*, 37–41.

Reid RJ, Mosley LM (2016) Comparative contributions of solution geochemistry, microbial metabolism and aquatic photosynthesis to the development of high pH in ephemeral wetlands in South East Australia. *Science of the Total Environment*, **542**, 334–343.

Reitzel K, Hansen J, Andersen F, Hansen KS, Jensen HS (2005) Lake restoration by dosing aluminum relative to mobile phosphorus in the sediment. *Environmental Science and Technology*, **39**, 4134–4140.

Reitzel K, Jensen HS, Egemose S (2013) PH dependent dissolution of sediment aluminum in six Danish lakes treated with aluminum. *Water Research*, **47**, 1409–1420.

Reynolds CS, Davies PS (2001) Sources and bioavailability of phosphorus fractions in freshwaters: a British perspective. *Biological Reviews*, **76**, 27–64.

Robinson B, Kim N, Marchetti M *et al.* (2006) Arsenic hyperaccumulation by aquatic macrophytes in the Taupo Volcanic Zone, New Zealand. *Environmental and Experimental Botany*, **58**, 206–215.

Rueda FJ, MacIntyre S (2009) Flow paths and spatial heterogeneity of stream inflows in a small multibasin lake. *Limnology and Oceanography*, **54**, 2041–2057.

Rutherford JC (1981) *Handbook on Mixing in Rivers*. Ministry of Works and Development, Wellington, New Zealand.

Rydin E, Huser B, Welch EB (2000) Amount of phosphorus inactivated by alum treatments in Washington lakes. *Limnology and Oceanography*, **45**, 226–230.

Rydin E, Welch EB (1999) Dosing alum to Wisconsin Lake sediments based on in vitro formation of aluminum bound phosphate. *Lake and Reservoir Management*, **15**, 324–331.

Ščančar J, Milačič R (2006) Aluminium speciation in environmental samples: A review. *Analytical and Bioanalytical Chemistry*, **386**, 999–1012.

Schafran GC, Driscoll CT (1987) Spatial and temporal variations in aluminum chemistry of a dilute, acidic lake. *Biogeochemistry*, **3**, 105–119.

Scheffer M, Carpenter S, Foley JA, Folke C, Walker B (2001) Catastrophic shifts in ecosystems. *Nature*, **413**, 591–596.

Scheffer M, Hosper S, Meijer M, Moss B, Jeppesen E (1993) Alternative equilibria in shalow lakes. *Trends in Ecology and Evolution*, **8**, 275–279.

Schindler DW (1977) Evolution of phosphorus limitation in lakes. *Science*, **195**, 260–262.

Schlesinger WH, Bernhardt ES (2013) *Biogeochemistry: An analysis of global change*. Academic Press, Waltham, MA, U.S.A.

Schlesinger WH, Cole JJ, Finzi AC, Holland EA (2011) Introduction to coupled biogeochemical cycles. *Frontiers in Ecology and the Environment*, **9**, 5–8.

Schoffman H, Lis H, Shaked Y, Keren N (2016) Iron–nutrient interactions within phytoplankton. *Frontiers in Plant Science*, **7**, 1–12.

Scholes P, Hamill K (2016) *Rotorua Lakes Water Quality Report 2014/2015. Environmental Publication 2016/06*. Bay of Plenty Regional Council, Whakatane, New Zealand.

Simpson MP, Bignall G (2015) Undeveloped high-enthalpy geothermal fields of the Taupo Volcanic Zone, New Zealand. *Geothermics*, **59**, 325–346.

Smith VH, Joye SB, Howarth RW (2006) Eutrophication of freshwater and marine ecosystems. *Limnology and Oceanography*, **51**, 351–355.

Smith VH, Schindler DW (2009) Eutrophication science: Where do we go from here? *Trends in Ecology and Evolution*, **24**, 201–207.

Smith VH, Wood SA, McBride CG *et al.* (2016) Phosphorus and nitrogen loading restraints are essential for successful eutrophication control of Lake Rotorua, New Zealand. *Inland Waters*, **6**, 273–283.

Søndergaard M, Jensen JP, Jeppesen E (2003) Role of sediment and internal loading of phosphorus in shallow lakes. *Hydrobiologia*, **506–509**, 135–145.

Søndergaard M, Lauridsen TL, Johansson LS, Jeppesen E (2017) Nitrogen or phosphorus limitation in lakes and its impact on phytoplankton biomass and submerged macrophyte cover. *Hydrobiologia*, 1–14.

Spears BM, Ives SC, Angeler DG *et al.* (2015) Effective management of ecological resilience - are we there yet? *Journal of Applied Ecology*, **52**, 1311–1315.

Spears BM, Maberly SC, Pan G *et al.* (2014) Geo-engineering in lakes: A crisis of confidence? *Environmental Science and Technology*, 9977–9979.

Sterner RW, Smutka TM, McKay RML *et al.* (2004) Phosphorus and trace metal limitation of algae and bacteria in Lake Superior. *Limnology and Oceanography*, **49**, 495–507.

Stumm W, Morgan JJ (1996) *Aquatic chemistry: Chemical equilibria and rates in natural waters*. Wiley, New York, NY, U.S.A.

Sullivan TJ, Cosby B (1998) Modeling the concentration of aluminum in surface waters. *Water, Air, and Soil Pollution*, **105**, 643–659.

Sullivan TJ, Driscoll CT, Gherini SA *et al.* (1989) Influence of aqueous aluminium and organic acids on measurement of acid neutralizing capacity in surface waters. *Nature*, **338**, 408–410.

Tanner CC, Clayton JS, Upsdell MP (1995) Effect of loading rate and planting on treatment of dairy farm wastewaters in constructed wetlands-II. Removal of nitrogen and phosphorus. *Water Research*, **29**, 27–34.

Tempero G (2015) *Ecotoxicological review of alum applications to the Rotorua Lakes. ERI report 52 for Bay of Plenty Regional Council*. University of Waikato, Hamilton, New Zealand.

Timperley MH (1983) Phosphorus in spring waters of the Taupo Volcanic Zone, North Island, New Zealand. *Chemical Geology*, **38**, 287–306.

Timperley MH, Huser BA (1996) Inflows of geothermal fluid chemicals to the Waikato River catchment, New Zealand. *New Zealand Journal of Marine and Freshwater Research*, **30**, 525–535.

Timperley MH, Vigor-Brown RJ (1986) Water chemistry of lakes in the Taupo Volcanic Zone, New Zealand. *New Zealand Journal of Marine and Freshwater Research*, **2086**, 173–183.

Tipping E, Rey-Castro C, Bryan SE, Hamilton-Taylor J (2002) Al(III) and Fe(III) binding by humic substances in freshwaters, and implications for trace metal speciation. *Geochimica et Cosmochimica Acta*, **66**, 3211–3224.

Toetz D (1971) Diurnal uptake of NO3 and NH4 by a Ceratophyllum-periphyton community. *Limnology and Oceanography*, **16**.

Trolle D, Hamilton DP, Pilditch CA, Duggan IC, Jeppesen E (2011) Predicting the effects of climate change on trophic status of three morphologically varying lakes: Implications for lake restoration and management. *Environmental Modelling and Software*, **26**, 354–370.

Turner BL, Frossard E, Baldwin DS (2005) *Organic phosphorus in the environment*. CABI Publishing, Wallingford, U.K.

Vanni MJ (2002) Nutrient recycling by animals in freshwater ecosystems. *Annual Review of Ecology and Systematics*, **33**, 341–370.

Vant WN, Davies-Colley RJ, Clayton JS, Coffey BT (1986) Macrophyte depth limits in North Island (New Zealand) lakes of differing clarity. *Hydrobiologia*, **137**, 55–60.

de Vicente I, Huang P, Andersen FØ, Jensen HS (2008a) Phosphate adsorption by fresh and aged aluminum hydroxide. Consequences for lake restoration. *Environmental Science and Technology*, **42**, 6650–6655.

de Vicente I, Jensen HS, Andersen FØ (2008b) Factors affecting phosphate adsorption to aluminum in lake water: Implications for lake restoration. *Science of the Total Environment*, **389**, 29–36.

Vitousek PM, Mooney HA, Lubchenco J, Melillo JM (1997) Human domination of Earth's ecosystems. *Science*, **277**, 494–499.

Vollenweider RA (1968) *Scientific fundamentals of the eutrophication of lakes and flowing waters, with particular reference to nitrogen and phosphorus as factors in eutrophication. Technical Report DAS/CS1/68.27 for the Organisation for Economic Co-operation and Development.* Organisation for Economic Co-operation and Development Council, Paris, France.

Vorosmarty CJ, Green P, Salisbury J, Lammers RB (2000) Global water resources: Vulnerability from climate change and population growth. *Science*, **289**, 284–288.

Warren L, Haack E (2001) Biogeochemical controls on metal behavior in freshwater environments. *Earth-Sciences Reviews*, **54**, 261–320.

Welch EB, Cooke GD (1995) Internal phosphorus loading in shallow lakes: Importance and control. *Lake and Reservoir Management*, **11**, 273–281.

Welch EB, Cooke GD (1999) Effectiveness and longevity of phosphorus inactivation with alum. *Lake and Reservoir Management*, **15**, 5–27.

Weng L, Van Riemsdijk WH, Hiemstra T (2012) Factors controlling phosphate interaction with iron oxides. *Journal of Environmental Quality*, **41**, 628–635.

Wetzel RG (1995) Death, detritus and energy flow in aquatic ecosystems. *Freshwater Biology*, **33**, 83–89.

Wetzel RG (2001) *Limnology: Lake and river ecosystems.* San Diego: Academic Press.

Williamson CE, Saros JE, Vincent WF, Smol JP (2009) Lakes and reservoirs as sentinels, integrators, and regulators of climate change. *Limnology and Oceanography*, **54**, 2273–2282.

Wilson CJN, Rowland J V. (2016) The volcanic, magmatic and tectonic setting of the Taupo Volcanic Zone, New Zealand, reviewed from a geothermal perspective. *Geothermics*, **59**, 168–187.

Wisawapipat W, Charoensri K, Runglerttrakoolchai J (2017) Solid-phase speciation and solubility of phosphorus in an acid sulfate paddy soil during soil reduction and reoxidation as affected by oil palm ash and biochar. *Journal of Agricultural and Food Chemistry*, **65**, 704–710.

Withers PJA, Jarvie HP (2008) Delivery and cycling of phosphorus in rivers: A review. *Science of the Total Environment*, **400**, 379–395.

Worsfold PJ, Monbet P, Tappin AD *et al.* (2008) Characterisation and quantification of organic phosphorus and organic nitrogen components in aquatic systems: A Review. *Analytica Chimica Acta*, **624**, 37–58.

Xing W, Liu G (2011) Iron biogeochemistry and its environmental impacts in freshwater lakes. *Fresenius Environmental Bulletin*, **20**, 1339–1345.

Xu R, Zhang M, Mortimer RJG, Pan G (2017) Enhanced phosphorus locking by novel lanthanum/aluminum–hydroxide composite: Implications for eutrophication control. *Environmental Science and Technology*, **51**, 3418–3425.

Xue P, Yan C, Sun G, Luo Z (2012) Arsenic accumulation and speciation in the submerged macrophyte *Ceratophyllum demersum* L. *Environmental Science and Pollution Research*, **19**, 3969–3976.

Zänker H, Hüttig G, Arnold T, Nitsche H (2006) Formation of iron-containing colloids by the weathering of phyllite. *Aquatic Geochemistry*, **12**, 299–325.

Zhang H, Davison W (1995) Performance characteristics of diffusion gradients in thin films for the in situ measurement of trace metals in aqueous solution. *Analytical Chemistry*, **67**, 3391–3400.

APPENDIX

Table A.1. Summary of results from 07/03/2017. The table includes cations in mg L^{-1} from TA, ICMPS, IC and FIA analysis.

Location				Cations														
07_03_17	Temp	pH(field)	pH(lab)	Na	K	Ca	Mg	Fe	Mn	Al	Ba	Sr	NH_4	Zn	Ni	Cu	Ag	U
Site18	38.0	6.0	5.9	312.11	17.29	14.12	5.79	2.31	1.07	0.03	0.000	0.095		0.01	0.00	0.00	0.00	0.00
Site16	20.1	6.2																
Site17	38.0	6.0	5.8	309.23	17.09	13.89	6.16	3.55	1.103	0.137		0.093		0.0056	0.00046	0.00057	-2E-05	4.1E-06
Site1	26.3	6.2	6.2	94.46	12.67	9.85	5.41	1.04	0.862	0.068	0.103	0.069	0.104	0.0029	0.00026	0.00027	9.3E-05	9.9E-06
Site6	22.5	6.6	6.8	143.97	14.22	11.66	6.84	1.78	0.995	0.038	0.105	0.082		0.0023	0.00023	0.00049	0.00014	1.6E-05
Site7	24.2	6.4	6.4	157.77	13.15	10.22	5.66	0.70	1.004	0.045	0.104	0.072		0.0019	0.00019	0.00023	0.00011	9.8E-06
Site2	26.0	6.3	6.4	120.89	13.11	10.18	5.63	0.93	0.911	0.063	0.102	0.071		0.0073	0.00025	0.00037	0.00012	7.9E-06
Site11	27.5	6.4	6.5	148.07	12.74	9.89	5.37	0.52	0.894	0.070	0.098	0.069		0.0019	0.00019	0.00014	0.00014	8.8E-06
Site8	22.7	6.8	6.6	160.77	12.78	10.14	5.67	0.21	0.502	0.081	0.083	0.070		0.0039	0.00026	0.00018	0.00012	8.9E-06
Site3	22.0	6.6	6.9	188.96	12.41	10.02	5.44	0.19	0.569	0.054	0.082	0.068	0.066	0.0464	0.0002	0.00013	0.00008	9.9E-06
Site12	23.2	6.7	6.8	126.43	12.55	10.13	5.48	0.21	0.917	0.039	0.090	0.069		0.0025	0.00068	0.00089	0.00015	6.8E-06
Site9	22.3	7.4	7.1	104.17	10.09	7.62	4.61	0.10	0.154	0.030	0.058	0.054		0.0007	0.00015		0.00017	8.8E-06
Site4	21.6	7.6	7.4	97.71	9.31	6.89	4.28	0.09	0.056	0.032	0.046	0.048			0.00013		8.7E-05	8.9E-06
Site13	22.2	6.8	6.8	124.06	10.78	6.91	3.60	0.07	0.067	0.014	0.064	0.048		0.0009	0.00014		0.00011	4.9E-06
Site10	22.5	6.4	7.7	90.92	8.75	6.56	4.18	0.02	0.016	0.013	0.051	0.046		0.0004	0.00017		0.00012	6.9E-06
Site5	22.2	8.2	7.6	88.94	8.65	6.45	4.08	0.02	0.023	0.013	0.050	0.045	0.028	0.0001	0.00011		8.4E-05	8.9E-06
Site14	23.0	6.9	7.1	127.33	12.01	7.18	3.44	0.06	0.061	0.011	0.072	0.051		0.0018	0.00015	3.1E-05	0.00011	6.8E-06
Site15	22.3	8.3	7.5	87.49	8.31	6.32	4.03	0.02	0.007	0.011	0.048	0.044	0.026	0.0022	0.00015		9.5E-05	6.8E-06

Table A.2. Summary of results from 07/03/2017. The table includes anions and totals in mg L^{-1} from TA, ICMPS, IC and FIA analysis.

Location	Anions										Totals			
07_03_17	Cl	HCO_3	Si	SO_4	B	NO_3	NO_2	PO_4	As	Se	CB%	TN	TP	DIN
Site18	302.00		73.23	38.10	1.62			0.051	0.030	0.002	-0.30001			
Site16														
Site17	298.00		73.08	68.90	1.62			0.008	0.032	0.003	-8.05532			
Site1	178.11	496.4	56.62	25.55	1.01	0.159	0.005	0.016	0.014	0.002	-71.5209	0.1711	0.00741	0.268
Site6	204.54	793.2	59.85	24.23	1.19			0.037	0.041	0.003	-72.6097			
Site7	180.83	122.6	57.96	25.67	1.07			0.011	0.016	0.002	-28.3894			
Site2	179.29	654.2	58.28	26.50	1.05			0.014	0.015	0.002	-72.3486			
Site11	177.92	147.5	57.44	25.85	1.03			0.011	0.011	0.002	-34.3226			
Site8	179.52	170.1	49.69	22.26	1.06			0.019	0.014	0.002	-33.3593			
Site3	176.60	128.5	49.61	23.51	1.02	0.085	0.005	0.010	0.009	0.002	-21.5084	0.2848	0.06684	0.156
Site12	176.02	120.3	54.91	24.90	1.03			0.018	0.013	0.002	-35.809			
Site9	153.49	98.3	23.27	14.25	0.82			0.011	0.017	0.002	-35.4274			
Site4	142.62	104.7	17.14	12.34	0.76			0.008	0.018	0.001	-37.2987			
Site13	162.12	108.3	22.05	10.16	0.96			0.009	0.017	0.002	-31.4312			
Site10	127.34	85.5	7.49	11.77	0.68			0.008	0.018	0.002	-33.7352			
Site5	126.89	106.9	7.55	11.30	0.67	0.017	0.004	0.006	0.018	0.001	-38.9765	0.7005	0.05226	0.049
Site14	143.34	102.8	27.68	10.66	1.06			0.011	0.017	0.002	-26.0398			
Site15	126.01	84.5	6.91	10.86	0.66	0.015	0.004	0.008	0.018	0.002	-35.1942	0.6854	0.0503	0.045

Table A.3. Summary of results from 16/03/2017. The table includes cations in mg L^{-1} from TA, ICMPS, IC and FIA analysis.

Location				Cations														
16_03_17	**Temp**	**pH(field)**	**pH(lab)**	**Na**	**K**	**Ca**	**Mg**	**Fe**	**Mn**	**Al**	**Ba**	**Sr**	**NH_4**	**Zn**	**Ni**	**Cu**	**Ag**	**U**
Site18	37.3	6	6	220.57	16.94	11.68	5.90	3.04	1.17	0.028	0.136	0.0932		0.0058	0.00093	0.00061	0.00025	
Site16	19.6	7.13	6.55	75.80	8.20	5.90	4.56	0.61	0.41	0.003	0.082	0.0458	0.052	0.0023	0.00072		0.00016	5E-06
Site17	37.2	6.1	6.16	217.30	16.63	11.83	5.50	2.93	1.20	0.239	0.138	0.0961		0.0069	0.00110	0.00108	0.00020	2E-06
Site1	26.57	6.84	6.14	123.46	11.49	8.78	4.80	0.77	0.71	0.054	0.093	0.0636	0.098	0.0072	0.00030	0.00019	0.00013	2.9E-06
Site6	25.32	7.14	6.45	126.88	11.00	8.20	4.84	0.58	0.71	0.043	0.094	0.0624		0.0030	0.00029	0.00016	0.00009	8E-06
Site7	25.29	7.16	6.46	135.43	11.66	8.66	4.99	0.35	0.76	0.046	0.097	0.0650		0.0017	0.00027	0.00031	0.00012	9E-06
Site2	26.02	6.91	6.11	125.60	11.57	8.96	4.95	0.53	0.70	0.046	0.089	0.0632		0.0050	0.00027	0.00025	0.00014	5.8E-06
Site11	25.43	7.07	6.51	122.85	10.37	7.82	4.73	0.29	0.57	0.040	0.085	0.0588		0.0041	0.00022		0.00016	1.3E-05
Site8	23.39	7.36	6.85	133.71	11.54	8.64	5.00	0.22	0.57	0.048	0.085	0.0643		0.0017	0.00023	0.00024	0.00014	1.2E-05
Site3	25.13	7.18	6.81	117.46	11.33	8.79	4.92	0.28	0.59	0.070	0.079	0.0616	0.04	0.0029	0.00034	0.00027	0.00010	4.8E-06
Site12	25.72	7.07	6.76	118.64	10.55	7.72	4.54	0.35	0.50	0.063	0.079	0.0579		0.0024	0.00023	0.00016	0.00020	1.3E-05
Site9	20.25	8.74	7.49	103.85	8.92	6.57	4.34	0.08	0.09	0.040	0.056	0.0501		0.0004	0.00020		0.00014	1.2E-05
Site4	19.99	8.92	8.19	94.28	8.73	6.35	4.23	0.09	0.09	0.042	0.052	0.0470		0.0020	0.00032	0.00022	0.00004	1.2E-05
Site13	24.95	7.29	7.54	117.71	9.79	7.12	4.40	0.31	0.36	0.065	0.067	0.0539		0.0015	0.00028	5.2E-05	0.00016	1.5E-05
Site10	19.85	8.82	7.64	79.63	7.51	5.38	3.58	0.00	0.00	0.007	0.055	0.0436		0.0006	0.00015		0.00014	8E-06
Site5	19.87	8.91	8.22	81.97	7.68	5.70	3.75	0.00	0.00	0.012	0.053	0.0419	0.234	0.0517	0.00023		0.00007	9E-06
Site14	23.27	7.48	7.73	89.14	8.16	5.82	3.91	0.05	0.06	0.019	0.051	0.0449		0.0019	0.00030		0.00015	0.00001
Site15	19.97	9.01	7.65	79.90	7.36	5.20	3.53		0.00	0.007	0.050	0.0407	0.166	0.0006	0.00041		0.00012	8E-06

Table A.4. Summary of results from 16/03/2017. The table includes anions and totals in mg L^{-1} from TA, ICMPS, IC and FIA analysis.

Location	Anions										Totals			
16_03_17	Cl	HCO_3	Si	SO_4	B	NO_3	NO_2	PO_4	As	Se	CB%	TN	TP	DIN
Site18	278.53		76.83	38.17	1.617			0.0622	0.0347	0.0035	-12.3			
Site16	114.19		44.48	7.88	0.596	0.204	0.005	0.0370	0.0089	0.0012	-10.074			0.261
Site17	275.91		77.16	59.84	1.478			0.0082	0.0322	0.0039	-19.14			
Site1	156.18	154.53	55.60	23.56	0.938	0.189	0.005	0.0116	0.0116	0.0015	-39.473	0.3533	0.07312	0.292
Site6	180.02	125.18	52.92	20.06	0.861			0.0142	0.0168	0.0019	-37.114			
Site7	173.81	115.15	56.39	23.13	0.935			0.0115	0.0114	0.0023	-33.04			
Site2	157.57	115.65	55.76	23.71	0.954			0.0109	0.0119	0.0023	-33.569			
Site11	159.55	251.04	53.17	20.55	0.837			0.0113	0.0129	0.0019	-50.832			
Site8	174.06	117.62	52.94	22.43	0.928			0.0171	0.0132	0.0020	-33.88			
Site3	157.78	111.56	54.63	23.27	0.947	0.093	0.005	0.0138	0.0102	0.0017	-35.597	0.1694	0.04653	0.138
Site12	160.25	202.99	49.93	20.88	0.867			0.0169	0.0138	0.0016	-47.42			
Site9	138.46	99.58	24.26	14.04	0.732			0.0107	0.0155	0.0012	-35.389			
Site4	125.41	94.18	21.82	13.81	0.690			0.0128	0.0157	0.0013	-36.051			
Site13	144.77	179.18	39.35	17.66	0.815			0.0125	0.0158	0.0016	-43.144			
Site10	116.16	95.70	6.29	9.30	0.582			0.0139	0.0165	0.0012	-40.296			
Site5	106.65	89.74	6.88	10.39	0.600	0.021	0.006	0.0132	0.0165	0.0013	-36.18	0.7477	0.05939	0.261
Site14	120.09	84.71	12.83	11.03	0.680			0.0098	0.0174	0.0014	-33.519			
Site15	116.11	97.82	6.22	9.21	0.597	0.022	0.005	0.0137	0.0161	0.0011	-41.164	0.6236	0.04646	0.193

Table A.5. Summary of results from 07/04/2017. The table includes cations in mg L^{-1} from TA, ICMPS, IC and FIA analysis.

Location				Cations															
07_04_17	Temp	pH(field)	pH(lab)	Na	K	Ca	Mg	Fe	Mn	Al	Ba	Sr	NH_4	Zn	Ni	Cu	Ag	Pb	Co	Hg
Site18	34.15	6.03	6.32	197.78	15.11	11.75	5.78	1.469	1.085	0.073	0.133	0.093	0.187	0.012		0.0024	0.0003	0.00003	0.00012	
Site17	34.24	6	6.15	188.77	15.23	11.65	5.73	0.477	1.068	0.009	0.134	0.092	0.172	0.021	0.00006	0.0023	0.0003		0.00013	
Site16	18.78	6.73	6.65	61.0502	7.52	5.60	3.90	0.421	0.290	0.004	0.071	0.042	0.043	0.009		0.0009	0.0002			
Site1S1	23.99	6.09	6.32	109.94	10.35	7.75	4.31	0.499	0.527	0.048	0.090	0.057	0.084	0.007	0.0002	0.0014	0.0004		4.3E-05	
Site1B1	23.92	6.1	6.34	96.99	10.37	7.69	4.30	0.474	0.521	0.045	0.091	0.058	0.135	0.006	0.0002	0.0014	0.0004	0.00047	4.5E-05	
Site1S2	23	6.3	6.41	110.1	10.65	7.90	4.46	0.546	0.544	0.041	0.088	0.056	0.087	0.006	0.0002	0.0013	0.0004		4.3E-05	
Site1B2	22.88	6.29	6.35	111.76	10.61	7.86	4.46	0.548	0.533	0.041	0.089	0.057	0.096	0.005	0.0002	0.0015	0.0005	0.00011	3.5E-05	
Site1S3	21.48	6.39	6.38	98.53	10.30	7.65	4.41	0.614	0.534	0.049	0.087	0.056	0.079	0.004	0.0002	0.0014	0.0005	0.00008	3.8E-05	
Site1B3	20.46	6.45	6.4	96.52	10.36	7.87	4.52	0.522	0.537	0.040	0.092	0.058	0.099	0.007	0.0001	0.0013	0.0004		3.7E-05	
Site1S4	22.2	6.38	6.38	83.22	10.47	7.83	4.42	0.483	0.529	0.044	0.091	0.059	0.116	0.005	0.0002	0.0013	0.0004		3.6E-05	
Site1B4	21.1	6.43	6.43	73.47	10.53	7.88	4.48	0.370	0.526	0.041	0.090	0.058	0.138	0.008	0.0002	0.0013	0.0003	0.00000	5.1E-05	
Site2S1	22.99	6.33	6.53	87.09	10.32	7.69	4.39	0.191	0.485	0.055	0.089	0.058		0.004	0.0002	0.0014	0.0004	0.00003	4.6E-05	
Site2B1	20.29	6.43	6.73	77.91	8.80	6.34	3.76	0.231	0.326	0.074	0.073	0.047		0.006	0.0001	0.0011	0.0003	0.00000	9E-06	
Site2S2	20.03	6.65	6.67	87.16	9.65	7.05	3.97	0.176	0.377	0.058	0.078	0.052		0.005	0.0002	0.0014	0.0004	0.00023	3.4E-05	
Site2B2	19.23	6.79	6.86	85.44	8.27	5.87	3.41	0.238	0.268	0.026	0.062	0.042		0.005	0.0003	0.0019	0.0005	0.00003	1.8E-05	
Site2S3	19.35	6.63	6.65	81.74	9.80	7.25	4.06	0.311	0.441	0.040	0.080	0.053		0.005	0.0002	0.0013	0.0004	0.00008	3.3E-05	
Site2B3	18.61	6.63	6.7	83.64	9.53	6.99	4.01	0.268	0.408	0.062	0.077	0.051		0.005	0.0002	0.0014	0.0004	0.00001	3.1E-05	
Site2S4	19.95	6.49	6.77	82.84	10.01	7.45	4.18	0.189	0.391	0.045	0.081	0.054		0.006	0.0002	0.0014	0.0004	0.00007	2.1E-05	
Site2B4	18.16	6.61	6.8	82.94	9.44	6.97	3.91	0.276	0.183	0.062	0.067	0.047		0.004	0.0001	0.0012	0.0003	0.00001	0.00001	
Site3S1	22.69	9.1	7.78	73.7252	7.91	4.98	2.96	0.225	0.008	0.134	0.009	0.026	0.021	0.001	0.0001	0.0012	0.0002	0.00008		0.00028
Site3B1	18.38	7.04	7	74.1676	8.56	5.76	3.25	0.245	0.273	0.080	0.052	0.037	0.074	0.003	0.0001	0.0009	0.0003	0.00006		0.00017
Site3S2	21.57	8.23	8.96	75.034	8.21	4.14	2.63	0.179	0.009	0.108	0.004	0.019	0.036	0.001	0.0000	0.0010	0.0004			0.00021
Site3B2	18.46	6.55	7.15	71.7038	8.33	5.66	3.15	0.206	0.173	0.075	0.050	0.036	0.116	0.003	0.0002	0.0011	0.0004	2E-05		0.00012
Site3S3	19.74	7.42	8.49	72.7004	7.61	4.35	2.61	0.223	0.008	0.141	0.009	0.024	0.034	0.001	0.0000	0.0009	0.0003			0.00005

Site3B3	18.63	6.59	7	71.8847	8.54	5.83	3.21	0.209	0.139	0.070	0.053	0.037	0.141	0.002	0.0001	0.0010	0.0005			0.00008
Site3S4	19.22	7.77	7.2	74.8216	8.23	5.13	3.01	0.188	0.007	0.090	0.031	0.032	0.031	0.005	0.0001	0.0010	0.0004			0.00014
Site3B4	18.51	6.82	6.88	72.7777	8.39	5.83	3.27	0.236	0.197	0.080	0.056	0.039	0.135	0.004	0.0001	0.0010	0.0003			0.00012
Site3S5	19.21	6.91	7.12	70.1384	7.91	5.03	2.88	0.131	0.006	0.055	0.034	0.033	0.037	0.002	0.0001	0.0009	0.0005			0.00003
Site3B5	18.66	6.83	6.82	72.2767	8.58	5.82	3.15	0.186	0.145	0.057	0.055	0.039	0.149	0.002	0.0004	0.0012	0.0004	0.00017		0.00007
Site3S6	18.99	6.93	6.94	72.8821	8.28	5.59	3.12	0.138	0.006	0.055	0.042	0.037	0.029	0.001	0.0001	0.0010	0.0003			0.00006
Site3B6	18.77	6.74	6.76	76.0083	8.42	5.85	3.19	0.179	0.045	0.071	0.051	0.039	0.162	0.008	0.0001	0.0010	0.0003			0.00007
Site3S7	18.32	7.06	6.59	78.0681	8.77	6.26	3.36	0.141	0.007	0.055	0.054	0.044	0.033	0.003	0.0001	0.0012	0.0003	5.06E-06		0.00009
Site3B7	18.5	6.8	6.7	76.628	8.49	5.89	3.19	0.130	0.030	0.046	0.053	0.041	0.156	0.003	0.0001	0.0013	0.0003	1.01E-05		0.00004
Site3S8	17.72	6.92	6.9	79.1153	8.72	6.21	3.26	0.118	0.009	0.046	0.056	0.043	0.043	0.002	0.0001	0.0012	0.0004	4.76E-05		0.00006
Site3B8	17.83	6.8	6.86	79.9202	8.90	6.41	3.37	0.186	0.106	0.077	0.058	0.044	0.084	0.007	0.0001	0.0011	0.0004			0.00004
Site3S9	17.6	6.99	6.88	78.5826	8.46	6.07	3.24	0.113	0.007	0.042	0.055	0.043	0.057	0.002	0.0001	0.0012	0.0004			0.00001
Site3B9	17.58	6.81	6.86	79.2853	8.76	6.19	3.22	0.144	0.136	0.040	0.058	0.043	0.080	0.002	0.0002	0.0013	0.0004	0.00010		0.00006
Site3S10	17.21	7.28	6.9	81.0313	8.74	6.46	3.34	0.113	0.060	0.029	0.059	0.046	0.056	0.004	0.0001	0.0013	0.0004			0.00007
Site3B10	16.63	7.01	6.9	78.01	8.36	6.18	3.17	0.143	0.053	0.045	0.057	0.044	0.076	0.003	0.0001	0.0010	0.0004			0.00004
Site3S11	18.1	7.5	6.93	88.3281	8.65	6.32	3.26	0.201	0.008	0.083	0.033	0.043	0.081	0.003	0.0002	0.0014	0.0005	1.8E-05		0.00008
Site3B11	17.1	6.74	6.78	87.7254	9.19	6.96	3.54	0.181	0.115	0.051	0.067	0.050	0.055	0.005	0.0001	0.0015	0.0003	4.4E-05		0.00004
Site3S12	24.14	9.16	8.59	87.2	8.45	6.17	3.17	0.116	0.064	0.033	0.054	0.044	0.062	0.003	0.0002	0.0013	0.0004	7.1E-06		0.00003
Site3B12	17.78	6.77	7.15	77.5055	8.46	6.14	3.07	0.130	0.135	0.037	0.054	0.043	0.079	0.005	0.0001	0.0011	0.0004			0.00003
Site4S1	19.16	6.77	6.84	79.8	9.08	6.48	3.66	0.151	0.260	0.040	0.072	0.048		0.013	0.0002	0.0014	0.0004	0.00036	4.3E-05	
Site4B1	18.7	7.03	7.04	63.9	7.87	5.54	3.13	0.095	0.178	0.033	0.063	0.042		0.006	0.0002	0.0011	0.0003	0.00007	2.5E-05	
Site4S2	18.54	7.33	7.24	66.48	8.04	5.86	3.38	0.039	0.072	0.019	0.060	0.043		0.015	0.0002	0.0014	0.0003	0.00020	2.3E-05	
Site4B2	18.55	7.22	7.27	82.35	7.83	5.61	3.34	0.037	0.073	0.012	0.058	0.043		0.001		0.0011	0.0000	0.00008		
Site4S3	17.38	7.39	7.43	73.61	7.66	5.52	3.38	0.031	0.077	0.016	0.059	0.043		0.003		0.0012	0.0001	0.00006		
Site4B3	17.46	7.43	7.32	77.13	7.43	5.59	3.35	0.033	0.063	0.015	0.057	0.043		0.005		0.0012	0.0001	0.00011	4E-06	
Site4S4	18.9	8	7.78	73.69	7.49	5.54	3.37	0.008	0.007	0.011	0.054	0.043		0.003		0.0013	0.0001	0.00011		
Site4B4	18.03	7.3	7.51	72.57	7.59	5.57	3.37	0.056	0.134	0.018	0.057	0.042		0.001		0.0010	0.0002			
Site5S1	18.66	7.82	7.67	85.23	7.18	5.35	3.30	0.002	0.002	0.006	0.051	0.041	0.076	0.001		0.0012	0.0001	0.00023		
Site5B1	18.49	7.75	7.56	80	7.32	5.37	3.34	0.059	0.020	0.029	0.055	0.043	0.079	0.002		0.0012	0.0002	0.00014		
Site5S2	18.78	8.08	7.72	71.56	7.42	5.59	3.47	0.003	0.006	0.004	0.054	0.042	0.097			0.0010	0.0001			

Site5B2	18.74	8.01	7.72	71.43	7.10	5.42	3.35	0.003	0.014	0.005	0.053	0.042	0.100	0.000		0.0012	0.0002	0.00010		
Site5S3	18.39	7.98	7.62	73.75	7.38	5.49	3.40	0.009	0.007	0.006	0.053	0.042	0.090	0.001		0.0012	0.0002	0.00006		
Site5B3	18.37	7.94	7.24	75.45	7.10	5.35	3.38	0.029	0.034	0.014	0.055	0.043	0.085	0.001		0.0010	0.0002			
Site5S4	17.56	7.98	7.72	70.95	6.88	5.29	3.31	0.005	0.006	0.009	0.051	0.042	0.091	0.001		0.0011	0.0002	0.00001		
Site5B4	18.19	7.59	7.68	75.14	7.16	5.44	3.47	0.015	0.016	0.012	0.054	0.044	0.121	0.003		0.0012	0.0001	0.00003		
Site15S1	19	7.96	7.81	76.57	7.20	5.52	3.50	0.008	0.005	0.009	0.054	0.043	0.091	0.002		0.0012	0.0002			
Site15B1	18.43	7.5	7.65	91.42	7.22	5.54	3.44	0.015	0.010	0.010	0.054	0.044	0.104	0.001		0.0011	0.0002			

Table A.6. Summary of results from 07/04/2017. The table includes anions and totals in mg L^{-1} from TA, ICMPS, IC and FIA analysis.

Location	Anions											Totals			
07_04_17	Cl	HCO_3	Si	S	B	NO_3	NO_2	PO_4	As	Se	Cr	CB%	TP	TN	DIN
Site18	240.15	167.98	66.24	43.82	1.445	0.255	0.005	0.005	0.018	0.0027	0.0023	-35.132	0.158	0.523	0.447
Site17	249.28	202.38	67.07	33.33	1.403	0.227	0.005	0.011	0.013	0.0029	0.0026	-39.102	0.310	0.572	0.404
Site16	114.72	488.47	37.09	6.15	0.508	0.264	0.005	0.040	0.007	0.0012	0.0007	-77.855	0.066	0.500	0.312
Site1S1	152.49	116.54	44.82	18.44	0.786	0.282	0.005	0.010	0.010	0.0016	0.0015	-37.326	0.061	0.500	0.371
Site1B1	151.01	103.55	44.94	18.56	0.777	0.754	0.006	0.013	0.010	0.0015	0.0015	-39.484	0.048	0.511	0.895
Site1S2	149.12	109.49	46.74	18.75	0.782	0.326	0.005	0.013	0.011	0.0018	0.0017	-35.486	0.094	0.509	0.418
Site1B2	129.94	126.93	45.49	18.51	0.805	0.392	0.006	0.015	0.011	0.0019	0.0016	-34.781	0.103	0.497	0.494
Site1S3	147.90	99.63	45.18	17.86	0.791	0.268	0.005	0.017	0.011	0.0018	0.0015	-37.433	0.114	0.479	0.352
Site1B3	148.56	102.23	45.27	17.93	0.796	0.419	0.006	0.015	0.011	0.0019	0.0013	-38.508	0.123	0.451	0.524
Site1S4	150.23	105.36	44.92	17.92	0.802	0.477	0.006	0.014	0.012	0.0018	0.0012	-44.019	0.074	0.467	0.599
Site1B4	154.25	107.79	45.06	17.40	0.833	0.689	0.007	0.011	0.011	0.0016	0.0012	-48.334	0.080	0.456	0.834
Site2S1	150.80	125.20	43.63	16.87	0.798			0.014	0.010	0.0014	0.0012	-45.581			
Site2B1	111.59	96.01	33.96	13.40	0.658			0.022	0.010	0.0012	0.0008	-38.814			
Site2S2	133.51	108.50	36.24	13.94	0.734			0.015	0.010	0.0017	0.0010	-40.448			
Site2B2	112.99	94.34	23.28	9.85	0.641			0.014	0.010	0.0013	0.0007	-34.976			
Site2S3	111.73	119.45	38.79	15.44	0.749			0.016	0.011	0.0016	0.0009	-41.042			
Site2B3	107.95	117.72	36.01	14.34	0.763			0.019	0.010	0.0012	0.0008	-39.277			
Site2S4	111.84	115.52	39.01	15.32	0.793			0.014	0.010	0.0018	0.0009	-39.695			
Site2B4	106.11	111.55	34.10	13.51	0.719			0.019	0.009	0.0013	0.0008	-38.01			
Site3S1	95.56	90.39	26.21	13.84	0.592	0.098	0.007	0.022	0.018	0.0010	0.0002	-40.938	0.332	1.847	0.126
Site3B1	93.11	97.98	27.30	13.46	0.589	0.148	0.007	0.024	0.009	0.0009	0.0006	-38.292	0.074	0.494	0.229
Site3S2	95.82	63.93	24.03	13.01	0.606	0.025	0.006	0.027	0.026	0.0010	0.0002	-33.044	0.373	2.300	0.067
Site3B2	93.00	107.69	26.64	12.54	0.577	0.139	0.007	0.020	0.008	0.0011	0.0006	-41.243	0.060	0.465	0.262
Site3S3	95.54	86.45	25.19	12.76	0.592	0.014	0.005	0.023	0.021	0.0011	0.0003	-39.048	0.261	1.744	0.053

Site3B3	95.40	151.60	27.75	12.89	0.596	0.071	0.007	0.022	0.008	0.0007	0.0005	-49.023	0.071	0.460	0.219
Site3S4	95.27	139.23	26.84	12.89	0.592	0.019	0.005	0.025	0.013	0.0010	0.0004	-47.027	0.187	1.202	0.055
Site3B4	97.35	331.53	27.87	12.89	0.588	0.080	0.008	0.025	0.009	0.0012	0.0006	-67.003	0.064	0.533	0.223
Site3S5	100.29	227.96	25.47	12.54	0.561	0.030	0.005	0.019	0.011	0.0010	0.0004	-60.628	0.149	0.992	0.072
Site3B5	98.22	181.56	27.33	12.16	0.580	0.088	0.007	0.019	0.008	0.0010	0.0007	-53.232	0.052	0.511	0.244
Site3S6	100.48	93.96	28.14	13.19	0.592	0.018	0.009	0.017	0.008	0.0008	0.0006	-40.024	0.163	1.185	0.056
Site3B6	112.50	102.07	28.37	12.75	0.604	0.121	0.008	0.018	0.010	0.0010	0.0006	-41.823	0.024	0.343	0.291
Site3S7	108.11	159.70	29.97	13.58	0.607	0.050	0.006	0.017	0.008	0.0009	0.0007	-49.439	0.408	2.514	0.089
Site3B7	107.25	96.56	29.73	13.54	0.594	0.116	0.008	0.014	0.009	0.0009	0.0006	-39.876	0.048	0.490	0.280
Site3S8	110.59	101.19	27.84	12.66	0.616	0.120	0.007	0.012	0.009	0.0011	0.0007	-39.631	0.048	0.497	0.170
Site3B8	110.80	108.92	29.01	13.52	0.626	0.111	0.007	0.018	0.009	0.0011	0.0008	-40.683	0.051	0.491	0.202
Site3S9	109.72	101.47	27.42	13.07	0.607	0.154	0.007	0.015	0.009	0.0010	0.0006	-40.167	0.061	0.696	0.218
Site3B9	111.41	94.92	29.21	13.17	0.608	0.112	0.007	0.015	0.009	0.0012	0.0007	-38.629	0.084	0.549	0.199
Site3S10	116.44	126.70	30.04	13.91	0.620	0.152	0.007	0.017	0.008	0.0012	0.0007	-44.558	0.077	0.670	0.215
Site3B10	116.20	102.89	28.36	12.67	0.596	0.138	0.007	0.015	0.009	0.0014	0.0005	-41.594	0.051	0.566	0.221
Site3S11	112.57	107.86	33.19	15.47	0.657	0.144	0.007	0.020	0.015	0.0014	0.0004	-38.644	0.065	0.616	0.232
Site3B11	123.76	118.32	32.97	14.62	0.652	0.157	0.007	0.016	0.009	0.0012	0.0007	-41.234	0.042	0.567	0.219
Site3S12	124.40	84.40	26.02	12.65	0.610	0.167	0.007	0.016	0.009	0.0014	0.0005	-37.804	0.108	0.732	0.236
Site3B12	109.08	108.39	25.51	12.54	0.591	0.153	0.007	0.016	0.009	0.0009	0.0005	-41.545	0.046	0.583	0.239
Site4S1	101.23	103.21	30.28	12.47	0.710			0.016	0.012	0.0014	0.0008	-37.042			
Site4B1	88.74	96.44	15.62	7.65	0.602			0.017	0.015	0.0014	0.0006	-39.902			
Site4S2	93.30	103.57	13.14	9.22	0.633			0.010	0.014	0.0013	0.0007	-41.474			
Site4B2	93.34	112.43	12.66	9.71	0.640			0.008	0.014	0.0011	0.0006	-36.774			
Site4S3	93.07	104.04	10.80	9.92	0.609			0.011	0.013	0.0011	0.0006	-39.023			
Site4B3	92.78	101.16	11.38	9.86	0.610			0.013	0.013	0.0014	0.0006	-36.821			
Site4S4	93.73	94.57	6.80	9.82	0.611			0.009	0.015	0.0011	0.0006	-37.405			
Site4B4	93.18	108.22	13.35	9.61	0.609			0.012	0.015	0.0012	0.0006	-40.181			
Site5S1	132.47	129.34	5.98	9.27	0.582	0.024	0.009	0.006	0.015	0.0012	0.0005	-45.761	0.040	0.530	0.109
Site5B1	130.39	85.68	6.71	9.65	0.598	0.024	0.008	0.010	0.015	0.0011	0.0005	-39.96	0.036	0.539	0.111
Site5S2	132.62	91.94	6.47	10.57	0.609	0.028	0.010	0.007	0.015	0.0010	0.0005	-45.417	0.044	0.567	0.135

Site5B2	132.60	102.22	6.32	9.81	0.601	0.026	0.011	0.008	0.015	0.0011	0.0006	-47.257	0.043	0.562	0.137
Site5S3	132.78	103.21	7.17	9.79	0.612	0.030	0.008	0.006	0.015	0.0011	0.0006	-46.217	0.033	0.507	0.128
Site5B3	132.81	278.13	7.46	9.77	0.577	0.031	0.009	0.011	0.015	0.0012	0.0006	-65.394	0.042	0.551	0.125
Site5S4	133.05	143.51	6.75	9.57	0.581	0.028	0.010	0.007	0.015	0.0012	0.0005	-53.764	0.037	0.540	0.129
Site5B4	133.10	131.87	7.03	10.06	0.590	0.030	0.020	0.011	0.016	0.0013	0.0006	-50.107	0.045	0.509	0.171
Site15S1	132.97	391.33	6.79	10.24	0.599	0.025	0.008	0.009	0.015	0.0012	0.0006	-71.968	0.037	0.561	0.124
Site15B1	133.12	173.49	7.08	10.37	0.618	0.026	0.011	0.011	0.015	0.0011	0.0006	-80.346	0.035	0.457	0.141